T-4295

SELECTIVE CATALYTIC REDUCTION OF NITRIC OXIDE OVER ACTIVATED CARBON-BASED CATALYSTS

ARTHUR LAKES LIBRARY
COLORADO SCHOOL OF MINES
GOLDEN, CO 80401

by

Sayed Naveed Ahmed

ProQuest Number: 10796532

All rights reserved

INFORMATION TO ALL USERS
The quality of this reproduction is dependent upon the quality of the copy submitted.

In the unlikely event that the author did not send a complete manuscript
and there are missing pages, these will be noted. Also, if material had to be removed,
a note will indicate the deletion.

ProQuest 10796532

Published by ProQuest LLC (2019). Copyright of the Dissertation is held by the Author.

All rights reserved.
This work is protected against unauthorized copying under Title 17, United States Code
Microform Edition © ProQuest LLC.

ProQuest LLC.
789 East Eisenhower Parkway
P.O. Box 1346
Ann Arbor, MI 48106 – 1346

T-4295

A thesis submitted to the Faculty and the Board of Trustees of the Colorado School of Mines in partial fulfillment of the requirements for the degree of Doctor of Philosophy (Chemical Engineering and Petroleum Refining).

Golden, Colorado

Date 4/25/93

Signed: Sayed Naveed Ahmed

Sayed Naveed Ahmed

Approved:

Dr. Robert Baldwin
Thesis Advisor

Golden, Colorado

Date 4/25/93

Dr. Robert Baldwin
Professor and Head,
Department of
Chemical Engineering

ABSTRACT

The objective of this work was the investigation of selective catalytic reduction (SCR) of nitric oxide using ammonia as a reductant over activated carbon catalysts. The focus of the research was to examine the physical and chemical properties of activated carbons which influence nitric oxide reduction under conditions simulating flue gas environment at temperatures of 150-300^{o}C. Such temperatures are lower than those normally employed when using conventional inorganic oxide SCR catalysts. Low temperature SCR provides flexibility in locating the catalyst bed under the high dust loadings that are expected from advanced fossil fuel combustion processes thus resulting in longer catalyst life.

The chemical properties of activated carbons, such as surface oxides and mineral matter appeared to play a more important role in nitric oxide reduction than the physical properties, such as BET surface area and pore structure. Activated carbons with high acidity, high concentration of surface oxides and low mineral content were found to be better catalysts for nitric oxide reduction. The presence of nitrogen and sulfur did not affect the activity. The importance of acidic surface oxides was confirmed by treating a coconut shell-based carbon with sulfuric acid which acted as an oxidizing agent and created acidic surface oxides. These surface oxides were determined to be predominantly carboxyl and carbonyl groups with the help of infrared spectroscopy and linear

temperature programmed desorption. Activated carbons which were synthesized by chemical activation using sulfuric acid also exhibited high activity due to the presence of acidic surface oxides (carboxyl groups). Gas phase oxygen was also found to be very important for nitric oxide reduction. Increasing oxygen concentration significantly improved nitric oxide conversion over activated carbon, perhaps by heterogeneous oxidation of nitric oxide to nitrogen dioxide which was readily reduced to nitrogen by ammonia.

TABLE OF CONTENTS

LIST OF FIGURES

LIST OF TABLES

ACKOWLEDGEMENTS

The author wishes to express his sincere appreciation to his advisor, Dr. Robert Baldwin, for his help during the course of this study. Thanks are also due to Dr. John Stencel and Dr. Frank Derbyshire for their help during this study.

The financial support of Center for Applied Energy Research, Lexington, KY and Colorado School of Mines is gratefully acknowledged.

Chapter 1

INTRODUCTION

A significant amount of work has been done in Japan and Western Europe towards control of nitrogen oxides (NO_X) emissions from combustion processes. Nine European countries, all in Western Europe, have national limits on NO_X emissions from coal combustion currently in force or agreed for future implementation. These countries are Austria, Belgium, Denmark, Germany, Italy, the Netherlands, Sweden, Switzerland and the United Kingdom (see Table I) (1).

In the United States, one third of the man-made NO_X comes from industrial sources, another third comes from motor vehicles and the final third comes from combustion processes (2). In recent years, NO_X emissions control has become a very important environmental issue in the United States. In 1977, coal accounted for 76% of the NO_X emissions from the electrical utilities sector (oil accounted for 12 % and gas 12 %). In 1987, the contribution from coal increased to 88% of the total emissions (oil 3% and gas 9%) (3). The new regulations in the United States have limited the emissions of NO_X to less than 615-900 mg/m^3 from coal combustion. Until the last few years, the primary focus in the United States has been on the reduction of sulfur oxide (SO_X) emissions, the level of which was about twice that of NO_X around 1950. Today, the emitted tonnages of SO_X and NO_X are almost equal due to more emphasis

Table 1.1 National NO_x emission standards, currently in force or planed to be implemented (1)

Countries	New plants mg/m^3	Existing plants mg/m^3
Austria	200-400	200-400
Belgium	200-800	*
Denmark	650	*
Germany	200-500	200-1300
Italy	650	1200
The Netherlands	400-800	1100
Sweden	140	140-560
Switzerland	200-500	200-500
United Kingdom	650	*

on SO_x control.

NO_x is considered to be a major air pollutant for the following reasons :

1) In the troposphere region (which extends up to 6-10 miles in altitude), nitrogen dioxide (NO_2) reacts with volatile organic compounds (VOC) to form ozone (O_3) in the presence of sunlight (4,5). The simplified chemistry of ozone formation is as follows:

$$NO_2 + hv\ (<398nm) \text{ ----------> } O + NO \quad (1.1)$$

$$NO + VOC \text{ ----------> } NO_2 + H_2O + C_x \quad (1.2)$$

$$O + O_2 \text{ ----------> } O_3 \quad (1.3)$$

In this region, the presence of ozone is undesirable due to the greenhouse effect and the role of ozone in formation of photochemical smog.

2) In the stratosphere region (which extends up to 31 miles), the VOC are absent as a result of which nitric oxide (NO) can react with O_3 according to:

$$NO + O_3 \text{ ----------> } NO_2 + O_2 \quad (1.4)$$

Without VOC, a NO_2-NO-O_3 steady state is reached (4,5). The presence of O_3 is desirable in this region because O_3 shields the earth from a large percentage of UV radiation which is a major cause of skin cancer in humans.

3) NO_x can also act as a primary acid precipitation precursor. Acid precipitation is composed mainly of dilute sulfuric acid and nitric acid. Nitric acid is formed by the gas phase oxidation of NO_2 according to :

$$NO_2 + OH \text{ ----------> } HNO_3 \quad (1.5)$$

4) Another major concern over NO_x emissions is related to the greenhouse effect. Nitrous oxide (N_2O) is an infrared absorbing gas along with other greenhouse gases like carbon dioxide, water vapor, methane and chloroflouro carbons (5).

NO_x emissions can be controlled through combustion measures and post combustion clean-up of flue gas. Combustion measures include atmospheric and pressurized fluidized bed combustion; air and fuel staging in the furnace; and low NO_x burners. These measures are outlined in the next chapter. Post combustion clean-up techniques include selective non-catalytic reduction (SNCR) and selective catalytic reduction (SCR). These techniques are also discussed in detail in the next chapter.

During SCR, NO_x (consisting of NO and NO_2) is catalytically reduced to nitrogen (N_2) with a reducing gas, the most common being ammonia (NH_3). The reactions are:

$$4NO + 4NH_3 + O_2 \text{ ----------> } 4N_2 + 6H_2O \quad (1.6)$$

$$2NO_2 + 4NH_3 + O_2 \text{ ----------> } 3N_2 + 6H_2O \quad (1.7)$$

Oxygen is shown in the above reactions because of its presence in the flue gas. This technique is called selective because otherwise NH_3 could also react with oxygen in flue gas and and contribute towards NO_x formation:

$$4NH_3 + 5O_2 \text{ ----------> } 4NO + 6H_2 \qquad (1.8)$$

Extensive operating experience has been gained with SCR in Japan and Germany for NO_x control. Efficiencies of 80-90% for NO_x removal have been achieved with this technique. To date, the most successful catalysts have been inorganic oxides or noble metals on different supports, such as vanadia/titania, iron oxide/alumina, platinum/alumina and palladium/alumina (2). The optimum temperature for SCR using these catalysts is between 350-450^oC. Due to this temperature limitation, the location of catalyst bed is restricted. If the catalyst bed is placed at the front of the pollution control train before the electrostatic precipitator and the SO_x scrubber, as shown in Figure 1.1, the flue gas temperature would be within the desired range for NO_x reduction but the catalyst life could be reduced because of high concentrations of particulates and catalyst poisons like arsenic compounds (2). If the catalyst bed is placed after the clean-up equipment, the catalyst life is improved but since the flue gas temperature is reduced by the gas clean-up equipment, an additional source of heating is required to reheat the flue gas to the desired temperature. To reheat the flue gas by 50^oC requires energy equivalent to about 2-3% of boiler capacity (6). A solution to this problem is to use a catalyst which would permit the NO_x decomposition to be carried out at lower temperatures.

ARTHUR LAKES LIBRARY
COLORADO SCHOOL OF MINES
GOLDEN, CO 80401

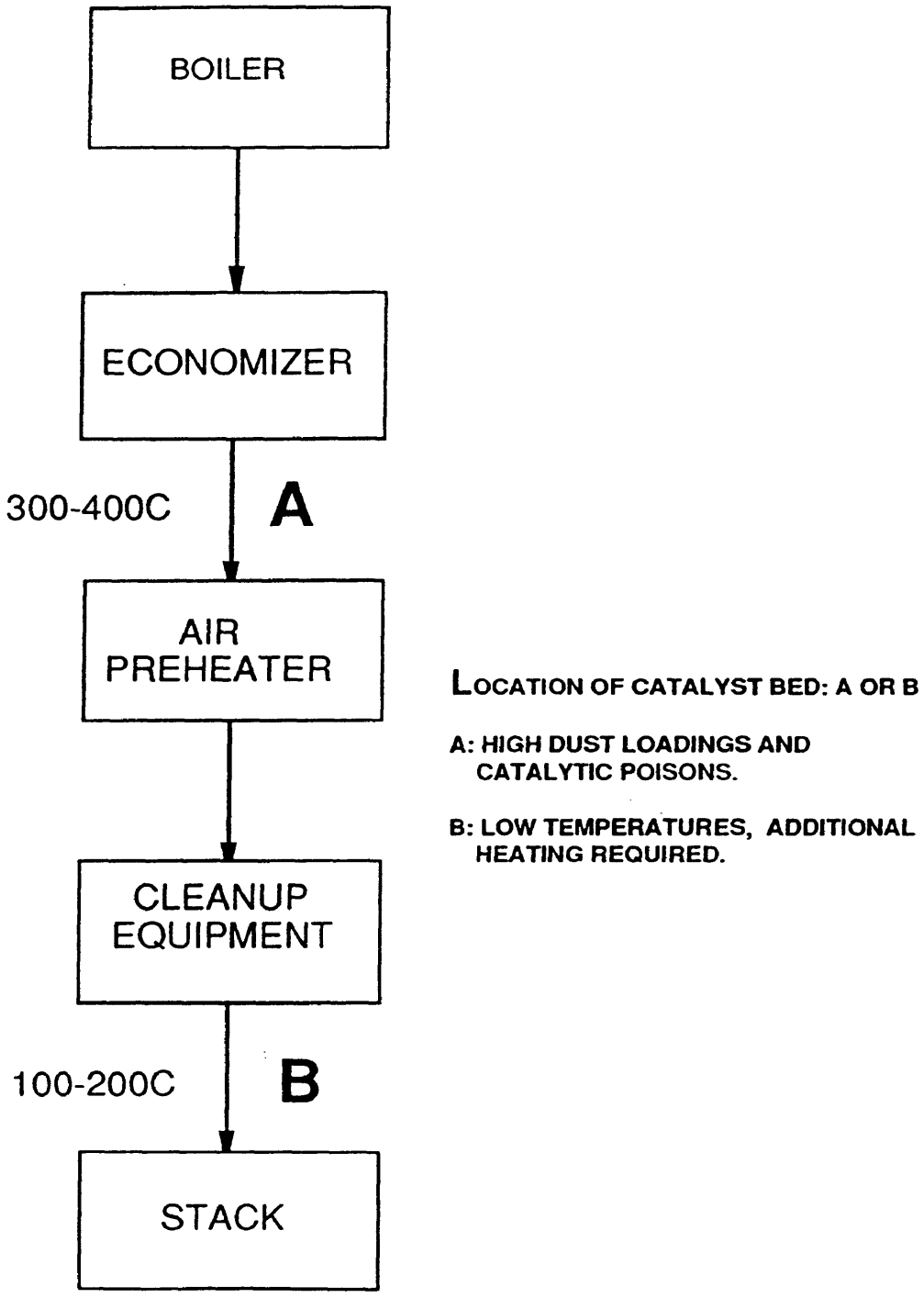

Figure 1.1 Flue gas train (coal fired power plants)

1.1 Objectives

The main objectives of this research were:

1) To determine if activated carbons could be used as catalysts for NO reduction at lower temperatures in an environment similar to that of flue gas generated from coal-fired power plants
2) To elucidate the characteristics that influence the activity of activated carbons for SCR of NO .

1.2 Experimental approach

The first step in this research was to determine if commercial activated carbons could be used for SCR of NO using NH_3 as the reducing gas and to investigate the characteristics of activated carbons that are important for this purpose. The results from this study are presented in Chapter 3.

The second step was to determine the effect of space velocity on the activated carbon activity. Space velocity is a very important parameter in determining the efficiency of catalyst. During the initial phase of this research it was found that oxygen plays an important role in NO decomposition and this was also investigated thoroughly. Also in this phase, the activity of activated carbon was compared with a commonly used commercial catalyst (vanadia/titania). These results are presented in Chapter 4.

Based on the results obtained from preliminary studies, the surface of commercial activated carbon was modified by an acid treatment (sulfuric acid). The effect of this treatment on activated carbon's activity was then investigated and these results are presented in Chapter 5.

In the last phase of the research, in-house activated carbons synthesized by chemical activation were used to study NO reduction. These results are presented in Chapter 6.

Chapter 2

GENERAL BACKGROUND

Nitrogen oxides are formed during combustion in the presence of oxygen. The main oxides are NO and NO_2 with NO contributing more than 90% of the total NO_x for most combustion processes (7). Other minor oxides formed during combustion are nitrous oxide (N_2O), dinitrogen trioxide (N_2O_3), dinitrogen tetraoxide (N_2O_4) and dinitrogen pentoxide (N_2O_5). NO is oxidized rapidly to NO_2 at room temperature but is stable at higher temperatures.

2.1 Formation of nitric oxide

There are three ways in which NO can be formed during combustion as discussed below :

2.1.1 Thermal nitric oxide

At combustion temperatures in excess of 1300^oC, oxygen (O_2) in combustion air is broken down to oxygen atoms which can then react with N_2 in air to form NO. This is also called Zel'dovich's mechanism (7):

$$O_2 \text{ ----------> } O + O \quad (2.1)$$

$$O + N_2 \text{ ----------> } NO + N \quad (2.2)$$

$$N + O_2 \text{ ----------> } NO + O \quad (2.3)$$

2.1.2 Prompt nitric oxide

As defined by Fenimore (7, 8), prompt NO is formed by a process in which NO is formed via solid intermediate products from fuel or air nitrogen in an early phase in the flame front with hydrocarbons participating:

$$CN + H_2 \text{ ----------> } HCN + H \quad (2.4)$$

$$CH + N_2 \text{ ----------> } HCN + N \quad (2.5)$$

The HCN eventually produces NO in the presence of O_2. The contribution by this pathway is very negligible.

2.1.3 Fuel nitric oxide

NO can also formed by oxidation of nitrogen-containing species in the fuel. The exact reaction mechanism is not fully known. The nitrogen content in coal varies between 0.5% and 2.0%. Heavy oil contains about 0.5%,while light oil and natural gas contain virtually nc organic nitrogen (7). Combustion tests of volatile nitrogenous compounds, and of devolatized char suggest that both volatile and nonvolatile nitrogenous constituents of the coal can contribute to NO formation by gas phase oxidation of devolatized fuel nitrogen and

heterogeneous oxidation of char nitrogen in the flame tail (8). A simplified scheme for NO_X formation from coal combustion is shown in Figure 2.1.

2.2 Combustion measures

NO_X formation can be reduced by either alternative combustion measures or post combustion control.

2.2.1 Fluidized bed combustion

This technology has emerged in the past decade. As the name implies, fluidized bed combustion (FBC) processes uses a fluidized bed for the coal combustion reactor with air acting as the fluidizing medium. Coal is usually present as a finely divided solid (1.5-3 mm diameter) in the combustion reactor. Either limestone (calcium carbonate) or dolomite (calcium magnesium carbonate), both of which occur widely, is also present in the combustion reactor. There are several advantages of FBC over pulverized and other conventional firing systems. In terms of NO_X, the primary advantage is related to lower operating temperatures. FBC operating temperatures are usually around 750-900^{o}C, whereas in a conventional pulverized firing system, the operating temperatures are normally in excess of 1500^{o}C. This is primarily due to the difference in the heat transfer coefficients between the bed and internal boiler tubes. In FBC, the particle convective component is responsible for a characteristic marked increase in the bed-to-surface heat transfer coefficient thus permitting operation at lower temperatures with no net reduction in the rate of heat transfer. As a result of lower operating temperatures, the formation of

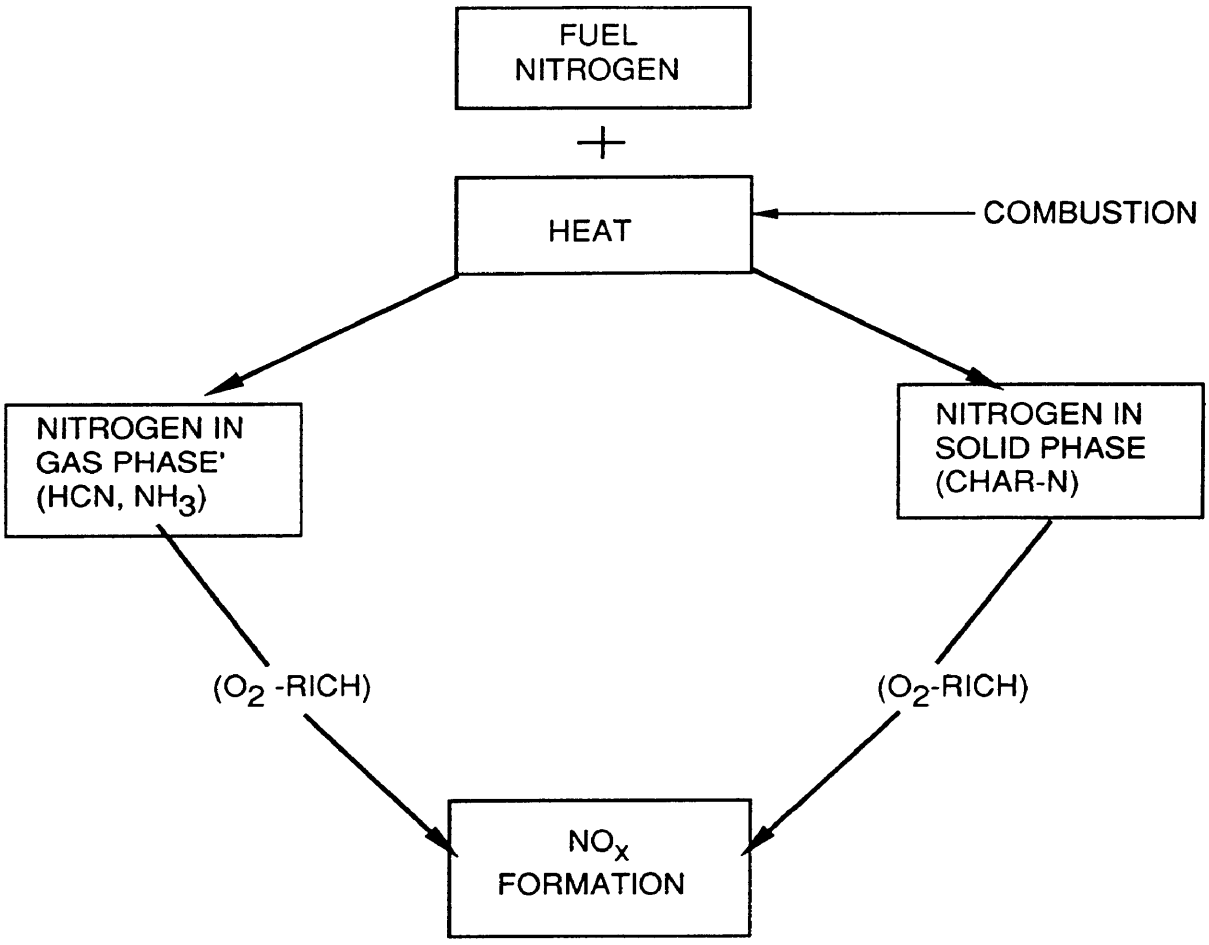

Figure 2.1 Conversion of fuel-N to NOx during coal combustion (9)

thermal NO_x is decreased. Fuel NO_x is also reduced, although to a lesser extend. Thermal NO_x however, contributes to less than 10% of the total NO_x emissions from FBC (7).

FBC includes atmospheric fluidized bed combustion (AFBC) and pressurized fluidized bed combustion (PFBC). The largest AFBC plant is a commercial unit operating at Paducah, Kentucky and has a capacity of 160 MW. The largest PFBC plant is a demonstration unit in Tidd, Ohio with a capacity of 80 MW.

2.2.2 Air staging

Excess combustion air can be reduced, resulting in a decrease in NO_x formation without causing problems such as unstable combustion, corrosion and increased unburnt carbon in fly ash. This reduction can be achieved by air staging. The air is either staged in the furnace or in the burner. Normally 10-20% of the total combustion air can be used for air staging.

2.2.3 Fuel staging

The aim of fuel staging is to reduce the already formed NO_x back to N_2 by creating a reducing environment in the furnace. A major portion of fuel, mainly coal, is burnt under an oxidizing atmosphere in the primary zone thus producing NO_x. Another small portion of fuel is burnt in the secondary zone in a reducing environment. This facilitates the formation of hydrocarbon radicals and carbon monoxide. These gases can then reduce the NO_x formed in the primary zone.

2.2.4 Fuel type

Coal-bound organic nitrogen occurs in aromatic ring structures such as pyridine, picoline, quinoline and nicotines (10). As stated earlier, the nitrogen content in coal can vary from 0.5 to 2.0%. Thus by selecting a fuel with low nitrogen content, the formation of NO_X could be greatly reduced. In general, NO_X emissions from low volatile coals, especially anthracites, are higher compared to emissions from high volatile coals. In Germany, plants using brown coal (lignite) were found to produce fewer NO_X emissions (11). The lower NO_X production was due to low nitrogen and high water content in these coals. The high water content decreased the flame temperature, which resulted in low thermal NO_X production.

2.2.5 Flue gas recirculation

Recirculation of flue gas is also used to decrease the flame temperature, thus resulting in lower NO_X formation. This technique reduces thermal NO_X formation but has little effect on NO_X formed from fuel-nitrogen.

2.3 Selective non-catalytic reduction

Combustion modifications are generally limited to 20-50% NO_X reduction. In addition to the combustion modifications discussed previously, there are various SNCR processes available, in which the NO-reduction is caused by the reaction with N-H or C-H based chemicals. SNCR is an attractive method as it does not require the use of a catalyst. However, this method gives lower NO_X reduction than SCR and requires a higher consumption of chemicals (12). The

most commonly used chemicals are urea ($CO(NH_2)_2$) and NH_3. The method of injection of these chemicals into the furnace is very crucial to the success of SNCR technologies. The key is to find the right injection point, where the temperature is optimum, and a maximum mixing can occur between the chemicals and NO_x. The optimum temperature for urea to react with NO_x is between 1000-1150^oC. The overall reaction scheme is (13):

$$\text{Urea} \text{ ----------> } NH_2 + NCO \quad (2.6)$$

$$NH_2 + NO \text{ ----------> } N_2 + H_2O \quad (2.7)$$

$$NCO + NO \text{ ----------> } N_2 + CO_2 \quad (2.8)$$

Urea works well in this temperature range, but at low temperatures use of urea results in lower reduction of NO and formation of secondary products such as NH_3 which can create problems at down-stream equipment. The efficiency of urea can be enhanced by addition of oxygenated hydrocarbons such as alcohols, and organic acids.

If NH_3 is used as a chemical, similar problems can be created at down-stream equipment by NH_3 slip. The optimum reaction temperature for NH_3 is between 950-1050^oC. In a test plant in Denmark, there have been problems concerning ammonia slip of as much as 12 ppm. Also in Germany, in one test plant, NH_3 slip over 10 ppm gave rise to extensive deposits on the air preheater when the wall temperature was below 280^oC (14). Another limitation on this process is that the temperature window over which these reagents are

effective is relatively narrow. SNCR processes in general are capable of 30-50% NO_x reduction (14).

Brian et al. (15) investigated the reaction of cyanuric acid $(HNCO)_3$ with NO:

$$2(HNCO)_3 + 9NO \text{ ---------> } 3H_2O + 7.5N_2 + 6CO_2 \qquad (2.9)$$

At 700°C, no NO reduction occurred when a quartz flow tube was used, whereas NO was efficiently reduced when an otherwise equivalent stainless-steel flow system was used.

Chen et al. (16) investigated the effectiveness of using selective reducing agents such as ammonium sulfate in combination with combustion modifications including staged combustion and fuel reburning using Indiana and Utah coal. Significant reductions in NO emissions were observed which could only be achieved by catalytic reduction which is discussed in the next section.

2.4 Selective catalytic reduction

The abatement of NO_x through combustion measures is less costly than that based on flue gas treatment (SCR) due to lower operating costs (see Table 2.1) (17). Due to new stringent NO_x regulations however, flue gas treatment is becoming inevitable. SCR has been found to be the most efficient way of reducing NO_x emissions of the various procedures. Plants are currently in operation where the NO_x emissions are reduced by more than 80-90%. The SCR technology was initially developed in Japan, where the first installation

Table 2.1 Comparison of NO_x removal technologies (17)

	Combustion Modifications	Over-Fire Air	Reburning	SNCR	SCR
NO_x Removal	10-30	15-30	40-60	30-70	60-90
Capital Costs ($/KW)	<1	5-10	35-45	10-20	75-150
Operating Costs (mill/KWh)	<1	<1	1-6	1-4	5-9

on a coal-fired unit started operating in 1980 (18). The first operation in Europe began in 1985. Application of SCR technology is relatively new in the United States. The testing of pilot scale plants is now underway in this country. The first SCR coal plant with a capacity of 140 MW is being built in New Jersey by Foster Wheeler and is expected to be in operation by mid 1993. It is estimated that the general cost of SCR for this plant will be between $2000-$4000 per ton of NO_x removed (17).

According to one source, by the end of 1990 FRG had the largest number of SCR installations (129 plants, 28,151 MWe), while Japan had 37 installations amounting to 9467 MWe (18).

During SCR, NO_x is catalytically reduced to N_2 by a reducing gas, the most common being NH_3. The reactions are:

$$4NO + 4NH_3 + O_2 \xrightarrow[\text{catalyst}]{} 4N_2 + 6H_2O \quad (2.10)$$

$$2NO_2 + 4NH_3 + O_2 \xrightarrow[\text{catalyst}]{} 3N_2 + 6H_2O \quad (2.11)$$

$$6NO + 4NH_3 \xrightarrow[\text{catalyst}]{} 5N_2 + 6H_2O \quad (2.12)$$

$$6NO_2 + 8NH_3 \xrightarrow[\text{catalyst}]{} 7N_2 + 12H_2O \quad (2.13)$$

SCR of NO_x proceeds via the first two reactions when oxygen is present, which is always the case for flue gas. This technique is called selective because

otherwise NH_3 could also react with O_2 in flue gas and contribute towards NO_x formation by the following reaction:

$$4NH_3 + 5O_2 \text{ ----------> } 4NO + 6H_2O \qquad (2.14)$$

At the same time, special consideration has to be given to the fact that the unreacted NH_3 can react with SO_x in the presence of water to form ammonium sulfate salts. This unwanted product can be responsible for corrosion and fouling of downstream equipment in the flue gas train.

The three very important characteristics of a potential SCR catalyst to be considered are its activity (function of temperature and space velocity), selectivity and life time. The most common catalysts used are noble metals, inorganic oxides and zeolites on different supports, as shown in Table 2.2.

2.4.1 Noble metals

The noble metal catalysts are intrinsically more active than metal oxides, but are less selective and are susceptible to poisoning by SO_x (2). Hence these catalysts are not used for coal or oil fired utilities, but are suited for gas turbines and automotive emissions, where SO_x concentrations are negligible. The optimum temperature for these catalysts is between 300-350^oC. The space velocity is a very crucial design parameter in a SCR system. For a gas turbine system, very high space velocities (about 60,000 hr^{-1}, STP) could be used for noble metal catalysts. The common structure for noble metal catalyst is a monolith format in which a corrugated metal sheet is coated with a thin layer of

Table 2.2 Catalysts for selective catalytic reduction (2)

Catalyst Type	key Components	Year
Noble Metal	Pt, Pd, Ru/Al_2O_3	1959
Metal Oxide	Fe_2O_3/Cr_2O_3	1965
Metal Oxide	$V_2O_5/MoO_3/WO_3/Al_2O_3$	1966
Metal Oxide	V_2O_5/TiO_2	1973
Metal Oxide	$V_2O_5/MoO_3/WO_3/TiO_2$	1973
Zeolite	Synthetic modernite	1978
Metal Oxide	$V_2O_5/TiO_2/SiO_2$	1989

an oxide support impregnated with noble metals. The advantage of this structure is its low pressure drop (2).

The reduction of NO to N_2 using noble metal catalysts with either NH_3 or carbon monoxide (CO) has been studied very extensively. The presence of O_2 seemed to have a positive influence on the rate of reduction over platinum (Pt), using NH_3 (19). Bauerle and Nobe (20) also found that the presence of O_2 increased the reduction of NO on Pt and palladium (Pd), but it decreased the reduction on ruthenium (Ru) and rhodium (Rh) in the presence of NH_3. In case of Pt, the maximum reduction occurred with 2% of O_2 present at 300°C. In the presence of O_2, considerable amounts of N_2O were also formed on Pt and Pd. This was accounted by NH_3-O_2 reaction shown below:

$$NH_3(g) + O_2 \text{ <====> } HNO(ads) + H_2O(g) \quad (2.15)$$

$$2HNO(ads) \text{ <=====> } N_2O(ads) + H_2O(ads) \quad (2.16)$$

NO can either be reduced directly or indirectly (through N_2O formation) by CO as shown (21):

$$CO + NO \text{ ----------> } CO_2 + 1/2N_2 \quad (2.17)$$

or

$$CO + 2NO \text{ ----------> } CO_2 + N_2O \quad (2.18)$$

$$CO + N_2O \text{ ----------> } CO_2 + N_2 \quad (2.19)$$

The SCR of NO using CO over polycrystalline Pt, Pd, and Rh was investigated by Hahn and Lintz (21,22) in the presence of O_2. NO was selectively reduced over Pt and Rh at low temperatures (300°C). At higher temperatures, the selectivity was decreased. At around 600°C, CO was completely oxidized by O_2 to CO_2 before it could reduce NO. Pd was found to be completely unsuitable for SCR of NO under any conditions.

Transient kinetics studies of the catalytic reduction of NO by CO on Pt showed that the main reaction proceeds over a wide range of reaction conditions via a dissociative mechanism as shown below (23):

$$CO(g) + S \leftrightarrows CO{\cdot}S \quad (2.20)$$

$$NO(g) + S \leftrightarrows NO{\cdot}S \quad (2.21)$$

$$NO{\cdot}S + S \leftrightarrows N{\cdot}S + O{\cdot}S \quad (2.22)$$

$$CO{\cdot}S + O{\cdot}S \leftrightarrows CO_2(g) + 2S \quad (2.23)$$

$$2N{\cdot}S \leftrightarrows N_2(g) + 2S \quad (2.24)$$

S in the above reactions represents an active site.

Ravindranathan et al. (24) studied the reaction of CO with NO over TiO_2-supported Ru and Rh. The reaction products for Ru were CO_2, N_2O and N_2. N_2O was formed by the following reaction:

$$NO(g) + S \leftrightarrows NO{\cdot}S \quad (2.25)$$

$$NO{\cdot}S + S \leftrightarrows N{\cdot}S + O{\cdot}S \quad (2.26)$$

$$NO{\cdot}S + N{\cdot}S \leftrightarrows N_2O{\cdot}S \quad (2.27)$$

$$N_2O{\cdot}S \quad <=======> \quad N_2O(g) \quad + \quad S \qquad (2.28)$$

On illumination with energy (< 390 nm), the rate of decomposition of N_2O to N_2 was increased significantly. Addition of Rh seemed to have a similar effect for N_2O decomposition. Eickel and Oh (25,26,27) showed that the addition of ceria (CeO_2) to Rh/Al_2O_3 can enhance the rate of NO reduction by CO. This was further confirmed by Cho (25), who studied this reaction using only Rh/CeO_2 at temperatures around 500°C. Iridium (Ir) is another member of the noble metals family which has been used for a NO-CO reaction. A conversion of 90 % was obtained over Ir/Al_2O_3 containing either 0.1 or 0.001% Ir (28), although the author of this particular source did not provide the temperature at which these studies were performed.

2.4.2 Zeolites

A zeolite is a porous crystalline solid with a well defined pore structure and large surface area consisting mainly of aluminum silicates. Zeolites can either be used in granular form or as monolithic layers. The use of zeolites for SCR was developed in Germany and are currently used in three SCR plants in Germany (6). Copper (CU)-exchanged zeolites have been studied for NO reduction by NH_3. Mizumoto et al. (29) investigated the mechanism of NO reduction by NH_3 over Cu(II) Y-type zeolites (Cu(II) NaY) by examining kinetic and isotopic studies. The rate of this reaction showed dependence on the partial pressures of both NO and NH_3, in accordance with Langmuir-Hinshelwood (LH) type rate equation:

$$r_{N_2} = \frac{k K_{NO} K_{NH_3} p_{NO} p_{NH_3}}{(1+K_{NH_3} p_{NH_3})^2} \qquad [2.1]$$

NH_3 was found to be very strongly adsorbed on the surface.

Cu-exchanged zeolites have also been investigated as catalysts for NO decomposition with and without O_2 (30). Cu-ZSM-5 was found to have the highest turnover frequency among zeolites. The activity of this catalyst levelled off around 500°C. The NO decomposition was inhibited by the presence of O_2 due to the formation of NO_2. Based on these results, the rate equation for NO decomposition in L.H. form was found to be as:

$$r_{N_2} = \frac{k p_{NO}}{1+ K_{O_2} p_{O_2}^{1/2}} \qquad [2.2]$$

The decomposition of NO was further studied using temperature programmed desorption (TPD)(31). Cu sites were found to be responsible for the the decomposition of NO, as NO did not decompose either on a parent zeolite or sodium exchanged zeolite ((Na)-ZSM-5). NO apparently decomposed to N_2O and NO_2, with further N_2O decomposition to N_2 and an oxygen atom.

Propane and propene have also been used as reductants over zeolites for NO reduction. The catalytic activity of Cu-exchanged zeolites for NO decomposition completely disappeared in the presence of SO_2, but the catalytic activity for NO reduction by propene was not affected by the presence of SO_2. The presence of O_2 also had a tremendous effect of the reduction with propene. Without O_2, the catalytic activity was almost zero (32).

A comparison of H-ZSM-5 (prepared by ion exchanging ZSM-5 with ammonium nitrate solution), H-mordenite (prepared by the same ion exchange method from commercial Na modernite), Na-ZSM-5, and silica gel showed that H-ZSM-5 and H-modernite had the highest activity of all the catalysts. Based on this finding, the active centers for SCR of NO using zeolites were assigned to the acid sites (33).

Fe-Y zeolites and Fe-modernite have also been used as catalysts for NO reduction in the temperature range of 350-700^{o}C (34). Zeolites have also been used as supports for noble metals. Four metal containing Na-Y zeolites(Pt, Pt_2Rh, $PtRh_2$, and Rh) were compared for NO reduction by CO. Bimetallic catalysts were found to have better activity than monometallic catalysts (35).

2.4.3 Metal oxides

Amongst metal oxides, vanadia (V_2O_5) on different supports (Al_2O_3, TiO_2 and SiO_2) is one of the most commonly used catalysts because of its very high activity for NO_x reduction. Other metal oxides that have been also studied for NO_x reduction include iron oxides (Fe_2O_3) and chromia (Cr_2O_3).

2.4.3.1 Vanadia

A great deal of research had been and is still being carried out on the use of V_2O_5 for NO_x reduction. V_2O_5 is not susceptible to SO_2 poisoning but due to its very high activity, it can oxidize SO_2 to SO_3 which can react with NH_3 to form ammonium sulfates and ammonium bisulfates thus creating problems at down-stream equipment.

The mechanism of NO reduction over V_2O_5 is not yet fully understood in terms of the role of NO and NH_3. Earlier work by Takagi and his co-workers (36,37) suggested that the NO-NH_3 reaction in the presence of O_2 over bulk V_2O_5 and V_2O_5/Al_2O_3 proceeds via the two adsorbates, NO_2 (ads) and NH_4^+(ads). Using FT-IR, they found that NO adsorbs as NO_2 on an oxidized or reduced surface of these catalysts but only in the presence of either O_2 or NO_2. In the absence of O_2, NO still adsorbed as NO_2 but only on active surface oxygen. The surface reaction followed the LH mechanism. O_2 was found to be necessary for substantial NO reduction,and this observation has been also confirmed by other workers (37).

Miyamoto et al. (38) did not agree with this mechanism. Their argument was that the conditions used by Takagi et al. (37) (reaction temperature roughly about room temperature, high NO and NH_3 concentrations of about 10,000 ppm) cannot occur in the actual SCR process. They proposed a dual site Eley-Rideal mechanism based on dilute gas conditions (see Figure 2.2):

1) NO does not adsorb on the catalyst surface either by homogeneous or catalytic oxidation of NO to NO_2.
2) NH_3 is strongly adsorbed adjacent to $V^{+5}=O$ as NH_4^+.
3) NH_4^+ adsorbed on the surface can react with gaseous NO to form N_2 at higher temperatures and also results in the formation of V-OH which is then oxidized by O_2 to $V^{+5}=O$.

TPD, TPR (temperature programmed reduction) and in-situ IR measurements conducted by Srnak et al. (39) showed that the adsorption of NH_3 on Lewis acid

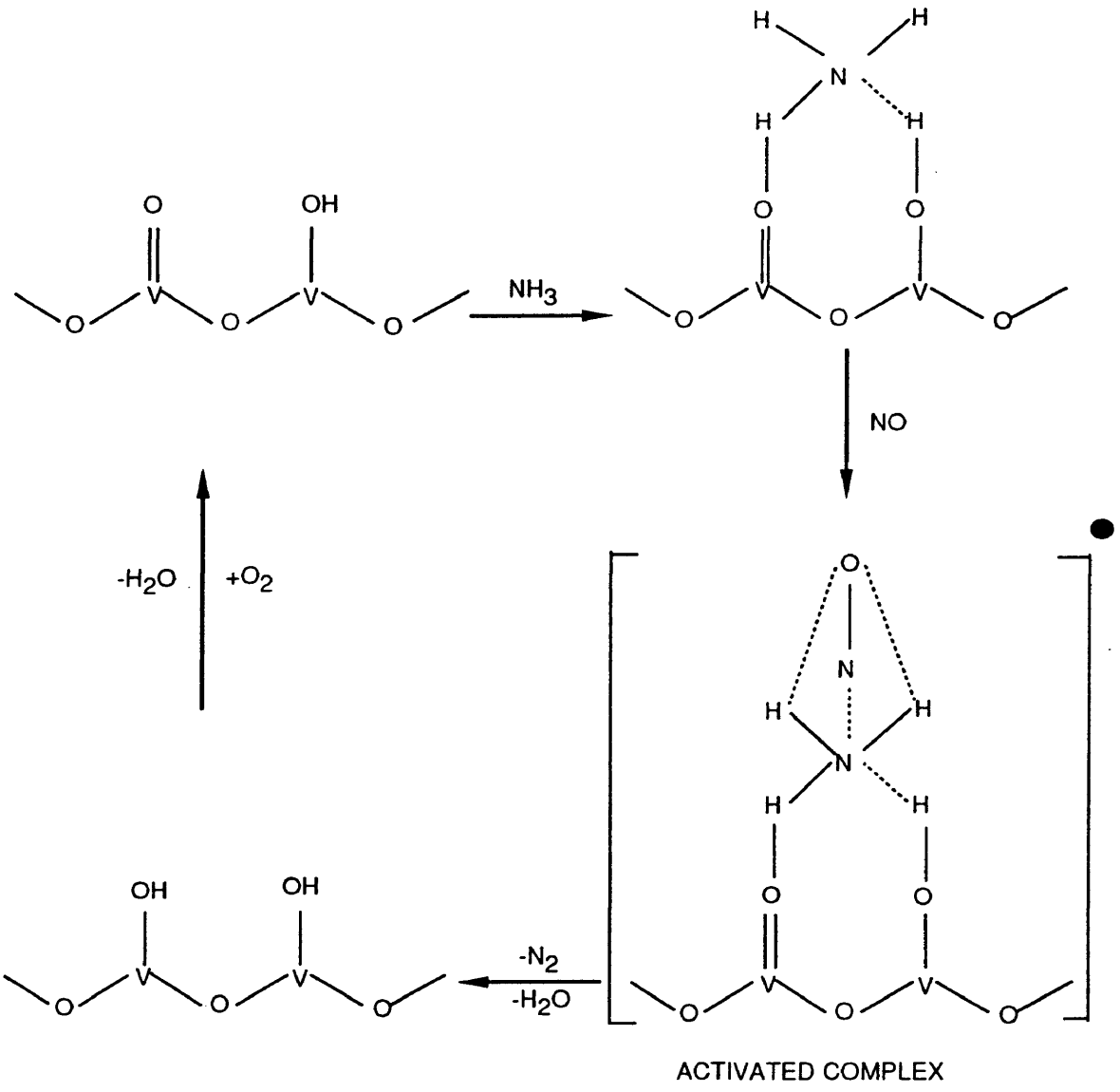

Figure 2.2 The mechanism of the NO-NH3 reaction on V_2O_5 (38)

sites was stronger than on Brönsted sites. NO did not adsorb in significant amounts on V_2O_5/TiO_2 under SCR conditions.

Odriozola et al. (40,41) studied the adsorption of NH_3 and NO on pure V_2O_5 and V_2O_5 supported on TiO_2, by Auger electron and temperature desorption spectroscopy using a ultra-high vacuum chamber. They proposed that the adsorption of NH_3 takes place mainly on vanadium causing the reduction of the original V^{+5} species and that the adsorption of NO takes place either on the reduced V_2O_5 or TiO_2. Oxidized V_2O_5 did not adsorb NO. The reduction of NO occurred through the migration of adsorbed species from the support to the vanadium sites. These results seemed to contradict Miyamoto's findings, who concluded that the reduction of V^{+5} to V^{+4} (in form of V-OH) was due to the reaction of adsorbed NH_3 with gaseous NO.

Recently Giandguido et al. (42) proposed a new mechanism based on measurements made using FT-IR to study the adsorption of NO and NH_3:

$$VO^{+2} + NH_3 \Longleftrightarrow [HO\text{-}V\text{-}NH_2]^{+2} \quad (2.29)$$

$$NO + [HO\text{-}V\text{-}NH_2]^{+2} \Longleftrightarrow [HO\text{-}V\text{-}NH_2\text{-}NO]^{+2} \quad (2.30)$$

$$[HO\text{-}V\text{-}NH_2\text{-}NO]^{+2} \Longleftrightarrow N_2 + H_2O + [V\text{-}OH]^{+2} \quad (2.31)$$

$$[VOH]^{+2} + 1/4O_2 \Longleftrightarrow VO^{2+} + 1/2H_2O \quad (2.32)$$

$$NH_3 + NO + 1/4O_2 \longrightarrow N_2 + 3/2H_2O \quad (2.33)$$

The first reaction step was breaking an N-H bond of molecularly coordinated ammonia. The results from these studies do not agree with the Odriozola et al.

(40,41) findings, which proposed spillover of the adsorbed NO species from the support to vanadium sites. It is clear that any of these different mechanisms could contribute to the main reaction to some extent depending on the reaction conditions.

Incorporation of SiO_2 into TiO_2 as a support has also been used to increase the overall activity of the catalyst compared to a single support. According to Rajadhyyaksho et al. (43), the catalytic activity of V_2O_5 supported on $TiO_2/SiO2$ was significantly greater than that of V_2O_5/SiO_2. The activity improved with increasing TiO_2 loadings. Bjorklund et al. (44) compared V_2O_5/TiO_2-SiO_2 samples with various V_2O_5 loadings ranging from 2-30 wt%. Characterization of these catalyst with FT-IR and XRD showed that V_2O_5 was highly dispersed on the support as an amorphous phase for catalysts with less than 20% loading. The sample with 10% loading showed the highest activity around 350°C. Studies by Handy et al. (45) have shown V_2O_5 to be less active and stable on amorphous supports compared to crystalline supports. The high activity of V_2O_5/TiO_2-SiO_2 results from high dispersion of V_2O_5 on TiO_2 which is in a partly crystalline form of anatase and possibly rutile.

The presence of water did not seem to affect the activity of V_2O_5/TiO_2 for SCR. Adsorption of water on the catalyst surface was weak compared to the adsorption of NH_3 (46).

A major concern on practical applications of SCR has been the deactivation of the catalyst. As stated earlier, one of the advantages of V_2O_5 over noble metals is its resistance towards SO_2 poisoning (provided it does not form ammonium salts by reacting with NH_3) in the flue gas. Unfortunately, there are

other chemical poisons, along with fly ash and dust, which are present in the flue gas that can affect the catalyst performance (6). Such poisons include alkali ions (Na, K, Ca and Mg). Gaseous arsenic has also been implicated as catalyst poison (2). Kasoaka et al. (47,48) found that, in the absence of SO_2, the severity of poisoning follows this order: KCl > NaCl > K_2SO_4 > Na_2SO_4. The poisoning effects disappeared in the presence of SO_2. According to Chen and Yang (48), Brönsted acid sites are the active sites of V_2O_5/TiO_2 for the reaction. Alkali metals poison the catalyst site by decreasing its Brönsted acidity, whereas SO_2 promotes the activity by increasing the Brönsted acidity. The presence of phosphorous not only poisons the active sites by forming phosphates, but it also blocks the pore structure of the catalyst. The negative effects of phosphorous on V_2O_5/TiO_2 have also been reported by Blanco et al. (49). In the presence of NH_3, acidic components such as SO_2 and HCl can also deactivate the catalyst by forming ammonium salts. The deactivating effect of SO_2 on the reaction rate of NO reduction with NH_3, using V_2O_5/Al_2O_3, was also investigated by Eldrige and Kittrell (50). SO_2 exposure to the catalyst seemed to effect the surface area and the pore size distribution, which was related to deactivating agents, ammonium sulfate and aluminium sulfate. However, the deactivated catalyst was completely regenerated by heat treatment around 500°C.

2.4.4 Iron oxide and chromia

Iron oxide catalyst is known to have a good activity for NO reduction. The optimum temperature for this catalyst is reported to be between 380-430°C (6).

A substantially greater amount of catalyst is needed compared to other conventional catalysts. The effect of support was also found to be very important, in that the activity per gram of Fe_2O_3/SiO_2 at 300°C was twenty times that of Fe_2O_3/SiO_2-TiO_2 although the difference in the surface area was only a factor of two (19). Fe_2O_3 has also been used in conjunction with Cr_2O_3. Willey et al. (51) investigated the mechanism of NO reduction by NH_3 over Fe_2O_3/Cr_2O_3; NO adsorption conformed to Freundlich isotherm, NH_3 was dissociatively adsorbed, and O_2 was needed to regenerate the active sites.

Amorphous Cr_2O_3 with high surface area has been found to be a highly active and selective catalyst for NO reduction by NH_3 at low temperatures (150°C) in the presence of O_2(52). Over 90 % conversion was achieved by this catalyst at a space velocity of 24,000 hr^{-1} with 2 % O_2. As compared to amorphous Cr_2O_3, crystalline Cr_2O_3 did not show such high activity. This could be explained in terms of the inherently high surface area of amorphous Cr_2O_3, however, there was a deactivation of the amorphous catalyst after a certain time period. The deactivation was not due to a change in a morphology of the catalyst according to X ray diffraction results. Further investigation showed that amorphous chromia had a higher coverage of labile oxygen species on the surface than did the crystalline chromia (53,54,55).

2.5 Activated carbon

Activated carbon is a generic term for a broad range of amorphous carbon-based materials which are very porous and have extended intraparticulate surface area. Commercially prepared activated carbons generally have a

specific surface area of 800-1500 m^2/g, contained predominantly within micropores (diameter less than 2 nm). By IUPAC classification, the pores are classified as following:

Micropores: Dp < 2 nm

Mesopores: 2 < Dp < 50 nm

Macropores: Dp > 50 nm

These materials may be either in granular or powder form. The granular form is characterized by a large surface area and small pores, whereas the finely divided powdered form is characterized by a low internal surface area and large pores (56). The elemental composition of activated carbon typically is comprised of 87.0% C, 0.5% H, 0.5% N , 1.0 % S and 5.0% O (57).

2.5.1 Manufacturing

Any material with a high carbon and low inorganic content can be used as a precursor for activated carbon. Low-ash content is essential to keep the ash content low in the final product. Commonly used precursors include wood, coconut shell, peat and low rank coal, although the bulk of activated carbon is produced from coconut shell and coal-based material. The type of precursor used affects the properties of the final product in terms of pore size distribution and texture (see Figure 2.3 and Table 2.3), which in turn often determines the application of the final product (56). Most commercial activated carbons are either prepared by physical activation (carbonization followed by activation) or chemical activation (carbonization and activation together).

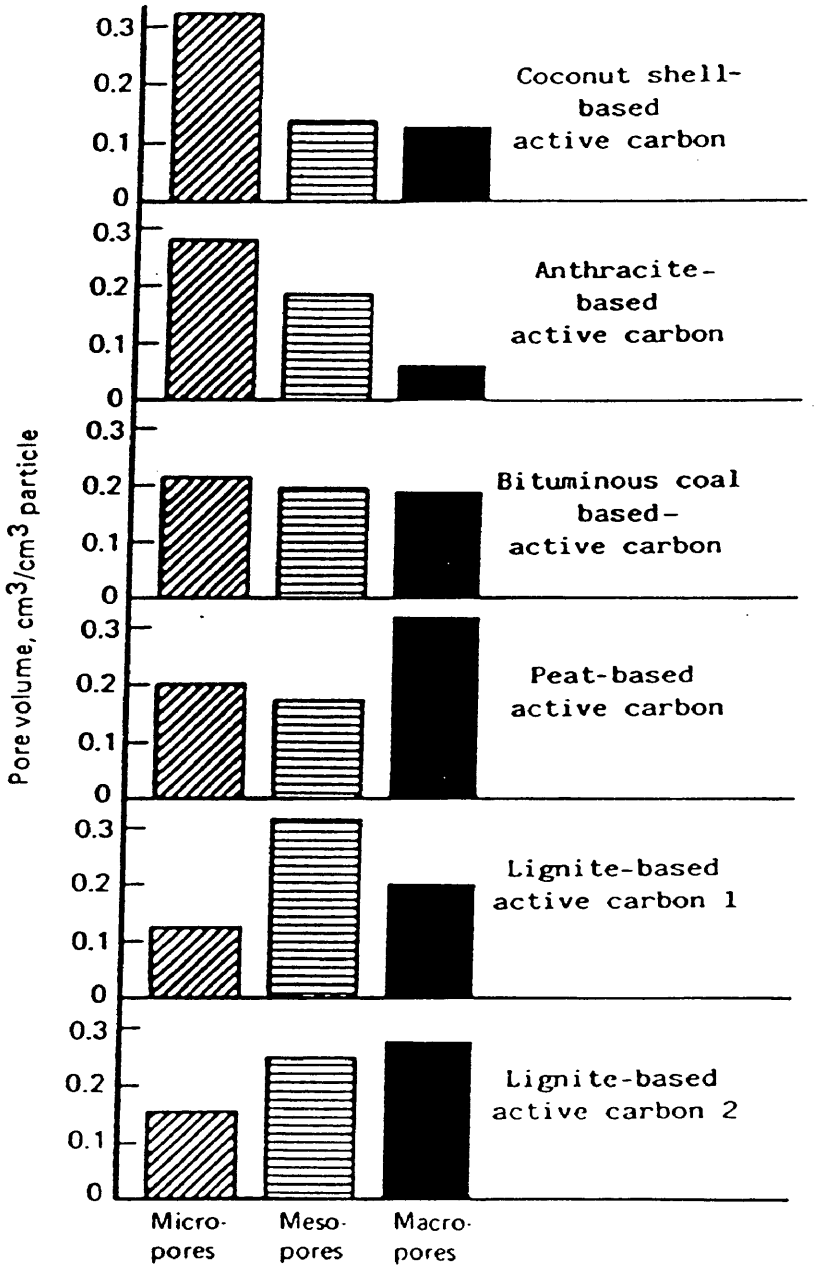

Figure 2.3 Effect of type of precursor on pore size distribution (56)

Table 2.3 The effect of the precursor on the texture and the subsequent application of activated carbon (56)

Raw material	Texture	Application
Soft wood	Soft, large pore volume	Aqueous phase adsorption
Hard wood	Soft, large pore volume	Aqueous phase adsorption
Nutshells	Hard, large pore volume	Vapor phase adsorption
Soft coal	Medium hard, medium. pore volume	Liquid and vapor phase adsorption
Hard coal	Hard, large pore volume	Gas vapor adsorption
Petroleum coke	Medium hard, medium pore volume	Waste water treatment

2.5.1.1 Carbonization

Carbonization is conducted in an inert atmosphere between 300-600^{o}C. During which, most of the non-carbon elements such as oxygen and hydrogen are eliminated as volatile gases leaving a fixed mass of carbon (called char for thermosetting precursor and coke for thermoplastic precursor). The residual carbon atoms group themselves into sheets of condensed aromatic rings with an irregular arrangement which creates interstices between them. These interstices give rise to pores. The quality and the yield of char is determined by the rate of heating and the final temperature. Lower heating rates result in a lower degree of volatilization and higher char yield because of increased dehydration and better stabilization of the polymeric components (56). Pore characteristics and other properties such as bulk density, mechanical strength and ignition temperature are strong function of carbonization temperature. In case of coal, mineral matter can affect the process of carbonization and the properties of activated carbon (58,59). For instance, alkali metal constituents such as Na, K and Ca can increase the activation rate (58). If the precursor is thermoplastic such as bituminous coal, the fluid phase development during carbonization could promote crystallite alignment and a loss of porosity. An essential prerequisite is that it must be intrinsically thermosetting or be converted from thermoplastic to thermosetting behavior by some process such as oxidation for the suppression of fluidity development in coal (60).

Although, carbonization modifies the pore structure inherent to the precursor, the pore structure is further developed by either activation route.

2.5.1.2 Physical activation

Physical activation is carried out between 800-1100^{o}C, in the presence of an oxidizing agent such as steam, carbon dioxide (CO_2) or a mixture of both. The oxygen in steam or CO_2 burns off the more reactive carbon from the carbon structure as CO and CO_2 by the following reactions:

$$C + H_2O \text{ ---------> } CO + H_2 \quad (2.34)$$

$$C + 2H_2O \text{ ----------> } CO_2 + 2H_2 \quad (2.35)$$

$$C + CO_2 \text{ ----------> } 2CO \quad (2.36)$$

The removal of carbon atoms increases the average size of the micropores already accessible to the gas and opens up closed porosity. The principal changes occur in the micropore region (60). The extent of burn-off depends on the nature of gas employed and the temperature of activation. A generalized schematic of the physical activation route is shown in Figure 2.4. All the possible steps that may be involved in the manufacture of activated carbon are shown, although only some of them will apply to any particular case.

2.5.1.3 Chemical activation

Chemical activation is carried out between 400-800^{o}C, using a chemical activating reagent such as zinc chloride, phosphoric acid and sulfuric acid. This route is usually taken when the precursors are cellulosic materials, wood being the most common (56,58). The starting material is first impregnated with the activating solution and then heat treated at a suitable temperature. A general

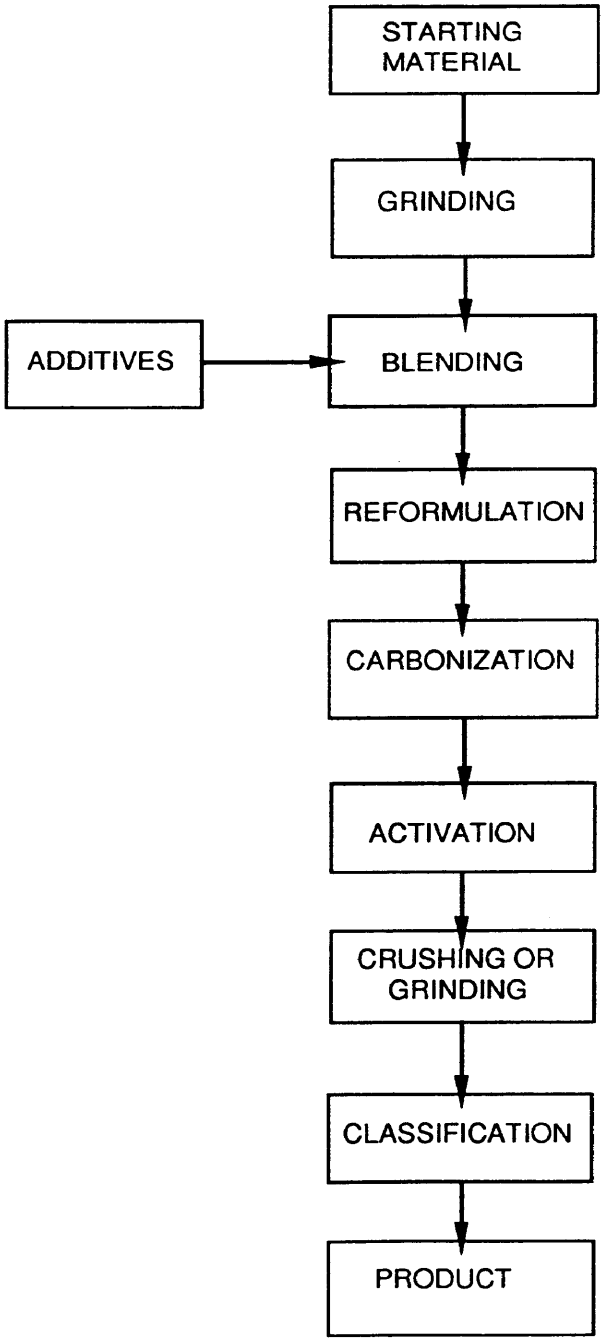

Figure 2.4 Physical activation route

ARTHUR LAKES LIBRARY
COLORADO SCHOOL OF MINES
GOLDEN, CO 80401

process flow sheet for the chemical activation process is shown in Figure 2.5. During calcination, the impregnated material dehydrates the raw material which results in the cross linking and increased aromatization of the carbon skeleton and the creation of a porous structure. According to Juentgen (60), cross linking inhibits shrinkage during heat treatment and helps to create the microporosity The pore size distribution of the carbons is reported to be dependent upon the ratio of chemical activant to the precursor. A high ratio leads to wider microporosity and more developed meso and macro porosity (60).

Zinc chloride ($ZnCl_2$) can act as an efficient activating agent in the temperature range of 600-700^oC, but the cost of $ZnCl_2$ and the low recovery may very well account for the preferred use of phosphoric acid in the industry.

Laine et al. (61) have studied the preparation and characterization of activated carbons from coconut shell impregnated with phosphoric acid. They were prepared using a one step carbonization and impregnation procedure. The optimum activation temperature for a higher surface area was found to be 450^oC. Higher surface area and mesoporosity were also found to be favored by increasing the acid concentration of the impregnating solution. Norit Ltd (U.K.) uses phosphoric acid to produce activated carbons from wood at a plant in Scotland. The most important unit of this plant is the recovery system (60,62). Kwok and Miller (63) suggested a different method for preparing activated carbon from petroleum coke by treating it with phosphoric acid and then activating it in steam between 700-900^oC to a weight loss of about 30%. The surface area of the final product was about 700 m^2/g.

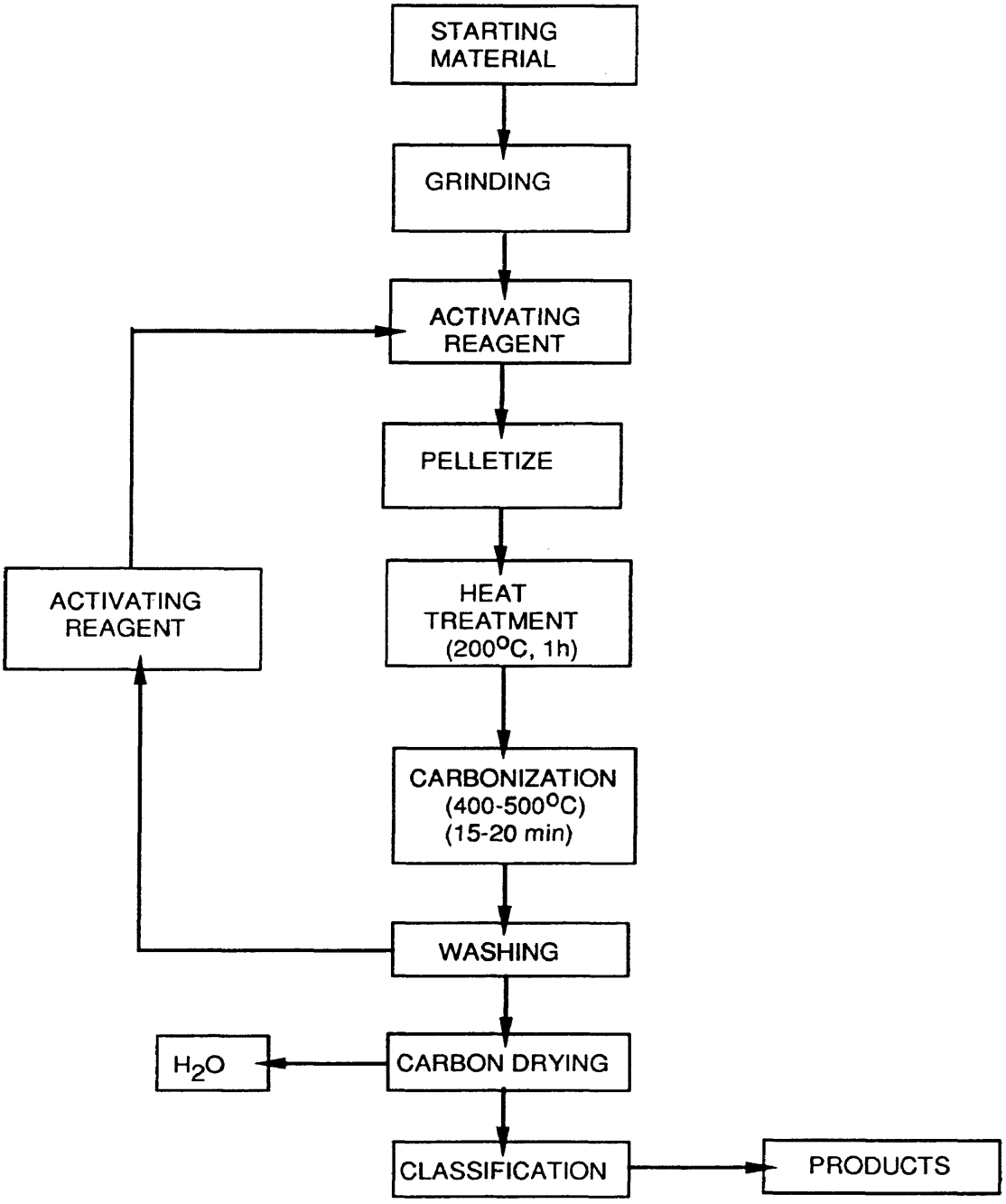

Figure 2.5 Chemical activation route

The application of chemical activation to coals has been very limited. A patent awarded to Carborundum Company (60, 64) describes a process for the production of activated carbon from sub-bituminous coal using an acid reagent (5% wt of conc. H_2SO_4, H_3PO_4 or HCl). The impregnated feed is heat treated at 450^oC in an inert atmosphere followed by steam activation around 900^oC.

2.5.2 Structure of activated carbon

Activated carbons have both physical as well as chemical structures. Both of these structures are very important depending on their application.

2.5.2.1 Physical structure

Figure 2.6 shows a schematic of the structure of activated carbon. The carbon atoms are mainly grouped into stacks of flat, aromatic sheets or planes, cross linked in a random manner by aliphatic bridging groups. The average width of these sheets is about 5 nm. The arrangement of these sheets is irregular and leaves free interstices between the sheets, thus giving rise to pore structure. The structure of activated carbon can also be considered as consisting of rigid interlinked clusters of microcrystallites (57), each microcrystallite comprising a stack of graphite planes (see Figure 2.7). These microcrystallites are interconnected by interaction of functional groups terminating at the graphitic planes. The intraparticle surface of activated carbon consists primarily of basal planes of the microcyrystallite, exposed within the micropore fissures during activation, as well as the edges of the graphitic planes comprising the sides of microcrystallite. The valence of the carbon

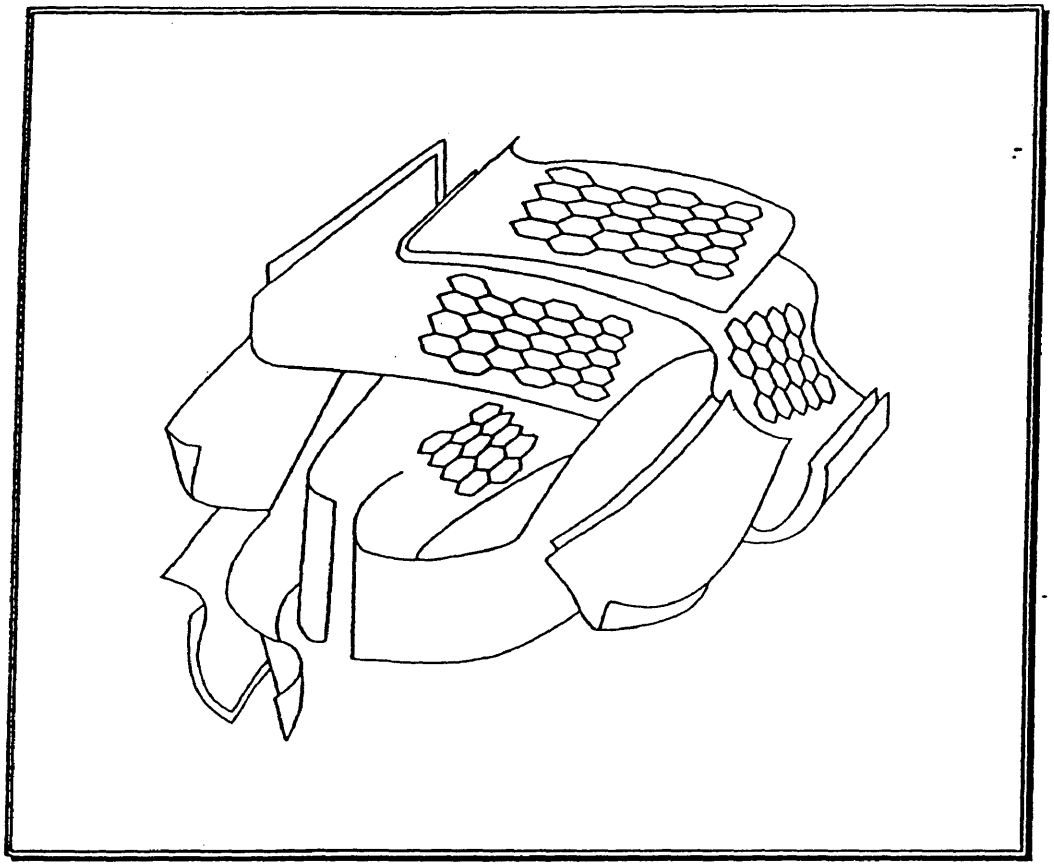

Figure 2.6 Schematic representation of the microstructure of carbons (56)

atoms located in the basal planes is fully satisfied (65). Adsorption on this type of surface would occur predominantly as a result of physical Van der Waals interactions.

2.5.2.2 Chemical structure

Carbon atoms located at the edges of the basal planes have only two of their possible three bonds formed with the neighboring carbon atoms (see Figure 2.7) in the same plane. These edge carbon atoms are more reactive than the carbon atoms located inside the basal plane. As a result, these edge carbon atoms are associated with appreciable amounts of heteroatoms such as oxygen, hydrogen, nitrogen, chlorine and sulfur (56). Carbon-oxygen surface structures are the most important in influencing surface characteristics and surface behavior. Activated carbon could be acidic or basic depending on the functional group present on the surface.

2.5.2.2.1 Acidic activated carbons

These type of activated carbons show acidic behavior and adsorb appreciable amounts of bases. The activation temperature significantly influences the nature of the carbon-oxygen surface complex. Low activation temperatures (physical activation) between 300-500^{o}C result in formation of acidic surface functional groups which are hydrophilic in nature (56,57). They are also formed during activation, when the activating agent is acidic in nature such as phosphoric, sulfuric or nitric acid. For example, Puri (56) found that treatment of charcoal with concentrated nitric acid resulted in a 20 % increase in

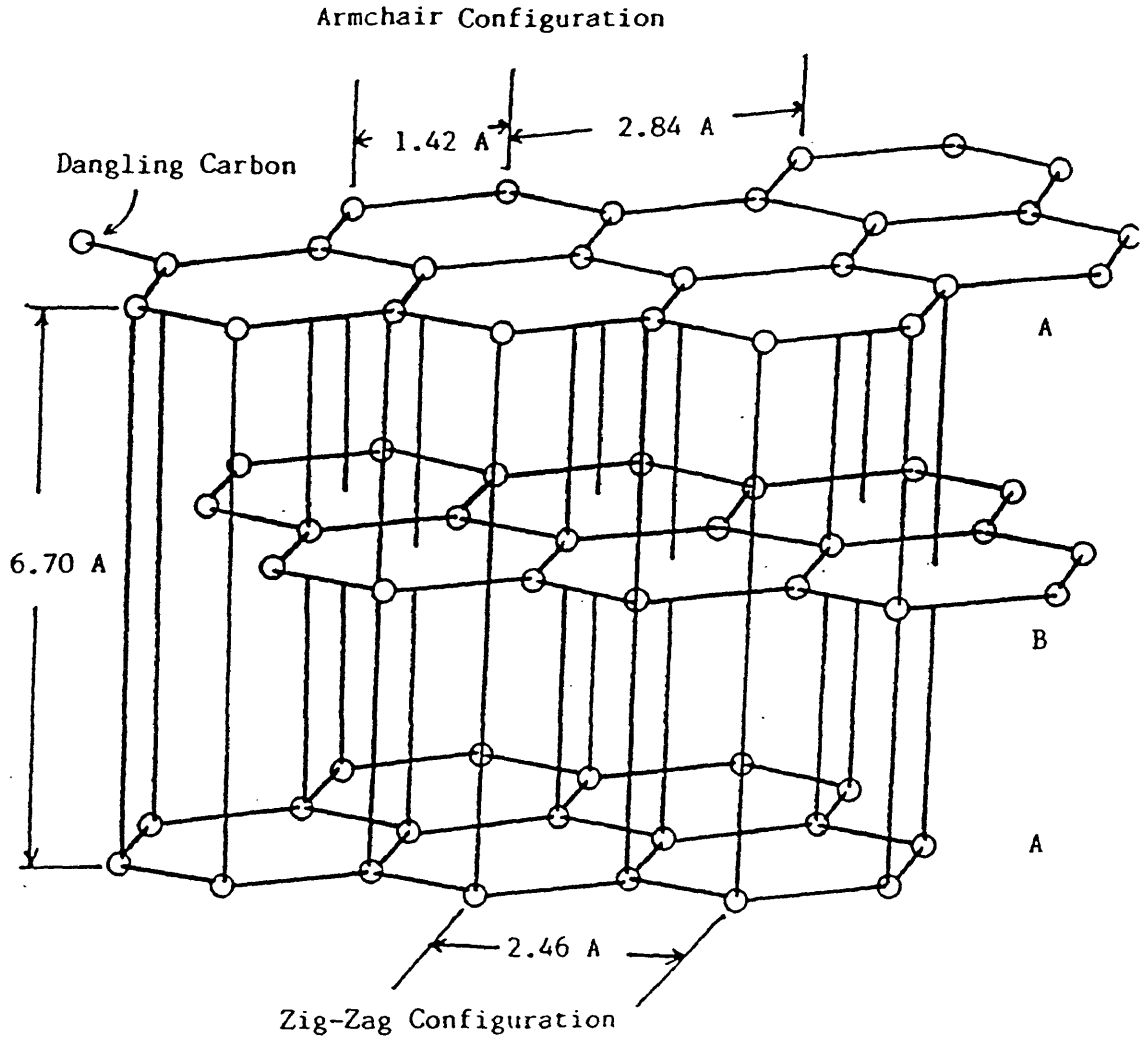

Figure 2.7 Structure of activated carbon (65)

oxygen. Attempts have been made to identify these functional groups using various techniques including IR spectroscopy, X-ray photoelectron spectroscopy, neutralization with bases and temperature programmed desorption. Some of the acidic surface oxides which have been identified so far include carboxylic, phenolic hydroxyl, lactones, carboxyl acid anhydrides, aldehydes and ketones, as shown in Figure 2.8.

2.5.2.2.2 Basic activated carbons

These type of activated carbons show basic behavior and adsorb appreciable amounts of acids. High activation temperatures of 800-1000^{o}C result in the formation of basic surface oxides. Garten and Weiss (57) proposed the presence of chromene groups on the surface. The formation of the basic oxides also accompanies the formation of hydrogen peroxide. This was accounted for by the side reaction of active methylene groups, $>CH_2$ or >CHR present in chromene (57,60). Later, Boehm and Voll suggested that the basic surface oxides are best represented by pyrone-like structures (57). Figure 2.9 depicts basic surface functional groups.

2.6 Activated carbon or active coke for nitric oxide reduction

Activated carbon has been used in pilot plants since 1985 to reduce NO_x and SO_x. The activated carbon produced from hard coal for flue gas cleaning is only produced in Germany and Japan (6). Berbau-Forshung of Germany developed a process for the simultaneous removal of NO_x and SO_2 using activated carbon. The process consists of two stage moving bed adsorbers.

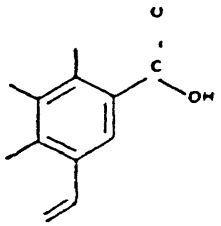

Carboxylic group

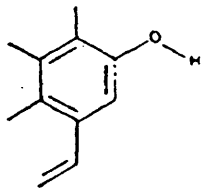

Phenolic hydroxyl group

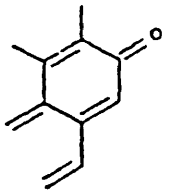

Quinone-type carbonyl group

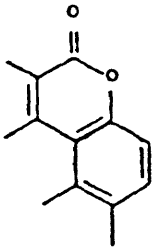

Normal lactone group

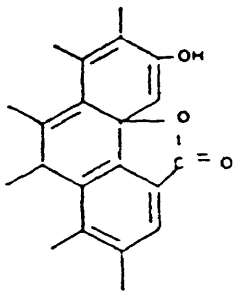

Fluorescein-type lactone group

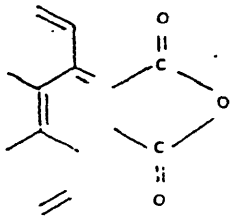

Carboxylic acid anhydride group

Figure 2.8 Acidic surface oxides on activated carbon (57)

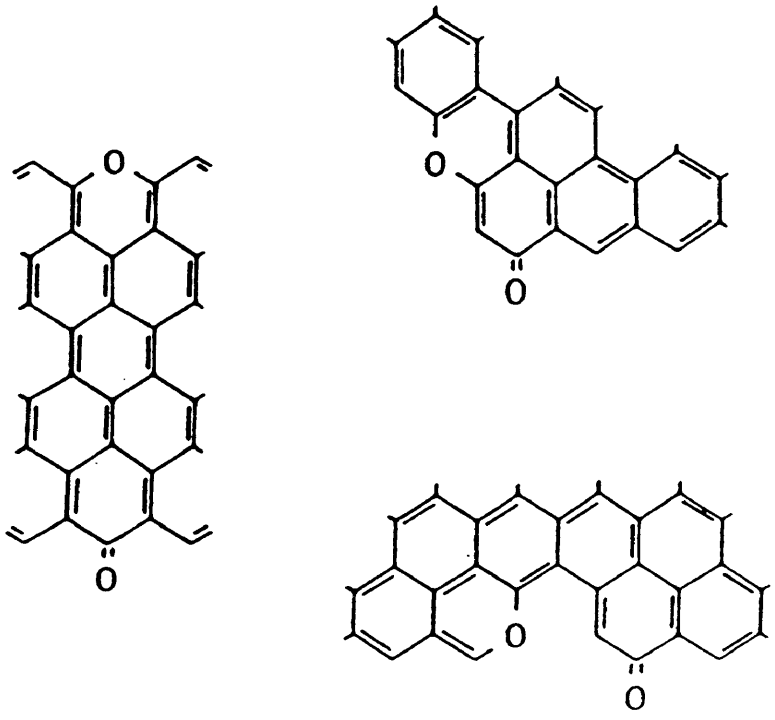

Figure 2.9 Possible structures of pyrones on activated carbons surface (56)

Most of the SO_2 is removed by adsorption in the first stage and NO_x is abated in the second stage by NH_3 injection. Both stages are designed as moving bed units. The catalyst used in this process is active coke (carbonized product) produced from finely ground preoxidized hard coal which is mixed with a binder, extruded to cylindrical pellets and carbonized. SO_2, adsorbed in the first stage, is retained in the pores as sulfuric acid in presence of water by the following reaction:

$$SO_2 + H_2O + 1/2O_2 \text{ ----------> } H_2SO_4 \qquad (2.37)$$

The H_2SO_4-loaded active coke is regenerated by heat treatment at 400°C and is then fed to the second bed. The removal efficiency for SO_2 is about 95% and about 80% for NO_x (66,67).

Kusabe et al. (68) studied the effect of SO_2 on active coke catalyzed reduction of NO by NH_3 using a two stage reactor. SO_2 was adsorbed on activated carbon in the first stage and NO was reduced to N_2 in the second stage. The SO_2, which escaped from the first reactor, reacted with NH_3 to form faceted fine crystals of $(NH_4)_2SO_4$ at 100°C and large planar particles of NH_4HSO_4 at 200°C. Simultaneously, the catalyst surface area reduced from 350 m^2/g to 9 m^2/g. The pores were found to be filled with ammonium salts. The catalyst activity decreased by 30-40% at low temperatures. Such deactivation was found to be very sensitive to temperature. Above 200°C, which is the melting point of NH_4HSO_4, the presence of ammonium salts had no effect on activity.

Juentgen and Kuehl (69) investigated the mechanism of NO reduction by NH_3 over active coke in the presence of water vapor and O_2. They concluded that the first step in the reduction is the oxidation of NO to NO_2. The intermediate reactions were strongly dependent on temperature. At lower temperatures (<100°C), adsorbed NO is converted to ammonium nitrate and ammonium nitrite. NO can only be converted into N_2 and H_2O via ammonium nitrite. At higher temperatures, all of NO is converted into ammonium nitrite. The intermediate reactions are as follows:

$$2NO(gas) \Longleftrightarrow 2NO(ads) \quad (2.38)$$

$$2NO(ads) + 1/2O_2 \Longleftrightarrow 2NO_2(ads) \quad (2.39)$$

At temperatures lower than 100°C

$$2NO_2(ads) \Longleftrightarrow N_2O_4(ads) \quad (2.40)$$

$$N_2O_4(ads) + 2NH_3 + H_2O \Longleftrightarrow NH_4NO_3 + NH_4NO_2 \quad (2.41)$$

$$NH_4NO_2 \Longleftrightarrow N_2 + 2H_2O \quad (2.42)$$

At temperatures greater than 100°C

$$2NO_2(ads) + 2NO \Longleftrightarrow 2N_2O_3(ads) \quad (2.43)$$

$$2N_2O_3(ads) + 2H_2O + 4NH_3 \Longleftrightarrow 4NH_4NO_2(ads) \quad (2.44)$$

$$4NH_4NO_2 \Longleftrightarrow 4N_2 + 8H_2O \quad (2.45)$$

Kleinschmidt (70) studied the kinetics of NO reduction by NH_3 in the presence of H_2O and O_2; and the reaction of NO with the catalyst itself in the absence of other reactants. In the absence of NH_3, there was no NO conversion. By changing the NO/NH_3 ratio, the reaction order of NH_3 was

determined to be zero, in other words, an excess of NH_3 had no effect on the conversion.

Recently, attention is being focussed on the use of active coke or activated carbon produced from brown coal. The advantage of this is the lower cost of production for coke from brown coal (10 % of the price for activated carbon from hard coal). Lenz et al. (71) studied the removal of SO_2 and NO_x from flue gas using brown coal coke. The coke was produced from pre-dried granular brown coal. The residence time of the coke in the hearth furnace was 45 minutes at 950°C. The removal of NO_x and SO_2 was found to be a function of the residence time of the flue gas in the reactor and the moisture content of coke. Approximately, 55 % of NO_x was converted to N_2 in a residence time of 15 to 20 seconds. NO_x removal efficiency decreased with an increase in the moisture content, but an opposite trend was observed for SO_2 removal.

Activated carbon has also been used as catalyst support for NOx reduction. Michiharu et al. (72) investigated the activity of ammonium halides supported on activated carbon for NO reduction by NH_3. The activated carbon was soaked in ammonium solution and dried at 130-190°C in air. Of all the ammonium halides, ammonium bromide showed the highest reactivity. Over 90 % of the NO was converted into N_2 at 100°C but only in the presence of O_2. Without O_2, the activity was zero. Kapteijn et al. (73) also investigated NO reduction by CO above 300°C over activated carbon supported alkali metals. The main products were N_2, CO, and CO_2. The activity increased with the atomic number: Na < K < Cs.

Chapter 3

COMMERCIAL ACTIVATED CARBONS

The main objective of the work presented in this chapter was to determine the characteristics of commercial activated carbons which were important for their activity for SCR of NO in the presence of NH_3 and O_2. The stoichiometry is shown by the following reaction:

$$4NO + 4NH_3 + O_2 \text{ ----------> } 4N_2 + 6H_2O \qquad (3.1)$$

As discussed in the previous chapter, activated carbons have been used in pilot plants in Germany to reduce NO_x emissions, but from the literature survey there appeared to be no strong evidence of any studies that have been performed to investigate the properties of activated carbons that are responsible for NO_x reduction.

The selectivity of these commercial samples was also investigated by studying NH_3 oxidation, given by the following reactions:

$$4NH_3 + 5O_2 \text{ ----------> } 4NO + 6H_2O \qquad (3.2)$$

$$2NH_3 + 2O_2 \text{ ----------> } N_2O + 3H_2O \qquad (3.3)$$

ARTHUR LAKES LIBRARY
COLORADO SCHOOL OF MINES
GOLDEN, CO 80401

Other reactions also possible under the experimental conditions include:

$$2NO + C \text{ ----------> } N_2 + CO_2 \quad (3.4)$$

$$2NO + O_2 + 2C \text{ ----------> } N_2 + 2CO_2 \quad (3.5)$$

The contribution of Reactions 3.4 and 3.5 toward NO reduction was also investigated using the commercial sample which showed the highest activity for NO reduction via Reaction 3.1.

3.1 Experimental

3.1.1 Gases

The following gas mixtures (certified standard), supplied by Liquid Carbonic, were used as received: 0.3 vol% NO/He, 0.3 vol% NH_3/He, 40.0 vol% O_2/He and 100.0 vol% He.

3.1.2 Catalysts

Four commercial activated carbon samples (labelled SP1, SP2, SP3 and SP4), originating from three precursors were used in powdered form (-50 mesh). Their origins and manufacturers are presented in Table 3.1. All of these samples were produced by the process of steam activation. The exact details of preparation of these samples is not known due to proprietary restrictions, except that SP1 was produced at a lower temperature than the other samples.

Table 3.1 Commercial samples origin and manufacturer

Sample	Precursor	Manufacturer
SP1	Coal	Carbotech
SP2	Peat	Norit
SP3	Coconut shell	Barneby & Sutcliff
SP4	Peat	Norit

3.1.3 Characterization

3.1.3.1 Nitrogen sorption

The surface area of the samples was obtained by nitrogen adsorption at 77 K using a Quantachrome Autosorb-6 analyzer. The sample was first out-gassed overnight under a vacuum of 10^{-2} torr and at a temperature of 200°C. It was then cooled with liquid nitrogen to 77 K. After the sample temperature was equilibrated, a known quantity of nitrogen gas was admitted into a sample cell. A sorption isotherm, providing 40 adsorption and 40 desorption points, was then obtained volumetrically. The surface area was calculated using the Brunauer-Emmett-Teller (BET) method, and the micropore volume was calculated using the t-method of deBoer et al. (74).

3.1.3.2 Mercury porosimetry

Specific volumes and surface areas of the meso- and macropore region were investigated by mercury porosimetry, using a Quantachrome Autoscan-60 porosimeter. The sample was first evacuated in the filling chamber to a vacuum of 20-30 torr before being allowed to take up mercury to atmospheric pressure. The macropore volume and surface area were calculated from the amount of mercury intruded at a pressure of 4250 psig. This value correlates to a pore diameter of 50 nm, which is the UIPAC defined minimum diameter of macropores. Mesopore parameters were obtained by subtracting macropore volume and surface area from the total values.

3.1.3.3 Ultimate and proximate analysis

Ultimate analysis was carried out using a Leco CHN-600 elemental analyzer and a Leco 432 sulfur analyzer (ASTM 4239 method C). Proximate analysis was carried out using a Leco TGA 500 proximate analyzer.

3.1.3.4 Mineral analysis

The sample was ashed in a muffle furnace at 750^{o}C for four hours (ASTM 3682). The ash was fused with lithium tetra-borate at 1000^{o}C for half an hour. The pellet was dissolved in 10 % HNO_3 and then analyzed by inductively coupled plasma using a spectrometric SMI III analyzer.

3.1.3.5 Ignition temperature

Ignition temperature of the samples was obtained using a Scientific Instrument thermogravimetric analyzer in a 20 vol % O_2/He environment.

3.1.3.6 pH analysis

The pH of the samples was obtained using a standard procedure (in industry) in which 3 g of the sample was mixed with 60 ml of distilled water and heated at 100^{o}C for three minutes. The solution was then filtered, allowed to cool to room temperature, and its pH was measured using an Orion Research microprocessor pH meter. This technique is only applicable to activated carbons which are manufactured by physical activation.

3.1.4 Equipment for activity measurements

The laboratory apparatus consisted of a fixed bed tubular reactor, gas mixing chamber, mass flow controllers, temperature controller, thermocouples and analytical equipment for analyzing products and reactants.

The mass flow control section consisted of five Tylan model FC-280 mass flow controllers along with a Tylan RO-28 readout and control units. The mass flow controllers were capable of delivering up to 200 SCCM for NO/He, NH_3/He and O_2/He and up to 1000 SCCM for He. The other mass flow controller was used in handling calibration gas for analytical equipment and was capable of delivering up to 1000 SCCM. Each stream was filtered through a 0.5 micron sintered metal filter before entering the flow controller. After passing through a block valve and a check valve, the gases entered the mixing chamber which was made up of 5.1 cm od stainless steel pipe filled with 3 mm glass balls. This arrangement allowed a thorough mixing of gases before entering the reactor. A three-way valve was installed before the reactor vessel which provided an option of bypassing the reactor vessel. The reactor vessel was a 1.9 cm od stainless steel tube with a 1.22 cm id and 30.54 cm in length. The fixed catalyst bed was positioned 20.34 cm from the gas entry port which was the bottom end of the reactor vessel, as shown in Figure 3.1. The bed was sandwiched between glass wool plugs and was supported by 3 mm glass balls. The reactor was enclosed in a tube furnace which was capable of heating the reactor up to 1000^{o}C. The furnace temperature was controlled by an Omega controller. Temperatures in the reactor were measured by three thermocouples installed at

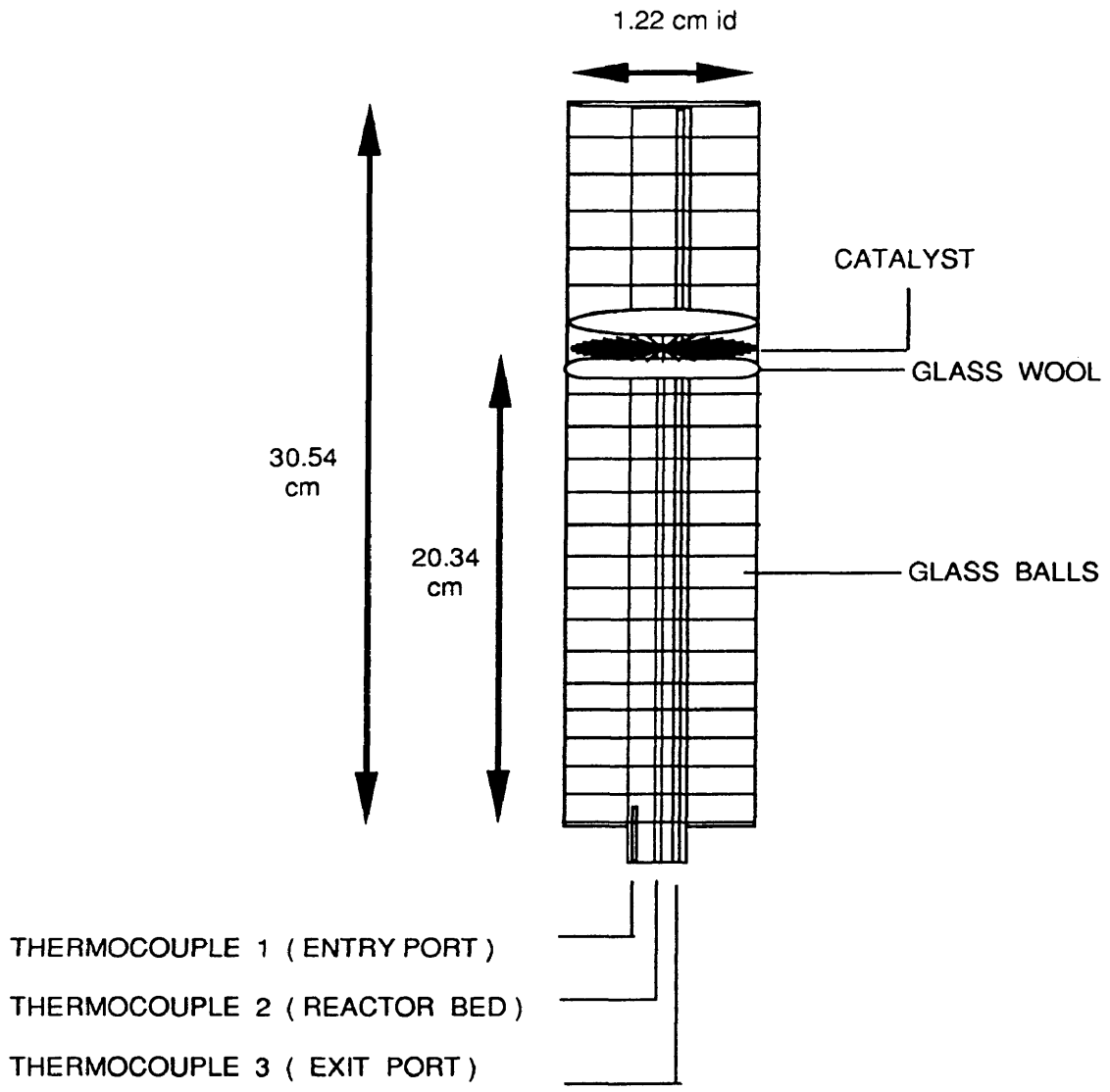

Figure 3.1 Reactor vessel

the gas entry port, at the fixed bed location and at the gas exit port. The schematic of the equipment layout is shown in Figure 3.2.

After passing through the reactor, a part of the stream was vented to the atmosphere and the remaining part was drawn into the analytical equipment which was divided into two sections. The first section consisted of infrared analyzer (Horiba PIR-2000R) for CO_2 and a chemiluminescence analyzer (Beckman Industrial) for NO/NO_x. Located prior to the analyzers was a 0.5 micron filter for particulate removal and a gas chiller to reduce the moisture content of the gas, as shown in Figure 3.3. The gas then encountered a pressure gauge and a rotameter used to monitor the flow conditions. The CO_2 infrared analyzer was based on non-dispersive infrared ray absorption. After passing through the CO_2 analyzer, the gas passed through the NO/NO_x analyzer. This analyzer utilized chemiluminescence as the method of NO concentration determination, which required the introduction of ozone (O_3) into the sample stream. Ozone for the chemiluminescent reaction is produced in a flow chamber where a stream of air or oxygen from an external cylinder is exposed to ultraviolet radiation from a source lamp. As NO and O_3 mixed in the reaction chamber, the chemiluminescent reaction produced light emission that was directly proportional to the concentration of NO:

$$NO + O_3 \text{ ----------> } NO_2^* + O_2 \qquad (3.6)$$

$$NO_2^* \text{ ----------> } NO_2 + h\nu \qquad (3.7)$$

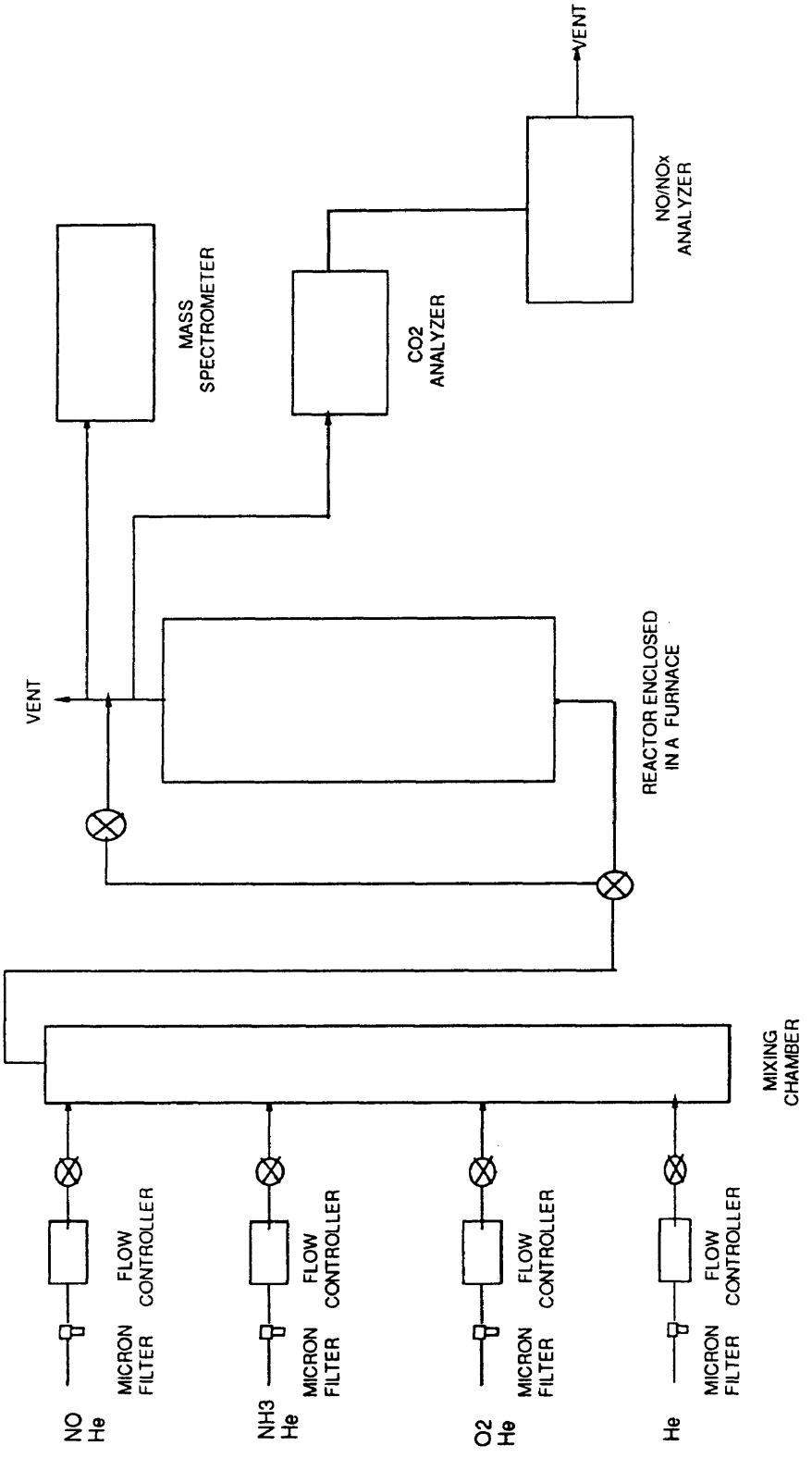

Figure 3.2 Equipment layout

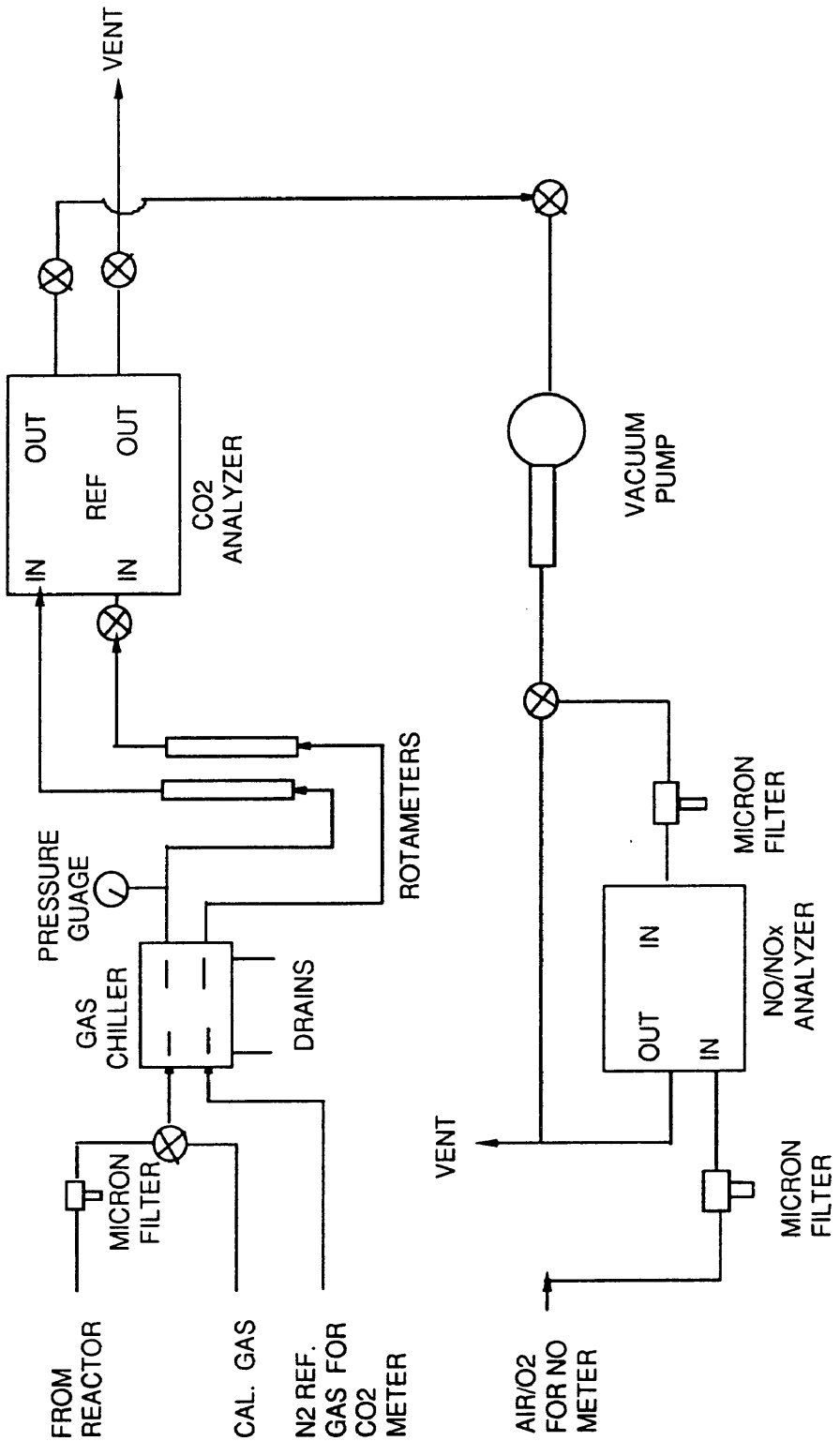

Figure 3.3 Analytical equipment

The NO_2 determination is identical to the NO determination except that, prior to entry into the reaction chamber, the gas is routed through a converter where NO_2 is converted into NO.

The second section consisted of the mass spectrometer (UTI 100-C) which included the quadrupole, RF generator and control console as shown in Figure 3.4. The sample gas to mass spectrometer was drawn from the reactor vessel through a thermal capillary, which was made up of a fused silica and had a 0.3 mm id.

3.1.5 Reaction conditions and procedure

Emphasis was placed on using conditions in the laboratory that would be similar to those of flue gas generated from power plants; hence, the NO and NH_3 concentrations were 700 ppm, O_2 was 4 % with the balance being He. In the test runs, the reaction temperature was varied from 150-300^oC. The total gas flow rate was 1000 SCCM, and the catalyst weight was 3 g thus making the space velocity equivalent to 20,000 $cm^3\ hr^{-1}\ g^{-1}$. The pressure inside the reactor vessel was maintained at approximately 1 atm by the part of effluent stream which was vented to the atmosphere.

All the flow controllers were calibrated to STP conditions using a bubble flow meter before starting this study and were then checked periodically throughout this research program. The calibration data is presented in Appendix A.

Prior to each test run, the catalyst sample was heated for four hours at 300^oC under a He flow to remove adsorbed moisture; and the CO_2 and NO/NO_x analyzers were zeroed and calibrated using standard gases. After bringing the

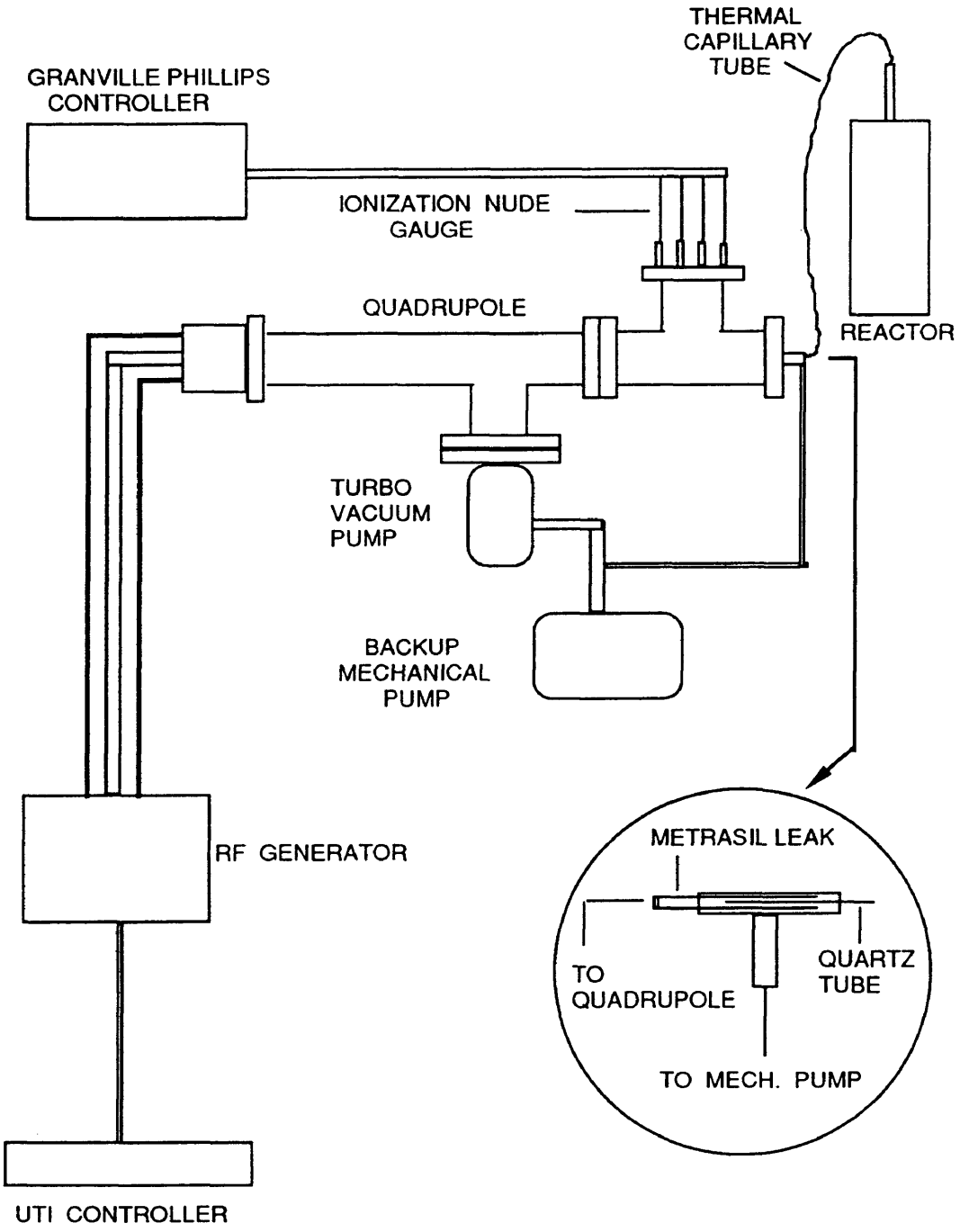

Figure 3.4 Mass spectrometer

reactor vessel to a desired temperature, half an hour was given for the temperature to stabilize within the reactor vessel under He flow of 1000 SCCM. Depending upon the run, appropriate reactant gases were introduced into the reactor vessel while keeping the total flow rate constant at 1000 SCCM at the expense of He. Unless specified otherwise, each test run for the activity was carried out for 4 hrs to ensure that steady state conditions were achieved before measuring the final NO conversion. At the end of each run, the whole system was purged with He to remove any contaminant gases.

The reproducibility of all the data was checked by repeating each test run at least once and in some cases twice.

3.2 Results and Discussion

3.2.1 Catalyst characterization

Typical isotherms obtained by the sorption of N_2 at 77 K onto the commercial samples are shown in Figures 3.5, 3.6, 3.7 and 3.8. The shape of these isotherms was close to Type I in the BDDT classification (75). Type I sorption isotherms are exhibited by microporous solids having relatively small external surfaces. The sloping pattern of the isotherm for SP4 also indicated the contribution to porosity by non-micropores. As the relative pressure approached 1.0, the adsorption of nitrogen in the gaseous phase shifted to a process of capillary condensation in which the pores were filled with liquid adsorbate. This accounted for the upswing in the adsorption curve. All the isotherms exhibited high pressure hysteresis similar to Type B by deBoer classification (76). Type B hysteresis is associated with slit-shaped pores.

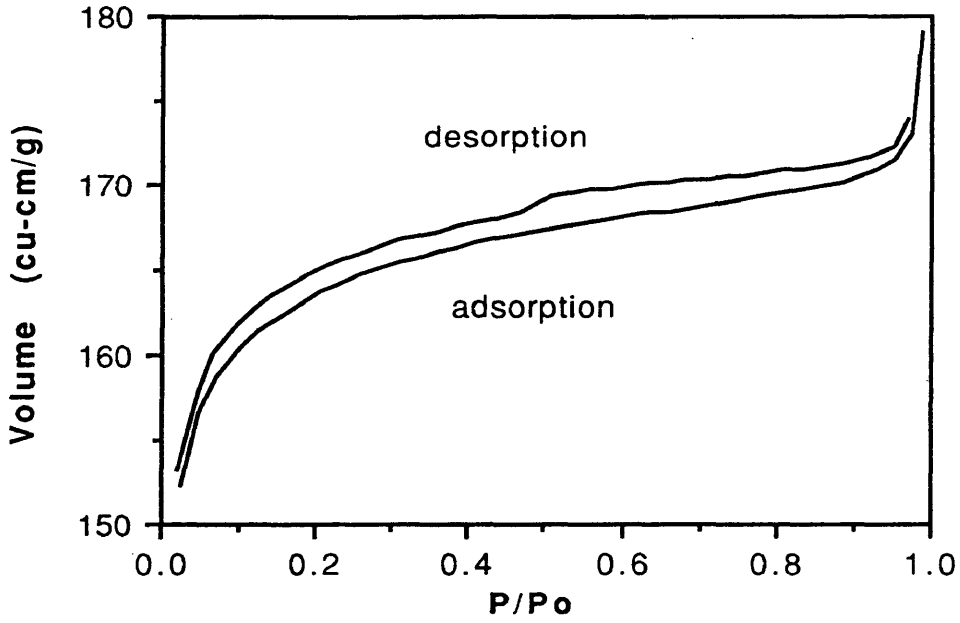

Figure 3.5 Nitrogen sorption isotherm at 77 K for SP1

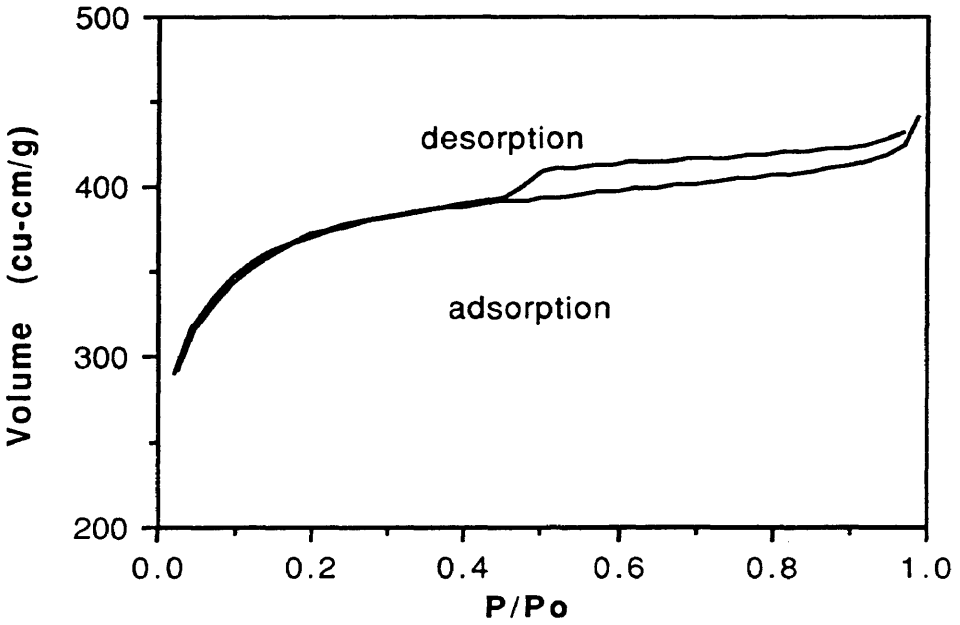

Figure 3.6 Nitrogen sorption isotherm at 77 K for SP2

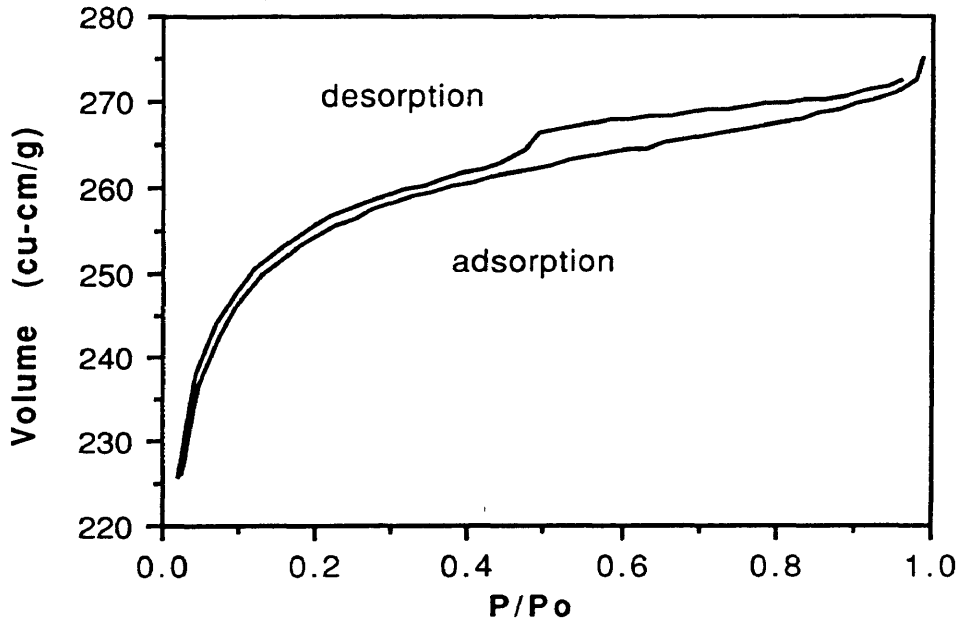

Figure 3.7 Nitrogen sorption isotherm at 77 K for SP3

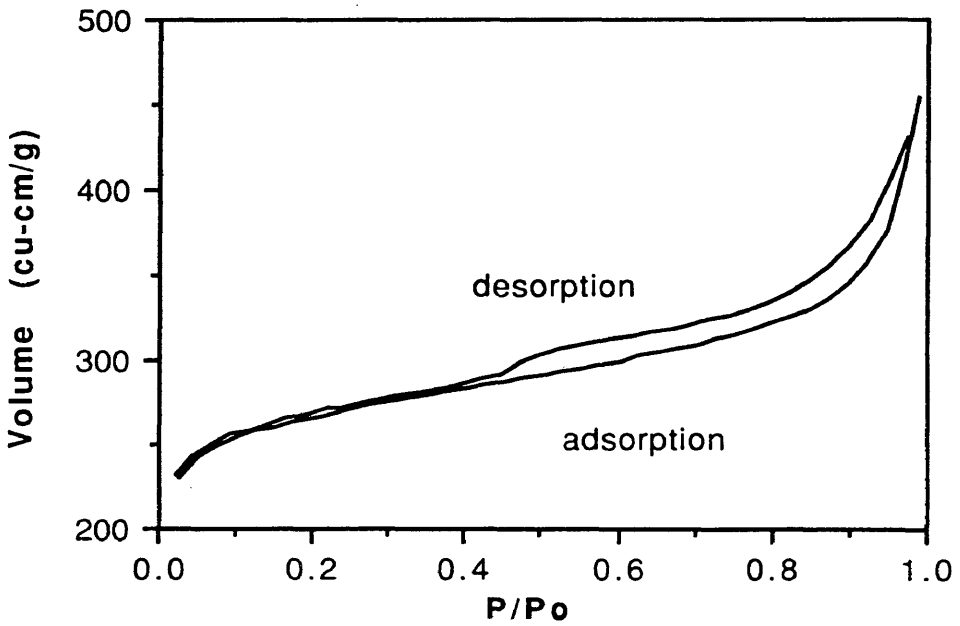

Figure 3.8 Nitrogen sorption isotherm at 77 K for SP4

Slit-shaped pores are expected in activated carbons because their porosity is thought to be due to the irregular arrangement of aromatic sheets consisting of carbon atoms (56).

A step at relative pressures of approximately 0.45 in the desorption cycle for all the samples was due to the change in the adsorbate phase from liquid to gas as suggested by Schofeild (77). These isotherms also exhibited open loop at low pressure hysteresis, although it is not apparent from the figures for SP2 and SP4. These results suggested that these samples contained very narrow micropores which may have resulted in severe activated diffusion of N_2.

All the samples had a very high BET surface area, as presented in Table 3.2, with SP2 exhibiting the highest surface area and SP1 the lowest of the four commercial samples. The observations about the samples' porosity, as obtained from the shape of the isotherms, were also confirmed by quantitative analysis, as these samples were highly microporous with very small pores. The average pore radius for all the commercial samples was less than 20 Å, with SP4 having the largest average pore radius (17.78 Å).

The mercury intrusion data is presented in Table 3.3. The contribution from non-micropores was very negligible.

The ultimate and proximate analysis data are presented in Tables 3.4 and 3.5. As shown, the main components of the samples were carbon and oxygen with lesser amounts of hydrogen, sulfur and nitrogen. The ash and moisture contents were also very low for all the samples.

Table 3.2 Commercial samples characterization using nitrogen adsorption at 77 K

Sample	BET surface area m^2/g	Micropore volume cm^3/g	Micropore surface area m^2/g	Average pore radius Å
SP1	466	0.239	440	11.70
SP2	1110	0.477	930	12.27
SP3	739	0.361	677	11.50
SP4	791	0.332	619	17.78

Table 3.3 Commercial samples characterization using mercury porosimetry

Sample	Macro volume cm^3/g	Macro surface area m^2/g	Meso volume cm^3/g	Meso surface area m^2/g
SP1	0.41	1.4	0.04	18.4
SP2	0.80	3.9	0.11	61.8
SP3	0.62	5.8	0.23	74.5
SP4	0.68	4.1	0.08	41.1

Table 3.4 Ultimate analysis of commercial samples

Sample	Carbon %	Hydrogen %	Nitrogen %	Sulfur %	Oxygen %
SP1	90.84	0.47	1.17	0.7	4.77
SP2	91.55	0.14	0.54	0.46	3.87
SP3	91.54	0.46	0.51	0.02	2.55
SP4	90.27	0.67	0.74	0.73	2.35

Table 3.5 Proximate analysis of commercial samples

Sample	Moisture %	Ash %	Volatile %	Fixed carbon %
SP1	2.70	2.05	12.6	82.6
SP2	4.39	3.44	0.5	91.7
SP3	2.67	4.92	30.0	62.4
SP4	3.54	5.24	26.6	64.6

The ignition temperatures and the pH of the activated carbon samples are presented in Table 3.6. The purpose of obtaining ignition temperatures for these samples was to ensure that reaction temperatures for NO reduction were less than the ignition temperature, thus preventing combustion of the samples. The ignition temperature of all the samples was higher than 450^{o}C.

3.2.2 Nitric oxide reduction by ammonia in the presence of oxygen

3.2.2.1 Activity measurements

The reactor vessel, glass wool and glass balls did not have any catalytic activity for NO conversion under the given conditions, as confirmed by the blank tests.

The conversion of NO was defined as:

$$\text{NO conversion (\%)} = X\ (\%) = \frac{([NO]_{in}-[NO]_{out})}{[NO]_{in}} \qquad [3.1]$$

where [NO] is the molar concentration. The reaction rate could be written as:

$$r_{NO} = K[NO]^{a}[NH_3]^{b}[O_2]^{c} \qquad [3.2]$$

where k is an observed rate constant. Since the concentration of O_2 was very high compared to other reactants and remained essentially constant throughout the course of the reaction, it can be combined with the observed rate constant. Other workers have reported the reaction rate to be first order with respect to NO

Table 3.6 Ignition temperature and the pH of commercial samples

Sample	Ignition temperature ^{o}C	pH
SP1	460	7.70
SP2	490	8.15
SP3	510	9.80
SP4	473	10.35

and zero order with respect to NH_3 (70). This is in agreement with our results which are presented in Chapter 4. Hence the final rate equation could be simplified to:

$$r_{NO} = K[NO]^1 \qquad [3.3]$$

where K is an observed empirical pseudo first-order rate constant. For a plug flow reactor, the design equation is given by:

$$\frac{W}{F^0_{NO}} = \int_0^x \frac{dX_{NO}}{-r_{NO}} \qquad [3.4]$$

where W is the mass of catalyst and F^o_{NO} is the inlet molar flow rate of NO. Using Equations 3.3 and 3.4, K can be obtained from the fractional conversion of NO by:

$$K = -\frac{F^o_{NO}}{[NO]_{in}W} \ln(1-X) \qquad [3.5]$$

For the purpose of comparison, the activity of the catalyst can be represented either by conversion of NO or by the observed pseudo first-order rate constant.

The NO conversion for the four samples, as a function of temperature, is presented in Figure 3.9. Sample SP1, which was produced from coal, had the highest activity between 150-300^{o}C. The NO conversion for SP1 was about 44

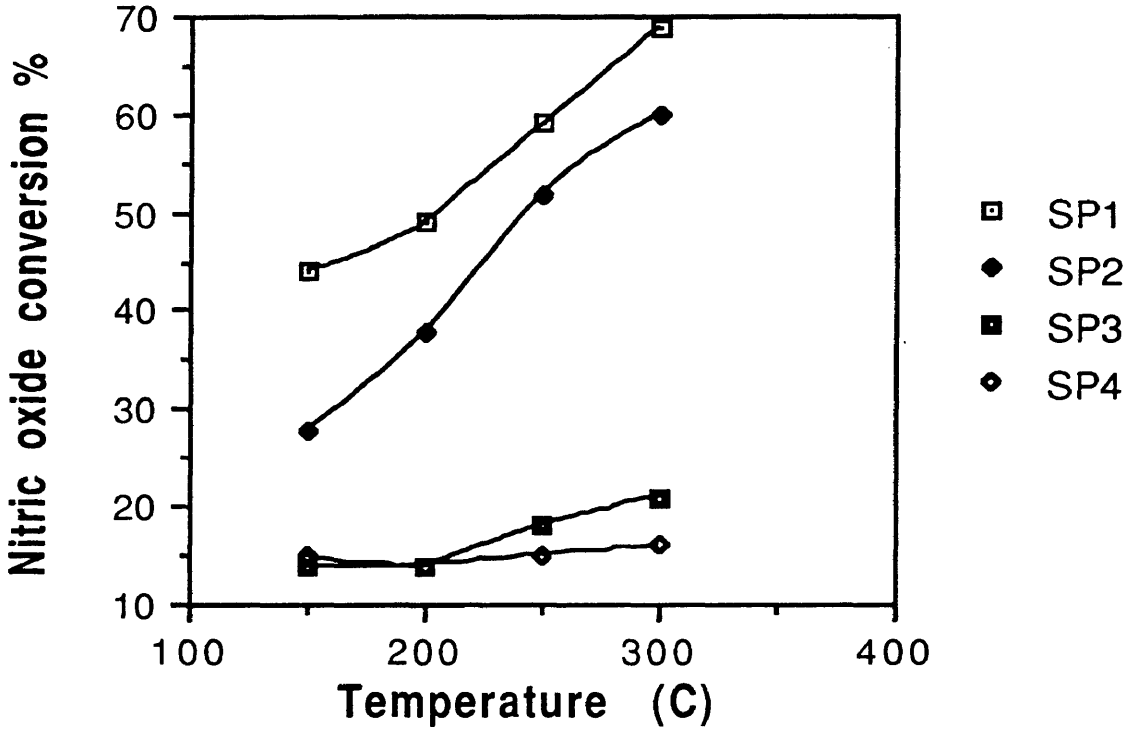

Figure 3.9 Comparison of activities of commercial samples

% at 150°C and 70 % at 300°C. Sample SP2, which was produced from peat, had the second highest activity for the given conditions. Samples SP3 and SP4, which were produced from coconut shell and peat, respectively, had very low activity, with SP4 having the lowest. The NO conversion for this sample was about 15 % at 150°C and 16 % at 300°C (thermodynamic equilibrium calculations for Reaction 3.1 are provided in Appendix B).

The temperature dependency of the SCR of NO for the samples is shown in the form of Arrhenius plots in Figure 3.10. The effect of temperature on the activity was as expected. The activity of SP1 and SP2 was very temperature sensitive, whereas for SP3 and SP4, catalytic SCR activity was found to be relatively temperature-insensitive. The activation energy was the highest (14.2 KJ/mole) in the case of SP2, as its activity almost doubled when the temperature was increased from 150°C to 300°C; and the lowest (1 kJ/mole) in the case of SP4, where the activity of this material remained almost constant when the temperature was increased.

Under the given conditions, there was a possibility that the following reaction could have taken place:

$$4NO + 4NH_3 + 3O_2 \text{ ----------> } 4N_2O + 6H_2O \qquad (3.8)$$

However, there was no indication of N_2O formation, as determined by the mass spectrometer.

The reaction temperatures were well below the ignition temperature, however at 300°C, their was evidence of very slight gasification of carbon to

ARTHUR LAKES LIBRARY
COLORADO SCHOOL OF MINES
GOLDEN, CO 80401

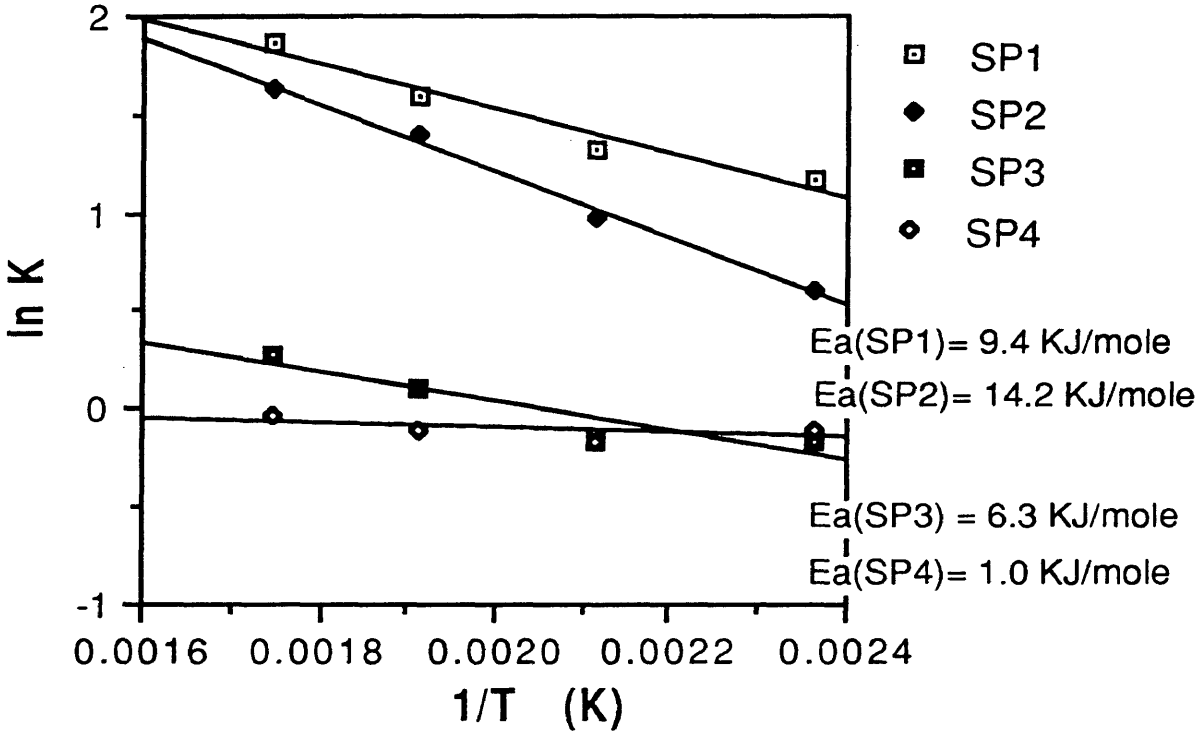

Figure 3.10 Temperature dependence for commercial samples

CO_2, which could only be detected by the mass spectrometer but not by the CO_2 infrared analyzer.

At higher operating temperatures there is a possibility that activated carbon may loose its activity when operated for longer periods due to the decomposition of surface oxides responsible for its activity (discussed in more detail in Chapter 5). Samples SP1 and SP2 were checked for their stability by being operated at 300°C for 72 hrs. Both the samples sustained their activity during this period which suggested that these catalysts were stable at high reaction temperatures.

3.2.2.2 Mass and Heat transfer limitations

In experimental studies of heterogeneously catalyzed reactions, special care has to be taken to avoid interference by physical transport phenomena such as interparticle mass and heat transfer and intraparticle mass and heat transfer so that the kinetic data obtained from the experimental reactor only represent the chemical event.

The effect of these limitations can be determined experimentally or can be estimated by calculation procedures (78,79). For interparticle limitations, the basis used for mass and heat transfer effects to become significant was a five percent change between the bulk and surface concentrations, and a 1°C gradient between the bulk and surface temperatures. Surface properties were estimated using the following equations:

$$C_b - C_s = \frac{r_p}{K_m a_m} \qquad [3.6]$$

$$T_b - T_s = (C_b - C_s)\frac{\Delta H}{C_p \rho}\left(\frac{P_r}{S_{ch}}\right)^{2/3} \qquad [3.7]$$

where:

C_b = bulk gas concentration

C_s = surface concentration

K_m = mass transfer coefficient

a_m = external surface per unit mass of catalyst

r_p = observed reaction rate per unit mass of catalyst

T_b = bulk gas temperature

T_s = surface Temperature

ΔH = heat of reaction

C_p = heat capacity of fluid

ρ = fluid density

P_r = Prandtl number

S_{ch} = Schmidt number

For Intraparticle limitations, mass transfer effects were investigated using Weiz and Prater criterion (79), also known as Damkohler number for diffusive transport, which is given below:

$$\frac{R r_p^2}{C_s D_e} << 1 \qquad [3.8]$$

where:

R = Observed reaction rate per unit particle volume

D_e = effective diffusivity

r_p = radius of the particle.

A tortuosity factor of 2 was used to calculate the effective diffusivity. This dimensionless group (Damkohler number) expresses the ratio of chemical reaction rate to diffusive flux. If it is less than 1 then the intraparticle mass transfer effects are insignificant.

Heat transfer effects were investigated using Anderson criterion (79) which is given below:

$$\frac{T_S R}{E} - \frac{\Delta H R r_p^2}{\kappa . T_S} > 0 \qquad [3.9]$$

where:

E = activation energy

R = gas constant

κ = thermal conductivity of the catalyst.

The intraparticle heat transfer effects can be assumed negligible if the L.H.S of the equation is greater than zero. For these calculations, it was assumed that between 150-300^{o}C, the controlling mechanism was the surface chemical reaction. The observed reaction rate used in the above expressions was calculated based on the initial concentration of the reactant (since the initial reaction rate is higher than the actual reaction rate).

The change in concentration between the bulk gas and the catalyst surface due to interparticle mass transfer limitations for the samples are presented in Figures 3.11-3.13. As can be seen, the effects of interparticle mass transfer were negligible for all the samples between 150-300^{o}C. Sample SP1 had the most prominent effect of all the samples. This was expected as this sample had shown the highest activity. As the reaction temperature increased, the concentration gradient between the bulk phase and the surface increased for SP1 and SP2; and remained somewhat constant for SP3 and SP4.

The temperature gradient due to interparticle heat transfer limitations was also very low for all the samples, as shown in Table 3.7. The SCR of NO is an exothermic reaction, but the temperature gradient across the film is also dependent on the concentration gradient across the film. Since the concentration gradient of the reactants was very low, the temperature at the surface was essentially identical to the bulk gas.

The mass and heat transfer effects due to intraparticle limitations were also found to be negligible for the samples, as shown in Tables 3.8 and 3.9. The Damkohler number was found to be less than one for all the samples for all the reactants. A trend similar to interparticle limitations was observed. Sample SP1 had the highest Damkohler number for given conditions. The Anderson criterion was also satisfied for all the samples.

3.2.2.3 Activity vs physical characteristics

The application of activated carbons as catalysts is often determined by their physical and chemical characteristics. Although physical characteristics such

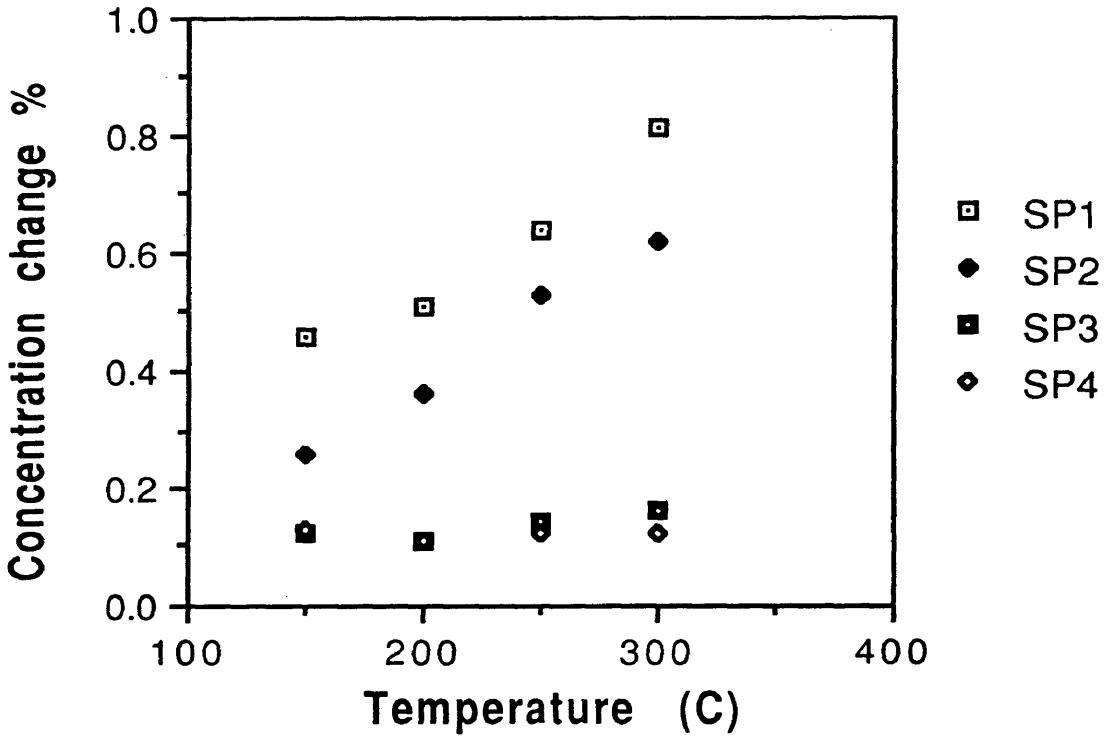

Figure 3.11 Effect of interparticle limitations on NO concentration

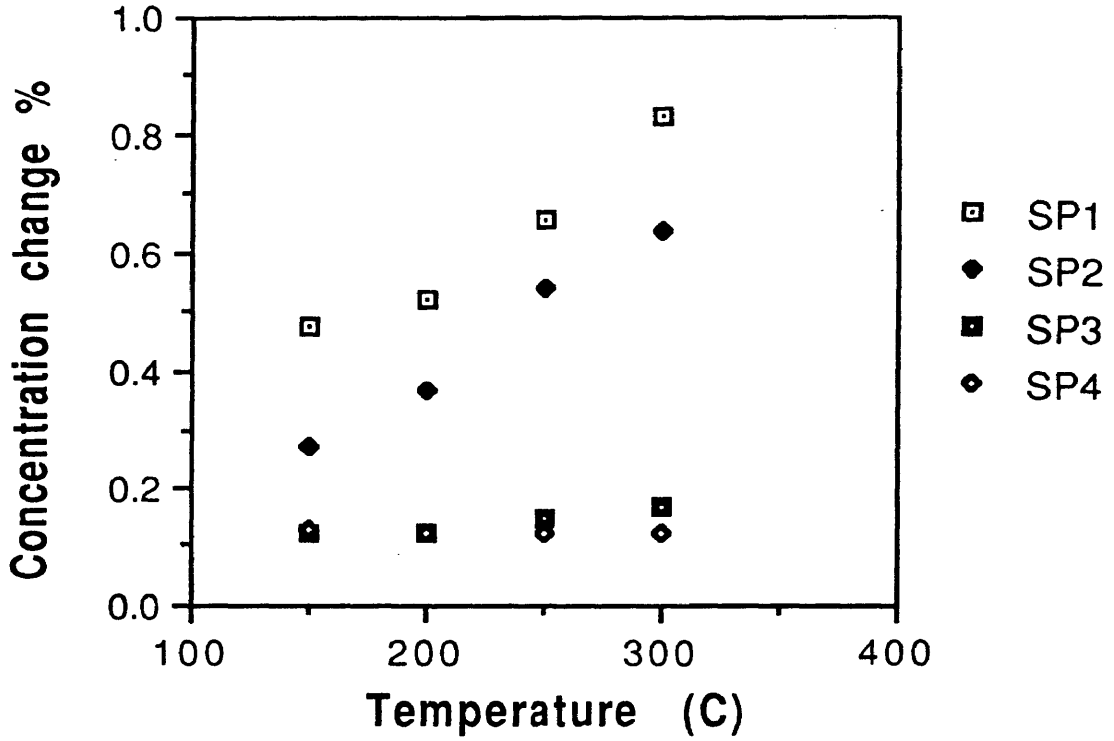

Figure 3.12 Effect of interparticle limitations on NH3 concentration

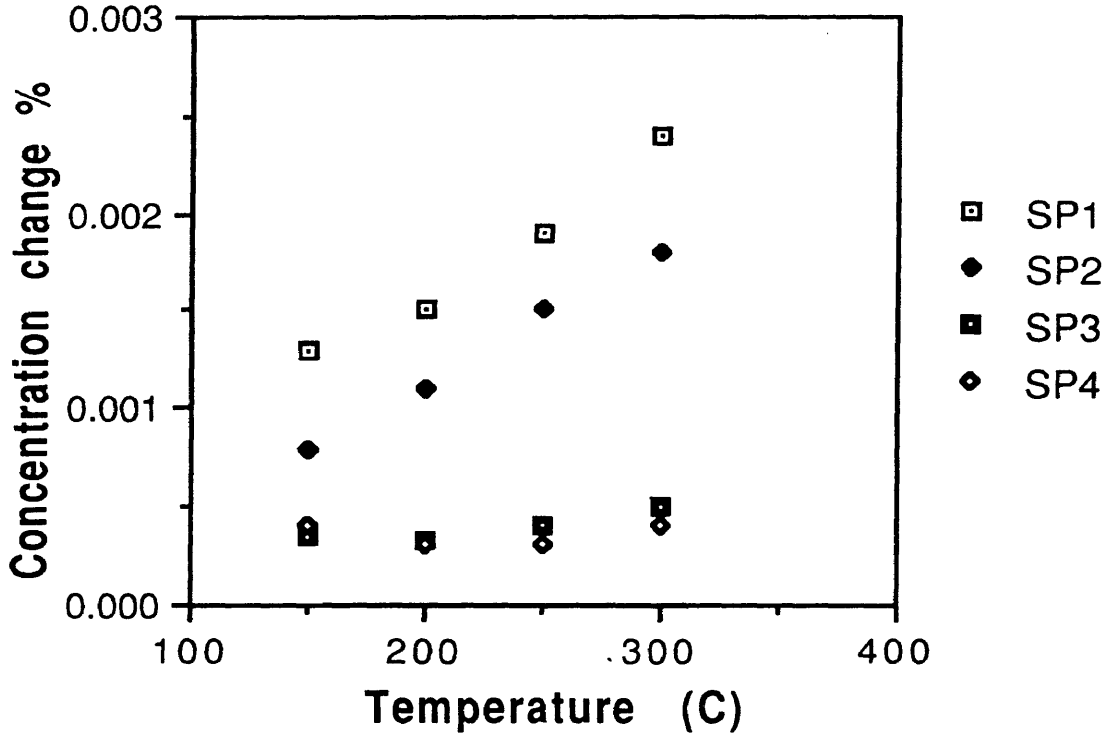

Figure 3.13 Effect of Interparticle limitations on O2 concentration

Table 3.7 Effect of interparticle limitations on temperature

Reaction temperature ^oC	SP1 (Tb-Ts)x10^4 ^oC	SP2 (Tb-Ts)x10^4 ^oC	SP3 (Tb-Ts)x10^4 ^oC	SP4 (Tb-Ts)x10^4 ^oC
150	1.5	0.8	0.4	0.4
200	1.8	1.2	0.4	0.4
250	2.4	2.0	0.5	0.4
300	3.3	2.5	0.7	0.5

Table 3.8 Effect of intraparticle limitations on concentration

Reaction temperature °C	NO Damkohler #	NH_3 Damkohler #	O_2 Damkohler #
SP1			
150	0.48	0.37	0.002
200	0.53	0.40	0.002
250	0.67	0.50	0.003
300	0.84	0.63	0.004
SP2			
150	0.27	0.21	0.001
200	0.38	0.28	0.002
250	0.55	0.42	0.002
300	0.65	0.49	0.003
SP3			
150	0.13	0.10	0.001
200	0.12	0.10	0.001
250	0.15	o.11	0.001
300	0.17	0.13	0.001
SP4			
150	0.14	0.10	0.001
200	0.12	0.09	0.001
250	0.12	0.09	0.001
300	0.13	0.09	0.001

Table 3.9 Effect of intraparticle limitations on temperature

Reaction temperature °C	NO Anderson #	NH_3 Anderson #	O_2 Anderson #
SP1			
150	0.37	0.37	0.37
200	0.42	0.42	0.42
250	0.46	0.46	0.46
300	0.51	0.51	0.51
SP2			
150	0.25	0.25	0.25
200	0.28	0.28	0.28
250	0.31	0.31	0.31
300	0.34	0.34	0.34
SP3			
150	0.56	0.56	0.55
200	0.62	0.62	0.62
250	0.69	o.69	0.69
300	0.75	0.75	0.75
SP4			
150	3.41	3.41	3.41
200	3.81	3.81	3.81
250	4.22	4.22	4.21
300	4.62	4.62	4.62

as BET surface area and pore size distribution influence the amount of internal surface accessible to reactant molecule, in the present study the NO conversion did not correlate with BET surface area, as shown in Figure 3.14. Sample SP1, with a relatively low surface area, had the highest activity whereas SP4 with an intermediate surface area, had the lowest activity. As shown in Figure 3.15, there was no correlation between activity and total pore volume which was obtained by nitrogen adsorption and mercury porosimetry. Sample SP1, with the smallest pore volume, had the highest activity while SP2, with the largest pore volume, had an intermediate activity. There was also no correlation between activity and average pore radius, as shown in Figure 3.16.

3.2.2.4 Activity vs chemical characteristics

Besides the physical characteristics, activated carbons also have chemical characteristics such as acidity or basicity, surface functionality and elemental composition which can influence their catalytic properties.

The activity of the samples correlated inversely with their pH, as shown in Figure 3.17. Since the pH is a measure of the sample's acidity or basicity, it is expected to influence the process of conversion chemistry and kinetics. From the trend observed in pH, it may be stated that NO conversion is favored by more acidic activated carbons.

The acidity or basicity of these samples can be influenced by the type and concentration of mineral matter and the surface oxides. An inverse correlation between the activity of these samples and their mineral matter content was obtained, as shown in Figure 3.18. Sample SP1 had the lowest mineral matter

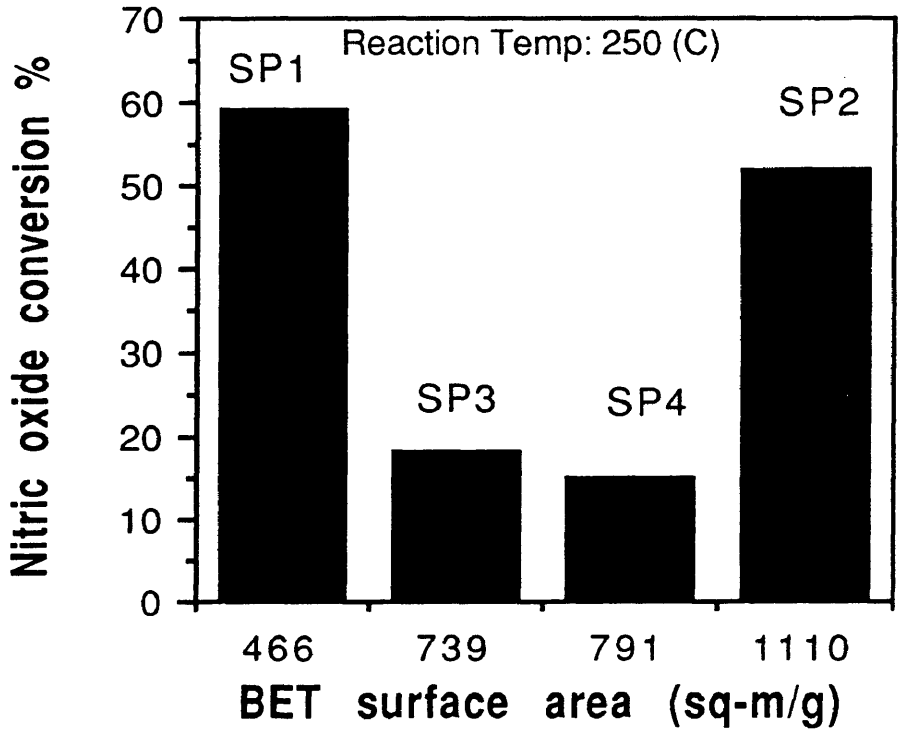

Figure 3.14 Effect of BET surface area on activity

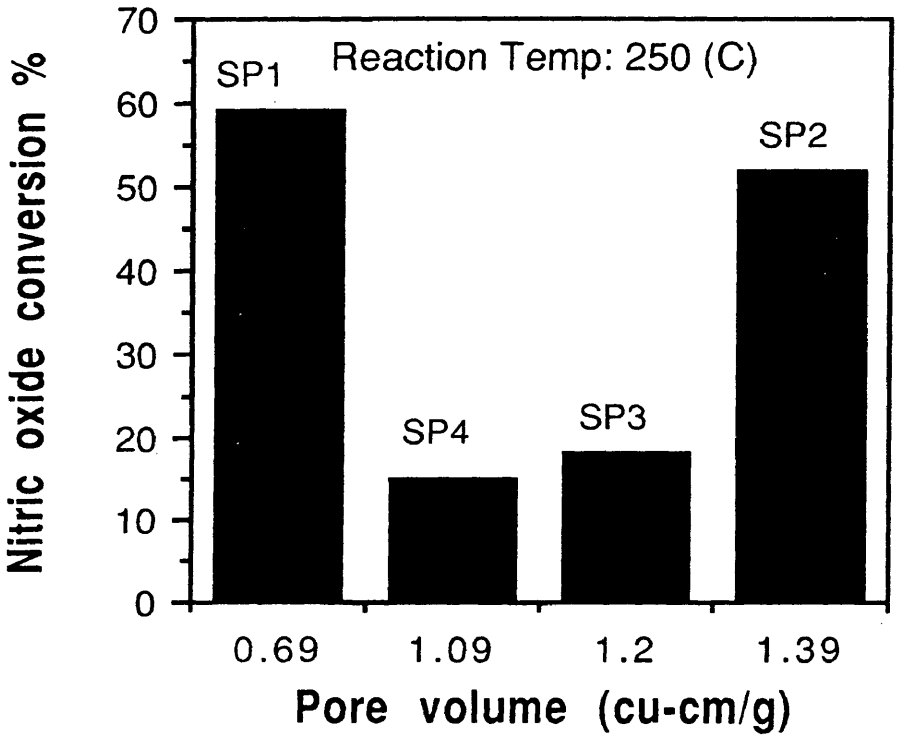

Figure 3.15 Effect of pore volume on activity

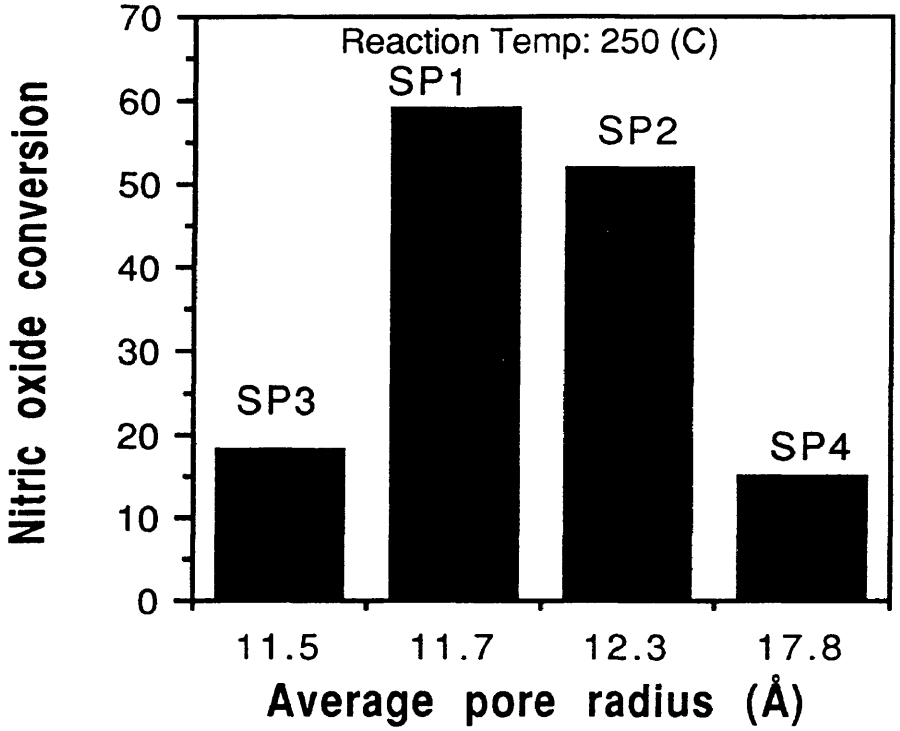

Figure 3.16 Effect of pore radius on activity

ARTHUR LAKES LIBRARY
COLORADO SCHOOL OF MINES
GOLDEN, CO 80401

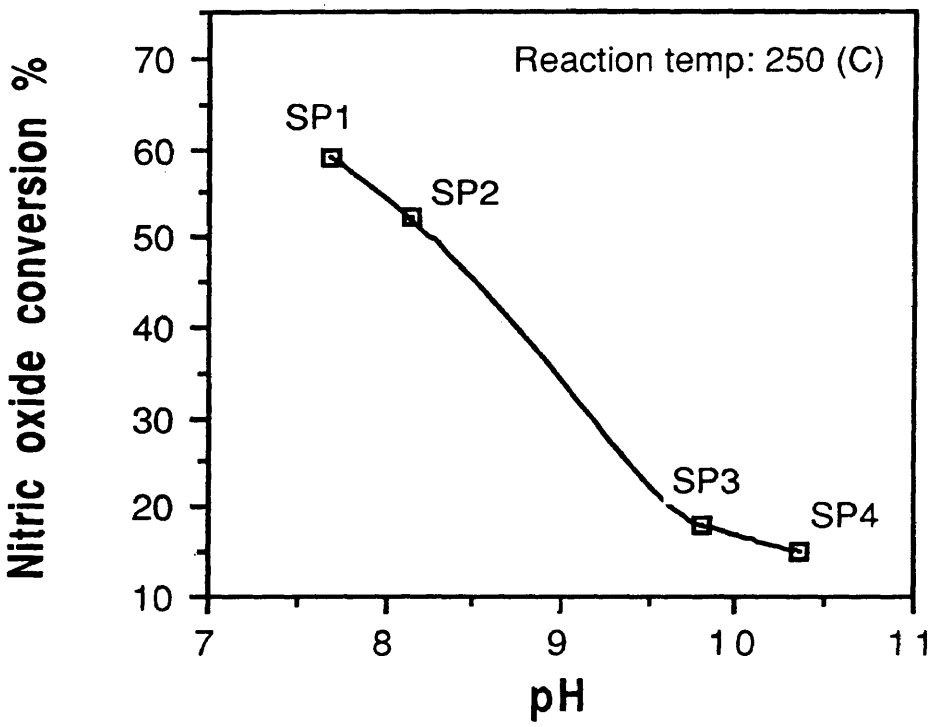

Figure 3.17 Effect of pH on activity

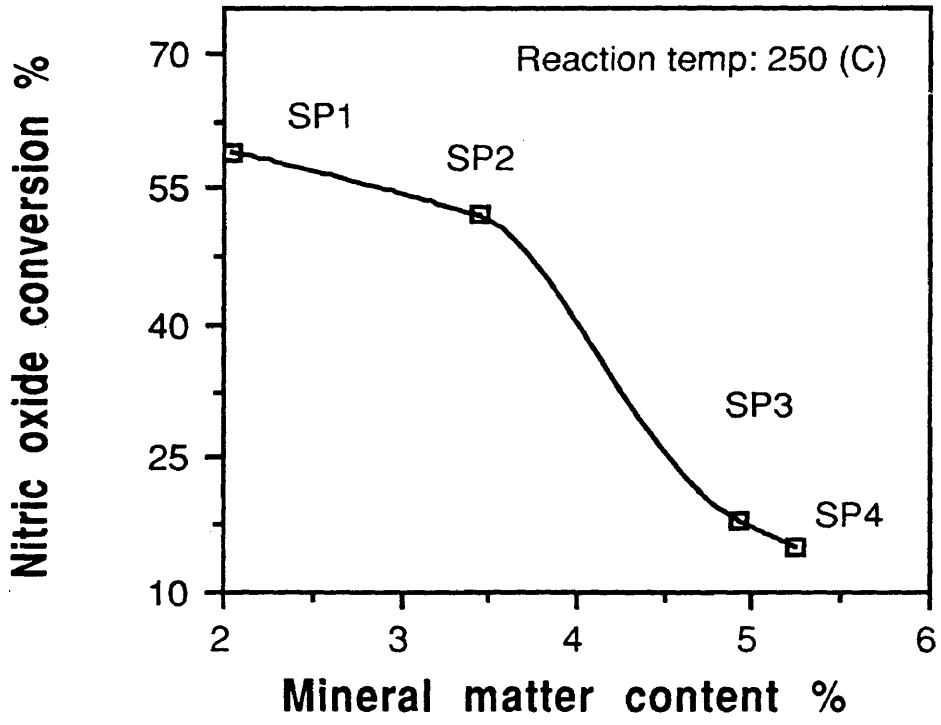

Figure 3.18 Effect of mineral matter on activity

content and SP4 had the highest. On further examination of the mineralogy of these samples, it was found that the presence of CaO, MgO and Na_2O had a negative effect on the NO conversion, as shown in Figure 3.19. The amount of these alkaline metal oxides was lowest in SP1 and highest in SP4. These alkaline metal oxides in the samples made them more basic, as indicated by their pH, which in turn influenced the NO conversion negatively.

It is important to point out that there may also be other minerals present in the samples which could not be identified that may have affected the activity. However, in general, the presence of alkaline metal oxides such as Na_2O, K_2O, CaO and MgO in flue gas has been associated with deactivation of SCR catalysts such as V_2O_5/TiO_2 (7). A comprehensive study of the effects of SCR process for all major poisons encountered in flue gas by Chen et al. (80) confirmed that the poisoning is caused by high basicity. According to Chen and Yang (48), acid sites are the active sites of a typical V_2O_5/TiO_2 SCR catalyst for NO reduction and these sites are destroyed by the presence of alkaline metal oxides. The same conclusion may be relevant for activated carbons.

To further examine whether pH and mineral matter affect activity, SP3 which had shown relatively low activity was washed with distilled water for 24 hrs and then dried in a vacuum oven at 100^{o}C for 24 hrs. The washing reduced the sample's pH from 9.55 to 8.23 and its mineral matter content from 4.92% to 2.31 %. The effect of this treatment on the mineralogy is shown in Figure 3.20. There was about a 20% decrease in the amount of the alkaline metal oxides. As expected, this treatment increased the activity of SP3 by approximately 25 % in the temperature range between 150^{o}C-300^{o}C, as shown in Figure 3.21.

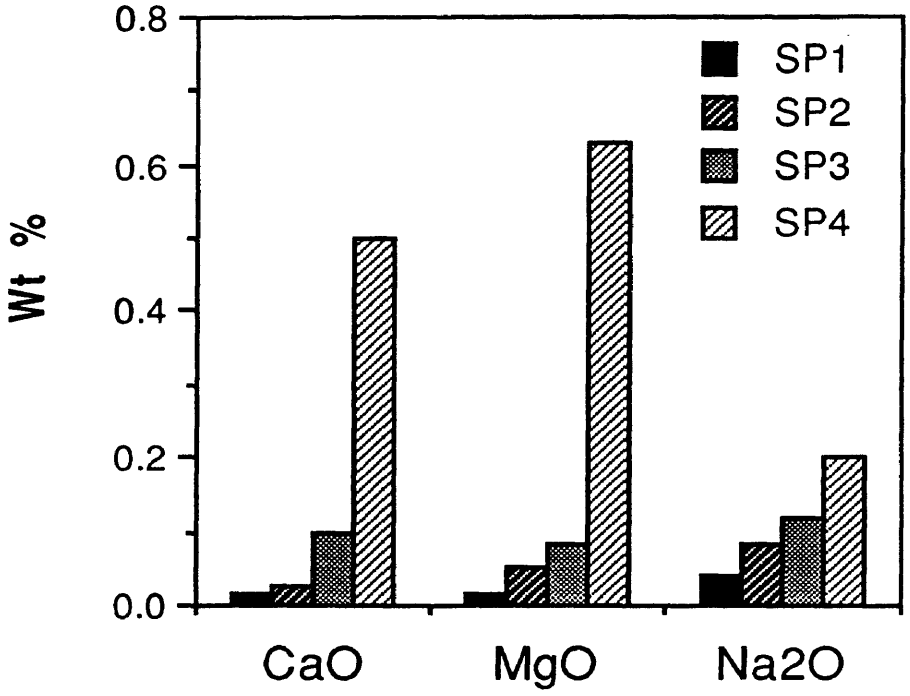

Figure 3.19 Mineral matter content of commercial samples

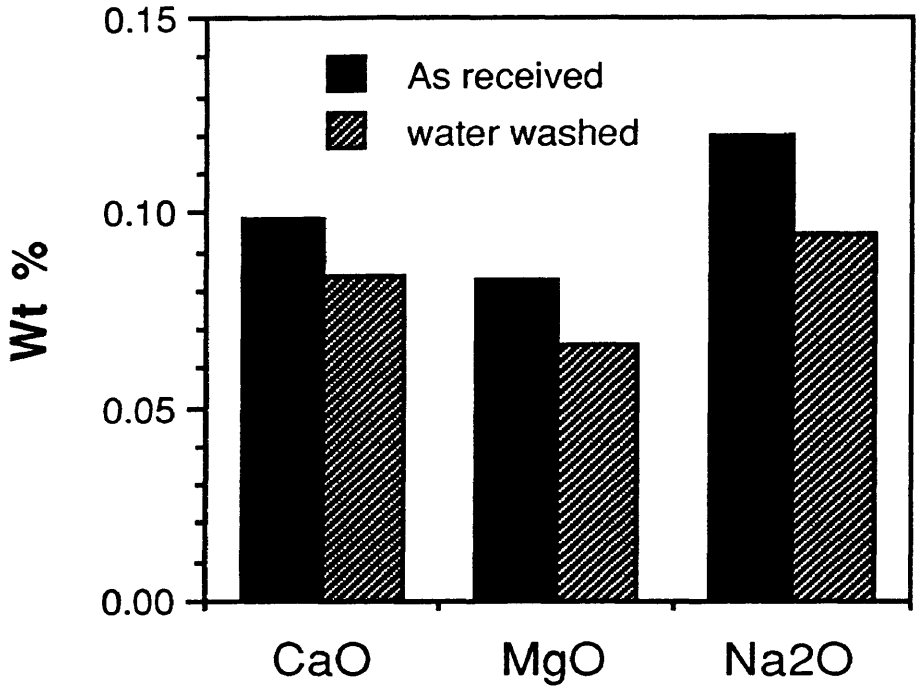

Figure 3.20 Effect of water washing on mineral matter of SP3

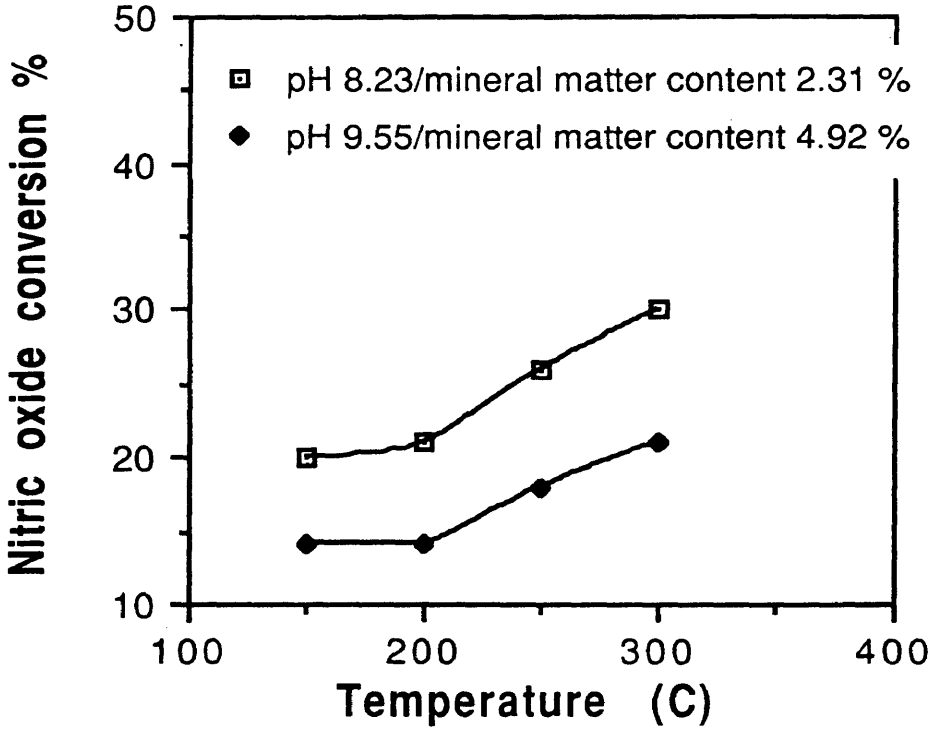

Figure 3.21 Effect of water washing on actvtiy of SP3

Lenz et al. (71) have also reported an increase in the activity of brown coal coke after being treated with hydrochloric acid for mineral matter removal.

The bulk oxygen content of these samples correlated directly with their activity, as shown in Figure 3.22. Such oxygen is possibly associated with surface and mineral oxides. However, SP1, with the highest oxygen content, had the lowest mineral matter content and SP4, with the lowest bulk oxygen content, had the highest mineral matter content. Similar trends were obtained for SP2 and SP3. Therefore, it may be concluded that the bulk oxygen content for these commercial samples represents primarily surface oxides associated with carbon rather than the mineral matter.

As stated earlier, the acidity or basicity of activated carbon is strongly influenced by surface oxides. Carbon-oxygen groups are one of the most important surface oxides in determining surface characteristics (56). These surface oxides can either be acidic or basic. Acidic surface oxides would include carboxyls, phenols and aldehydes, whereas basic surface oxides would include chromenes and pyrones (56,57). The activation temperature for the char (carbonized product) significantly influences the nature of the carbon-oxygen surface complex. Acidic surface oxides are formed when the activation temperature is low (300-500^{o}C); basic surface oxides are formed when the activation temperature is high (800-1000^{o}C) (56). The exact synthesis method for these commercial samples is not known, except that SP1 was activated at a lower temperature as compared to other samples as also indicated by its pH.

Mochida et al. (81) suggested the following scheme for NO and NH3 adsorption:

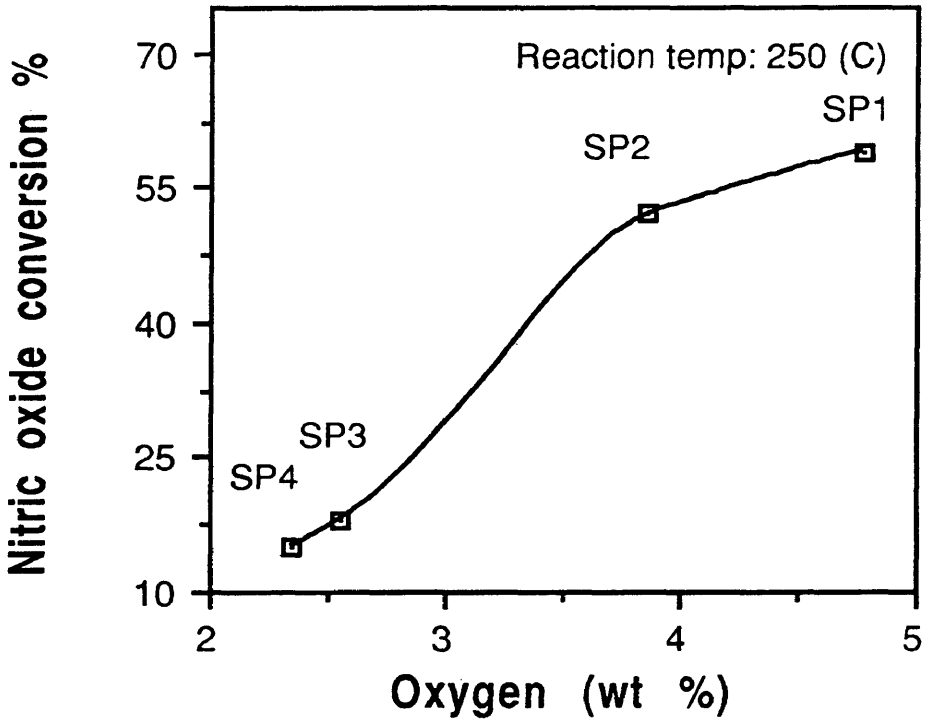

Figure 3.22 Effect of bulk oxygen on activity

$$NO + O{=}Carbon \text{ ----------> } NO_2\text{-Carbon} \quad (3.9)$$

$$NH_3 + HO\text{-Carbon} \text{ ----------> } NH_4O\text{-Carbon} \quad (3.10)$$

Based on this proposal, the NO conversion over activated carbon would be determined by the adsorption of the reactant gases, mainly NO and NH_3, on the surface oxides of the activated carbon. This observation is in agreement with the results from the present study which also suggest that surface oxides are important for NO conversion.

Other heteroatoms such as nitrogen and sulfur are also associated with activated carbons. These heteroatoms are basically derived from the precursor material and become a part of the chemical structure of activated carbon (56). The nitrogen content of these samples did not correlate with their activity as shown in Figure 3.23. However, SP1 had the highest nitrogen content and the highest activity of all the samples. Contrary to this finding, Juentgen and Kuehl (69) reported a correlation between the activity of activated carbon and its nitrogen content. Activated carbons prepared from nitrogen-containing materials such as polyacrylonitrite, urea resin, malamine resin and aniline-formaldehyde have shown higher activity for SO_2 removal but not for NO reduction by NH_3 (82). Although not shown here, the activity of these commercial samples did not correlate with their sulfur content.

3.2.3 Ammonia oxidation

Eldridge and Kittrell (50) reported a decrease in the activity of V_2O_5/Al_2O_3 at higher temperatures (>400^oC) due to the side reaction of NH_3 with O_2 thus

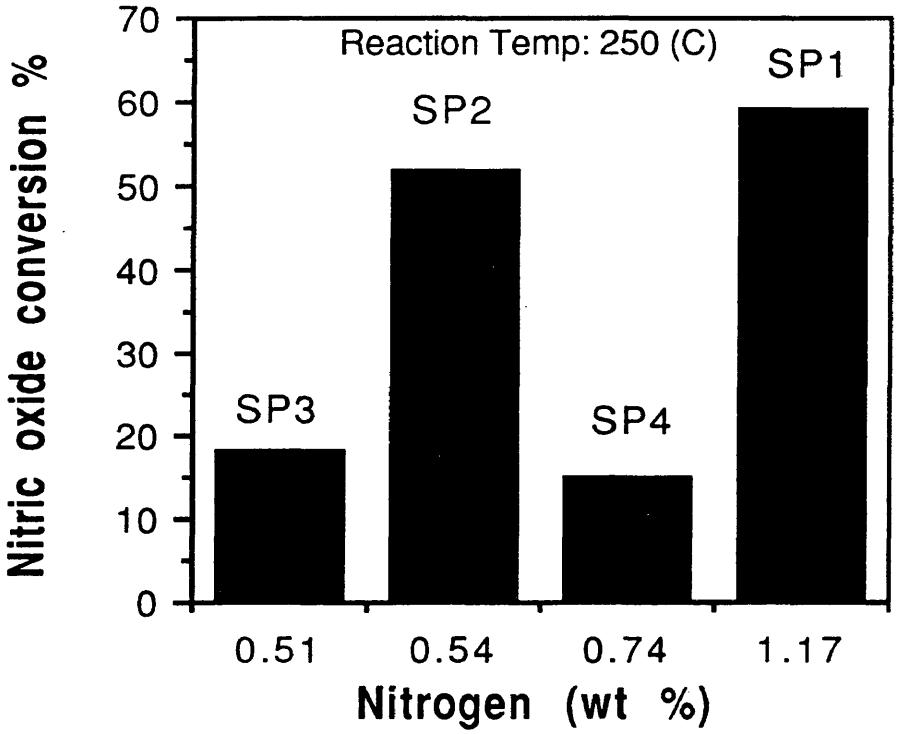

Figure 3.23 Effect of nitrogen on activity

forming NO. The activation energy for NH_3 oxidation was found to be 4 times that of NO reduction. All the commercial samples were tested for the non-selective formation of NO and N_2O by reacting NH_3 with O_2 in the absence of reactant NO (Reaction 3.2 and Reaction 3.3, equilibrium calculations are provided in Appendix B). There was no formation of NO or N_2O for SP2, SP3 and SP4 . However, there was a slight formation of NO for SP1, as shown in Figure 3.24, amounting to approximately 1 ppm at 300°C. These results suggested that all the activated carbon samples tested were very selective for NO reduction under the given reaction conditions.

3.2.4 Nitric oxide reduction by activated carbon alone

Bedjai et al. (83) reported high NO conversion using activated carbon at temperatures greater than 500°C:

$$2NO + C \text{ ----------> } N_2 + CO_2 \qquad (3.11)$$

Edward (84) also reported over 80 % conversion of NO by highly graphitized carbon black around 1000°C. Sample SP1, which showed the highest activity of all the commercial samples for Reaction 3.1 was used to study the NO reduction by activated carbon alone between temperatures of 150-300°C. The NO conversion was found to be extremely low in this temperature range, as shown in Figure 3.25. At 150°C, the conversion was about 3 % and at 300°C, it was about 6 %. At temperatures around 150-200°C, about one hour was required to attain steady state. Activated carbon, due to its high surface area, is

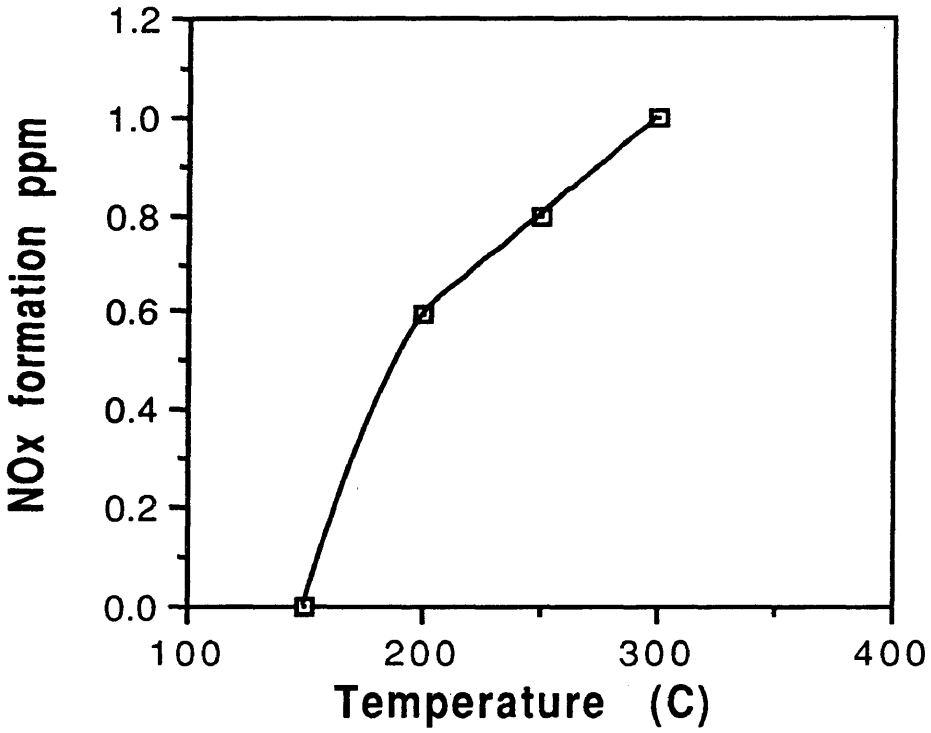

Figure 3.24 Ammonia oxidation over SP1

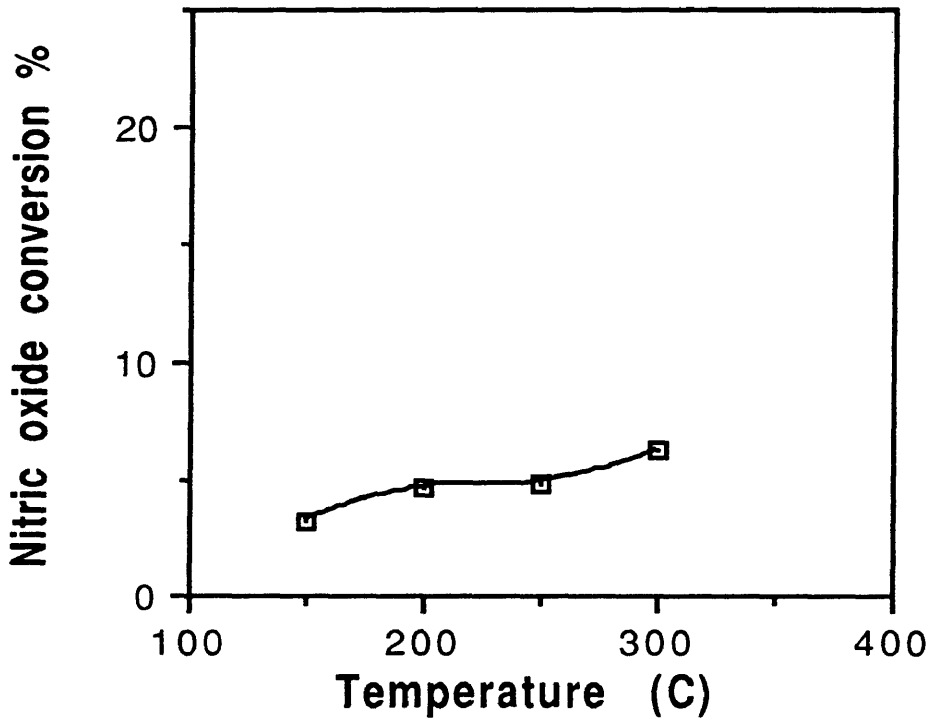

Figure 3.25 Nitric oxide reduction by SP1

a very good adsorbent. The initial measured decrease in NO concentration is consequently attributed primarily to its adsorption and not its removal by chemical reaction. As adsorption is an exothermic process, the adsorptive capacity of activated carbons decreases when the temperature is increased. In turn, the time required to reach steady state decreased with increasing temperature. At 300^{o}C, this process took about thirty minutes.

3.2.5 Nitric oxide reduction by oxygen and carbon

Sample SP1 was used to study the following reaction:

$$2NO + O_2 + 2C \text{ ----------> } N_2 + 2CO_2 \qquad (3.12)$$

Even in the presence of O_2, the NO reduction was very low and decreased further with increasing temperature, as shown in Figure 3.26. At 150^{o}C, the conversion was about 5% and at 300^{o}C , it was about 1%. Richter et al. (85) also reported the same temperature dependence in the range of 90-150^{o}C. As seen from this figure, the decrease in NO concentration at the outlet was also due to partial oxidation of NO to NO_2 and not only due to NO reduction to N_2.

$$NO + 1/2O_2 \text{ ----------> } NO_2 \qquad (3.13)$$

It is well known that the oxidation of NO to NO_2 is favored at low temperatures which may partially account for the temperature dependence. At low temperatures (150-200^{o}C), it took about three hours before steady state

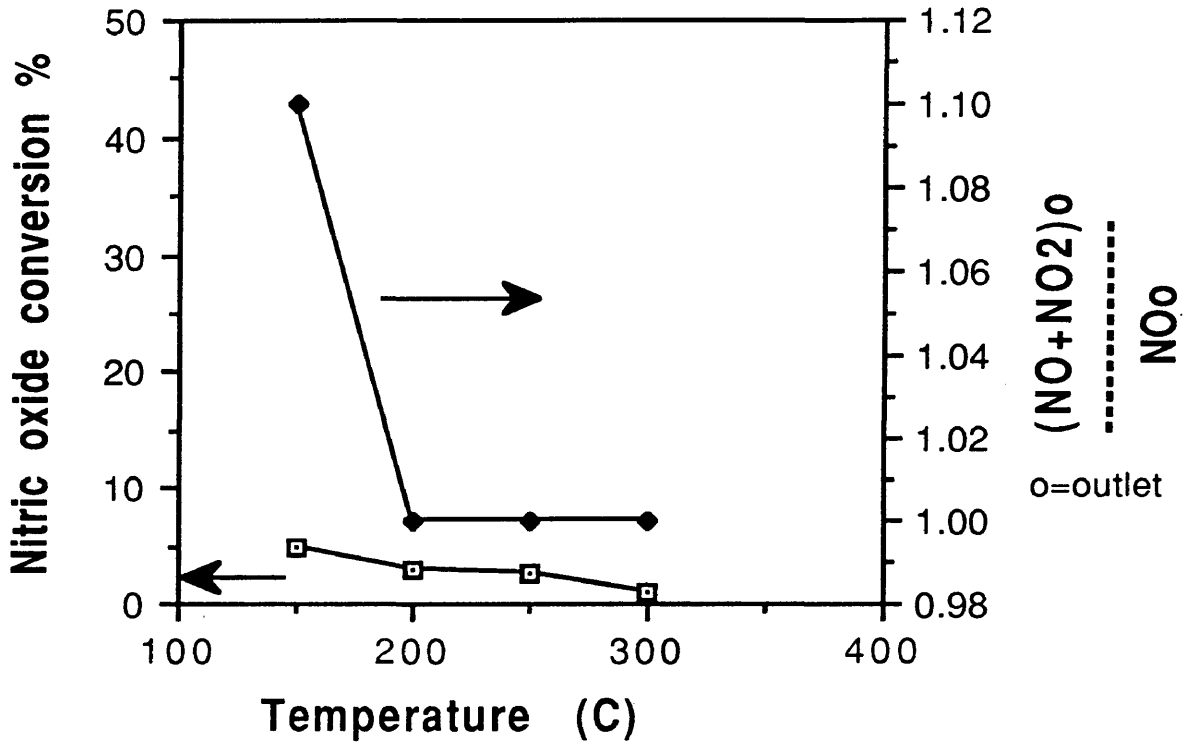

Figure 3.26 Nitric oxide conversion in presence of oxygen over SP1

appeared. This was due to the presence of O_2 which facilitated the adsorption of NO on activated carbon. This is discussed in more detail in Chapter 4.

3.3 Conclusions

The activity of commercial activated carbons did not correlate with physical properties such as BET surface area and pore structure. Rather, chemical properties affected the NO reduction by NH_3. Low pH activated carbons had higher activity for NO reduction implying that activated carbons which were more acidic in nature were better catalysts for NO reduction. The presence of mineral matter such as Na_2O, K_2O and CaO was unfavorable for NO reduction activity, but higher surface oxygen content increased the activated carbon's activity. Discrepancies between the expected performance of an activated carbon, based upon surface area and pore size distribution, and actual performance can be explained by these chemical properties.

The contribution of side reactions towards NO conversion over activated carbon was very low under the conditions employed in this study.

Chapter 4

EFFECT OF SPACE VELOCITY, GAS PHASE OXYGEN AND AMMONIA ON NITRIC OXIDE REDUCTION OVER ACTIVATED CARBON CATALYST

For a given system, the catalyst activity would depend on the reactants' concentration, reaction temperature, and space velocity. The effect of temperature on NO conversion has already been discussed in Chapter 3. The objective of the work presented in this chapter was to study the effects of: space velocity; gas phase O_2; and NH_3/NO ratio on NO reduction over activated carbon.

Space velocity (the ratio of the feed rate in volumetric units to the volume of reactor) is a very crucial design parameter in a SCR system. For a gas turbine system, very high space velocities (about 60,000 hr^{-1}, STP) are used and for a fossil fuel system, the catalyst operates at low space velocities (5000-10,000 hr^{-1}, STP). The effect of varying the space velocity was investigated simultaneously with the effects of O_2.

Oxygen is inherently present in the flue gas stream, but plays a very important role in NO reduction using NH_3. This role was investigated by studying the effects of varying O_2 concentration on NO conversion. For this purpose, the following three reactions were studied with and without activated carbon:

$$6NO + 4NH_3 \text{ ----------> } 5N_2 + 6H_2O \quad (4.1)$$

$$4NO + 4NH_3 + O_2 \text{ ----------> } 4N_2 + 6H_2O \quad (4.2)$$

$$6NO_2 + 8NH_3 \text{ ----------> } 7N_2 + 12H_2O \quad (4.3)$$

The role of O_2 was further investigated by studying the adsorption of reactants (NO,NH_3 and NO_2) on activated carbon at various O_2 concentrations. The effect of the NH_3/NO ratio on NO conversion was also investigated by changing NH_3 concentration.

As stated in Chapter 2, V_2O_5/TiO_2 is one of the most commonly used commercial catalysts for SCR, with typical operating temperatures of 350-450°C. But due to its high activity, it can also oxidize SO_2 (present in flue gas) to SO_3 which can react with NH_3 to form ammonium salts, thus creating problems at down-stream equipment. Activated carbon and commercial V_2O_5/TiO_2 catalysts were compared for their activity under identical experimental conditions.

4.1 Experimental

4.1.1 Gases

In addition to the gas mixtures described in Chapter 3, 0.3 vol % NO_2/He and 3.0 vol% NH_3/He supplied by Liquid Carbonic were also used in this study.

4.1.2 Catalysts

Sample SP1, which showed the highest activity of the commercial activated carbon samples in a previous study, was used for conversion and adsorption

studies. The other commercial catalyst (V_2O_5/TiO_2) was supplied by United Catalyst Inc.

4.1.3 Characterization

The characterization of SP1 has already been discussed in Chapter 3. The catalyst V_2O_5/TiO_2 was characterized using nitrogen adsorption and mercury porosimetry. These techniques have been discussed in Chapter 3.

4.1.4 Activity measurements and procedure

The equipment setup and the procedure for measuring NO conversion have been described in Chapter 3.

4.1.5 Reaction conditions for activity measurements

Prior to each experiment, the catalyst was heated at 300°C under a He flow to remove any adsorbed moisture. In all the experiments, the reaction temperature varied from 150-300°C and the total gas flow rate was maintained at 1000 SCCM.

4.1.5.1 The effects of space velocity and oxygen

The space velocity was varied from 10,000 - 40,000 hr^{-1}. It was calculated using the following equation:

$$\text{Space velocity} = \frac{q}{W.\rho_b^{-1}.} \qquad [4.1]$$

where q is the volumetric flow rate of feed at STP, W is the mass and ρ_b is the bulk density of the catalyst.

Simultaneously, the O_2 concentration was varied from 0-8 % with an increment of 2 %. The experiments without O_2 represented Reaction 4.1 and those with O_2 represented Reaction 4.2. The NO and NH_3 concentrations were each 700 ppm.

The NO_2 reduction using NH_3 (Reaction 4.3) was investigated using 700 ppm of each reactant gas at a space velocity of 10,000 hr^{-1}.

4.1.5.2 The effect of ammonia

The effect of NH_3 on NO conversion was studied using 700 ppm of NO and 4 % of O_2 (Reaction 4.2), at a space velocity of 10,000 hr^{-1}. The NH_3 concentration was varied from 700 ppm to 1050 ppm.

4.1.5.3 Comparison of activated carbon with vanadia/titania

Sample SP1 was compared with V_2O_5/TiO_2 catalyst at two space velocities: 7,500 hr^{-1} and 10,000 hr^{-1}, respectively. The NO and NH_3 concentrations were 700 ppm and O_2 concentration was 4 %.

4.1.6 Adsorption measurements

Adsorption studies were performed using a Scientific Instrument thermogravimetric analyzer attached to a VG, Micromass mass spectrometer (TGA/MS). Prior to gas adsorption, the sample was heated at 100^oC under a He flow for thirty minutes to remove moisture. The sample was then

equilibrated to a desired temperature. Appropriate gas was then introduced in the system until the sample surface was saturated. Subsequent to adsorption, the sample was heated to 250°C at a rate of 10°C/minute. The weight changes were monitored by TGA and the desorbed gases by MS.

4.1.7 Conditions for adsorption measurements

In all TGA/MS experiments, the temperature varied from 50-200°C unless specified otherwise, the total gas flow rate was 400 SCCM, and the sample weight was 15 mg. The NO_2 , NO concentrations were 1500 ppm and NH_3 concentration was 10,000 ppm. In the experiments for NO and NH_3 adsorption, O_2 concentration was varied from 0-15 % and in the case of NO_2, O_2 was not used.

4.2 Results

4.2.1 The effects of space velocity and oxygen

Results for NO conversion as a function of space velocity and gas phase O_2 concentration at 150°C, 200°C, 250°C and 300°C are shown in Figures 4.1-4.4. The NO conversion was effected by space velocity; as expected it increased with decreasing space velocity. This effect was more prominent at low space velocities. This is understandable because changing the space velocity from 40,000 hr^{-1} to 20,000 hr^{-1} was equivalent to changing the catalyst weight from 1.05 g to 2.1 g (bulk density of 0.7 g/cm^3) at a given flow rate, whereas changing the space velocity from 20,000 hr^{-1} to 10,000 hr^{-1} was equivalent to changing the catalyst weight from 2.1 g to 4.2 g. The effect of

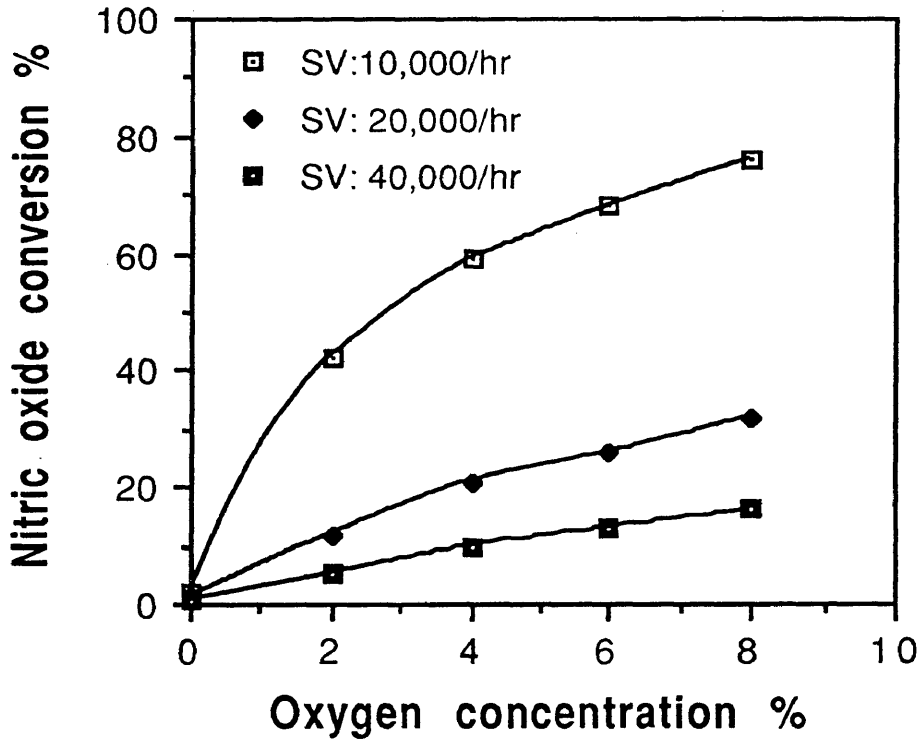

Figure 4.1 Effect of oxygen and space velocity on activity at 150C

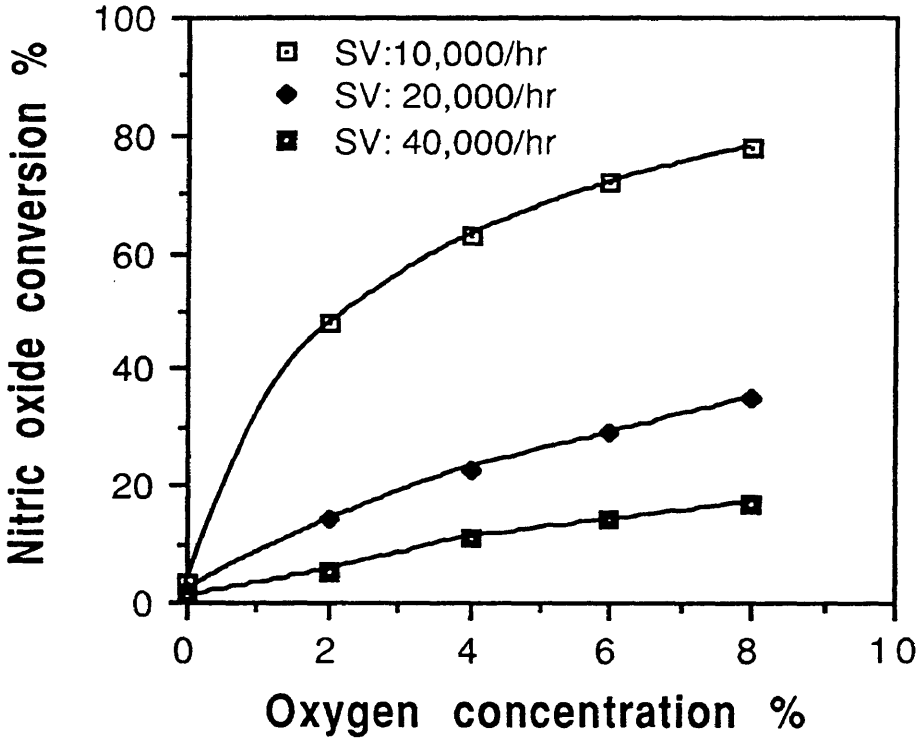

Figure 4.2 Effect of oxygen and space velocity on activity at 200C

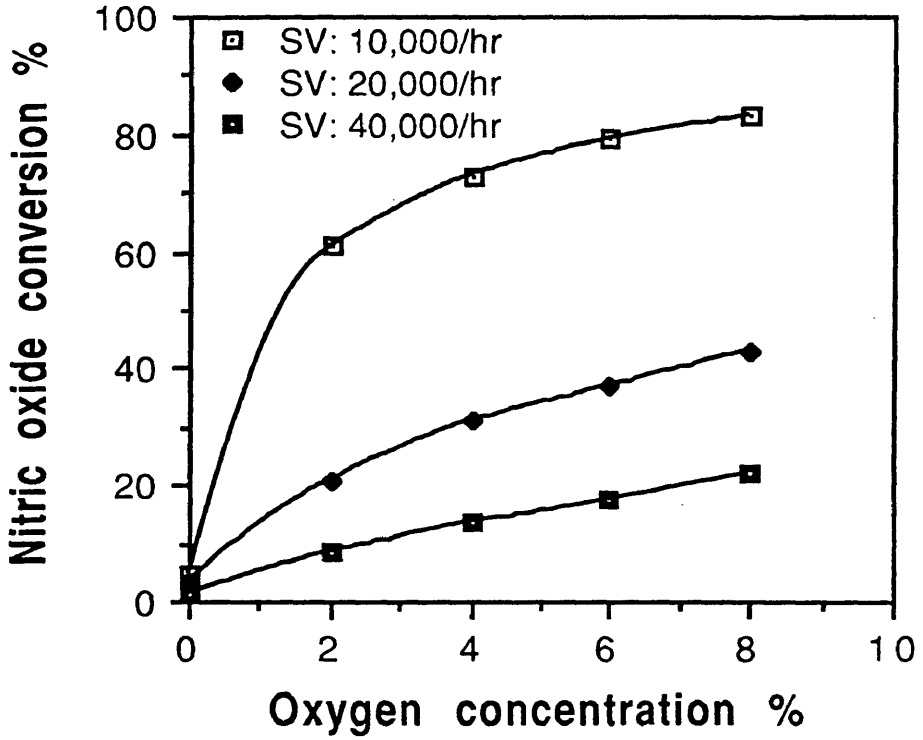

Figure 4.3 Effect of oxygen and space velocity on activity at 250C

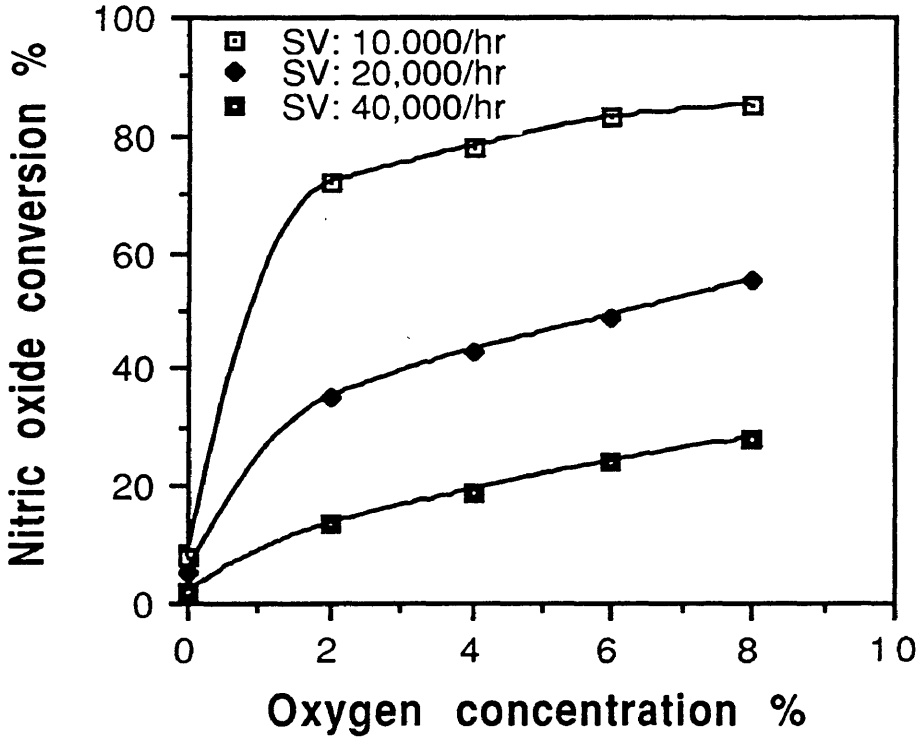

Figure 4.4 Effect of oxygen and space velocity on activity at 300C

space velocity was also greater at low temperatures. For example, changing the space velocity from 20,000 hr^{-1} to 10,000 hr^{-1} almost tripled the NO conversion at 150°C, whereas it only doubled at 300°C.

The effect of O_2 concentration on the NO conversion was similar for all temperatures (Figures 4.1 - 4.4). The NO conversion was very low in the absence of O_2 (Reaction 4.1). The NO conversion increased considerably when O_2 was introduced. The extent of improvement tended to decrease with an increase in O_2 concentration. For example, at a space velocity of 10,000 hr^{-1} and at a reaction temperature of 150°C, the NO conversion increased from 2.2 % to 42.5 % when the O_2 concentration was changed from 0 to 2 %; and it only increased from 68 % to 76 % when the O_2 concentration was increased from 6 % to 8 %. The incremental increase in conversion with increasing O_2 concentration was also not substantial at higher reaction temperatures. For example, at a space velocity of 10,000 hr^{-1} when the O_2 concentration was increased from 2 % to 8 % the NO conversion increased from 43 % to 76 % at 150°C whereas it only increased from 72 % to 85 % at 300°C.

Figure 4.5 shows the space velocity as a function of conversion using Equation 3.5 for the reaction temperatures of 150-300°C. As seen from this figure, straight lines were obtained for all the reaction temperatures which suggested that the reaction order was one with respect to NO.

Reduction of NO_2 using NH_3 in the absence of O_2, as a function of temperature, is shown in Figure 4.6. Even without O_2, the NO_2 conversion was very high and increased further with increasing temperature. At 150°C, the conversion was about 80 % and at 300°C, it was about 95 %.

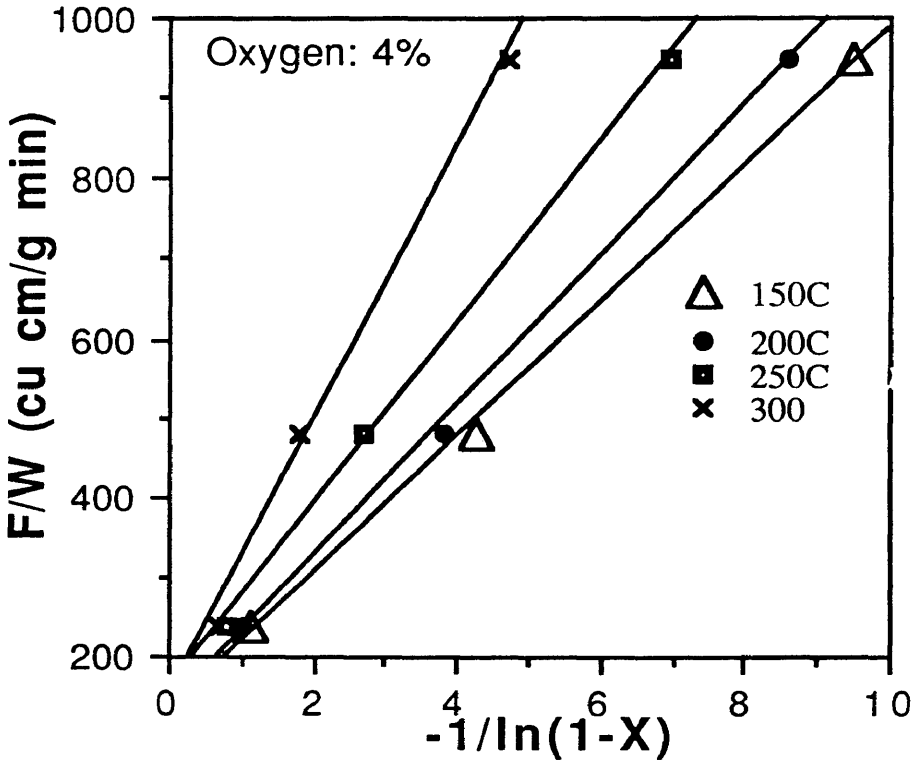

Figure 4.5 Determination of reaction rate order with respect to nitric oxide

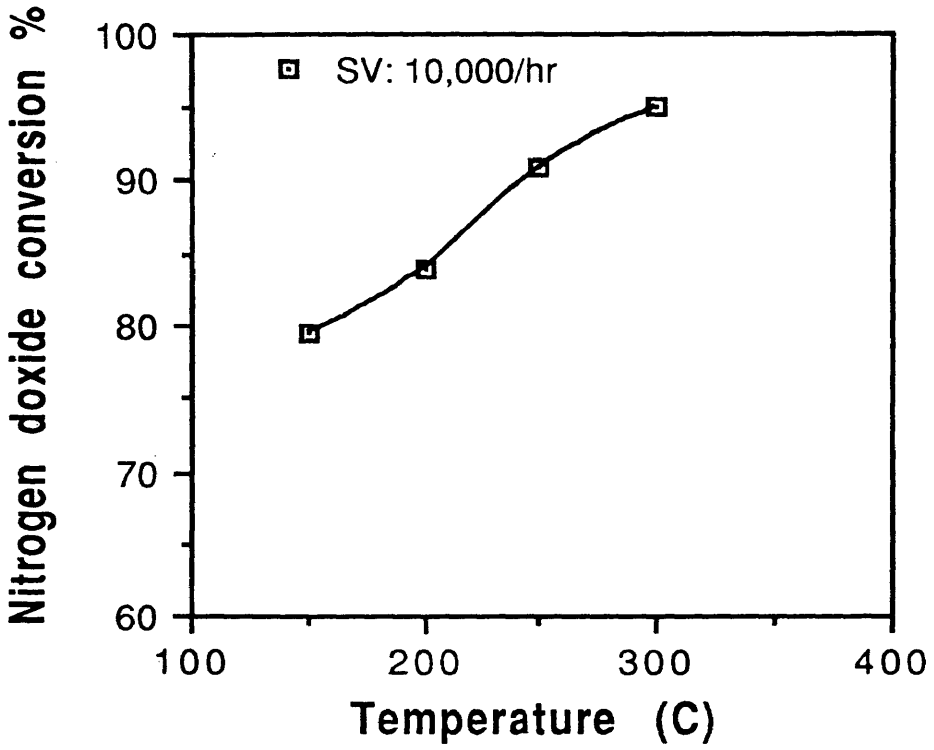

Figure 4.6 Nitrogen dioxide reduction using ammonia

Figure 4.7 shows the comparison of NO_2 conversion with NO conversion at various O_2 concentrations, as a function of temperature at a space velocity of 10,000 hr^{-1}. NO_2 conversion was higher than NO conversion with or without O_2. But with increasing O_2 concentration, NO conversion approached that of NO_2 for reaction temperatures in the range of 150-300°C.

NO reduction using NH_3 with and without O_2 was zero when activated carbon was not present. Even increasing the reaction temperature had no effect on NO conversion in the absence of activated carbon. However, NO_2 reduction using NH_3 was quite significant even without activated carbon, as shown in Figure 4.8, although not as high as when activated carbon was present. NO_2 conversion was about 45%, at 150°C and about 58 %, at 300°C without activated carbon compared with 80 % and 95 % in the presence of activated carbon.

The TGA data pertaining to NO adsorption on activated carbon using various O_2 concentrations at temperatures of 50-200°C is shown in Figure 4.9. As adsorption of NO is an exothermic process, the amount of adsorption decreased with increasing temperatures. Above 200°C, the amount of reactants that were adsorbed was below the detection limit. The amount of NO adsorbed was very low without O_2 and increased along with increasing O_2 concentration. At 50°C, the amount of NO adsorbed without O_2 was about 10 mg/g-sample and it was about 65 mg/g-sample with 15 % O_2. It was determined from separate experiments that the weight gained by the sample due to adsorption (at various O_2 concentration) was a fair representation of the NO-O_2 system and not just because of variation in O_2 concentration.

ARTHUR LAKES LIBRARY
COLORADO SCHOOL OF MINES
GOLDEN, CO 80401

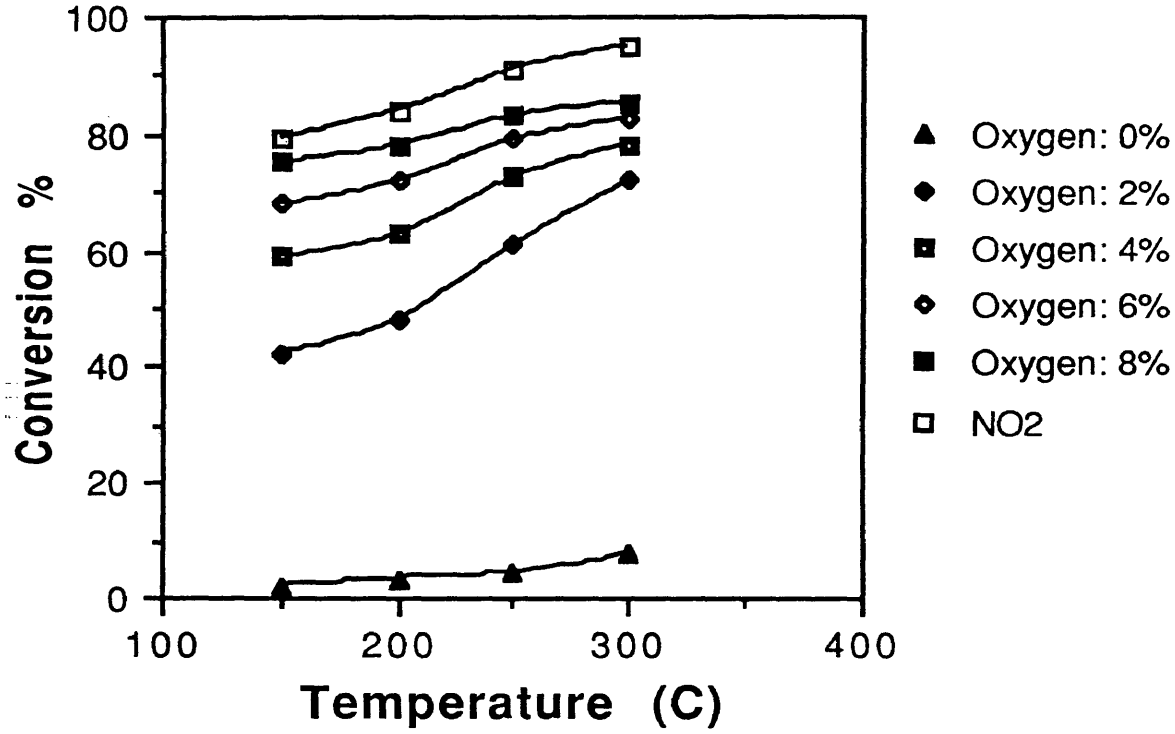

Figure 4.7 Comparison of NO, NO/O2 and NO2 conversion

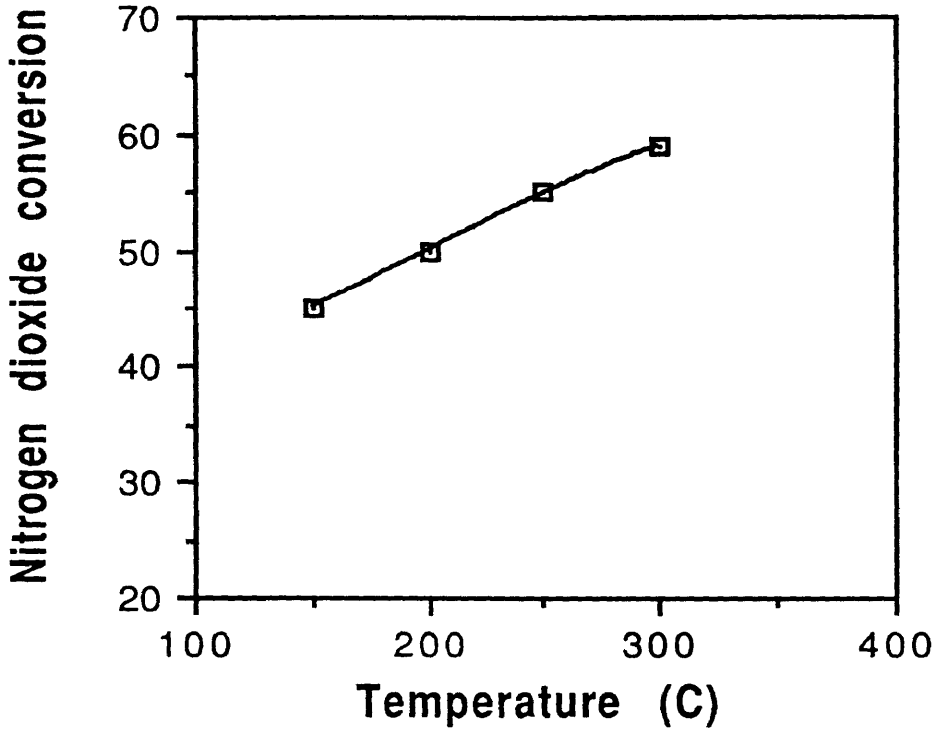

Figure 4.8 NO2 reduction using NH3 without activated carbon

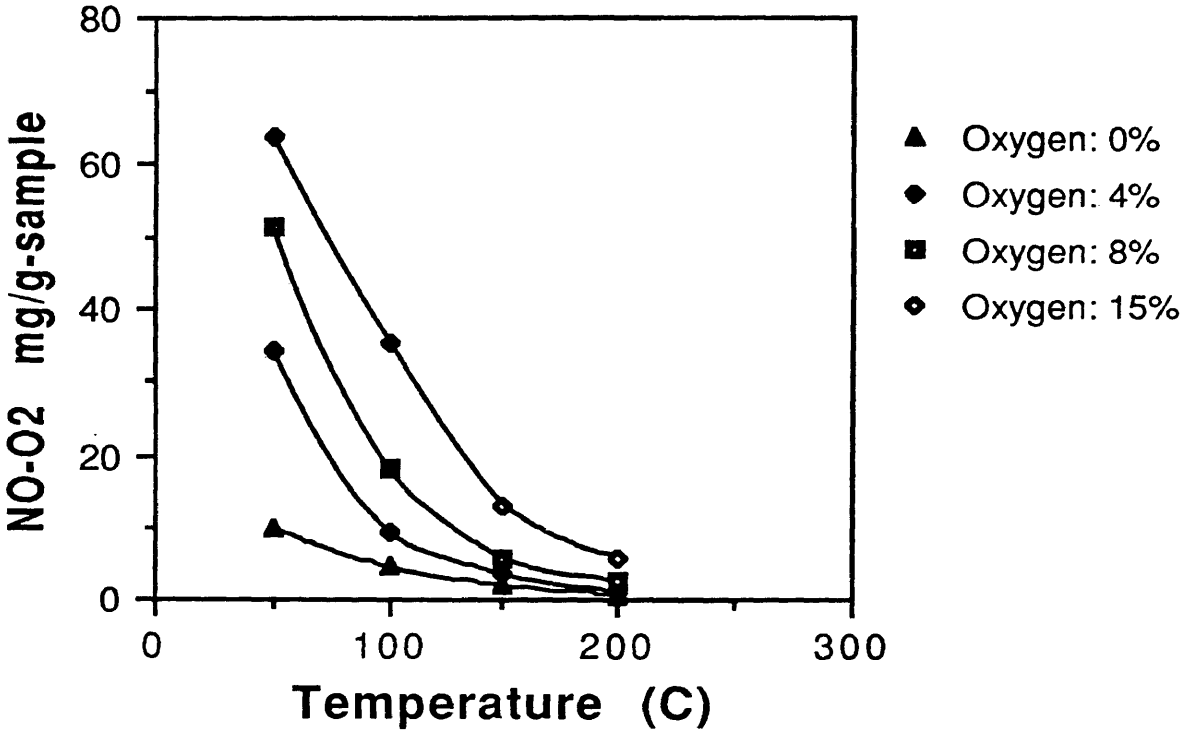

Figure 4.9 The effect of oxygen on nitric oxide adsorption

The MS data for desorption of surface complexes on subsequent heating is shown in Figure 4.10. The data is only shown for surface complexes formed by NO adsorption at 50°C for various O_2 concentrations. The amount of surface complexes decreased with increasing adsorption temperatures therefore the surface complexes formed at higher adsorption temperatures could not be detected by MS upon desorption. Upon desorption, the main surface complex was identified as NO_2. Increasing the O_2 concentration increased the amount of surface complexes as indicated by the amount of NO_2 evolved for various O_2 concentration.

The NO_2 adsorption was quite substantial even without O_2, as shown in Figure 4.11. As expected, NO_2 adsorption decreased with increasing temperature. A comparison of NO_2 adsorption with NO adsorption (at various O_2 concentrations) shows that the amount of NO_2 adsorbed was considerably more than the amount of NO adsorbed with or without O_2, as shown in Figure 4.12.

The TGA data on NH_3 adsorption on activated carbon using various O_2 concentrations at temperatures of 50-150°C is shown in Figure 4.13. As can be seen, the presence of O_2 did not affect NH_3 adsorption.

4.2.2 The effect of ammonia

The relationship between the NO conversion and inlet NH3/NO ratio is shown in Figure 4.14. It can be seen that both conversions (NH3/NO:1 and NH_3/NO: 1.5) as a function of temperature were nearly identical implying that an excess of NH_3 had no affect on conversion under the experimental conditions.

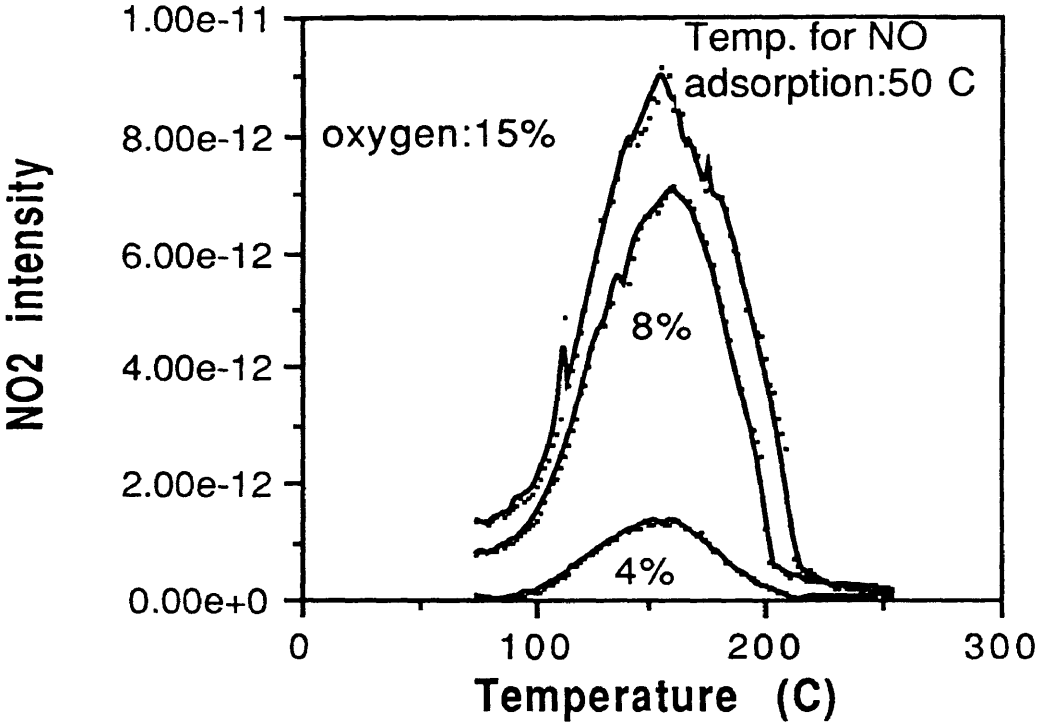

Figure 4.10 NO2 desorption profiles for various O2 concentrations

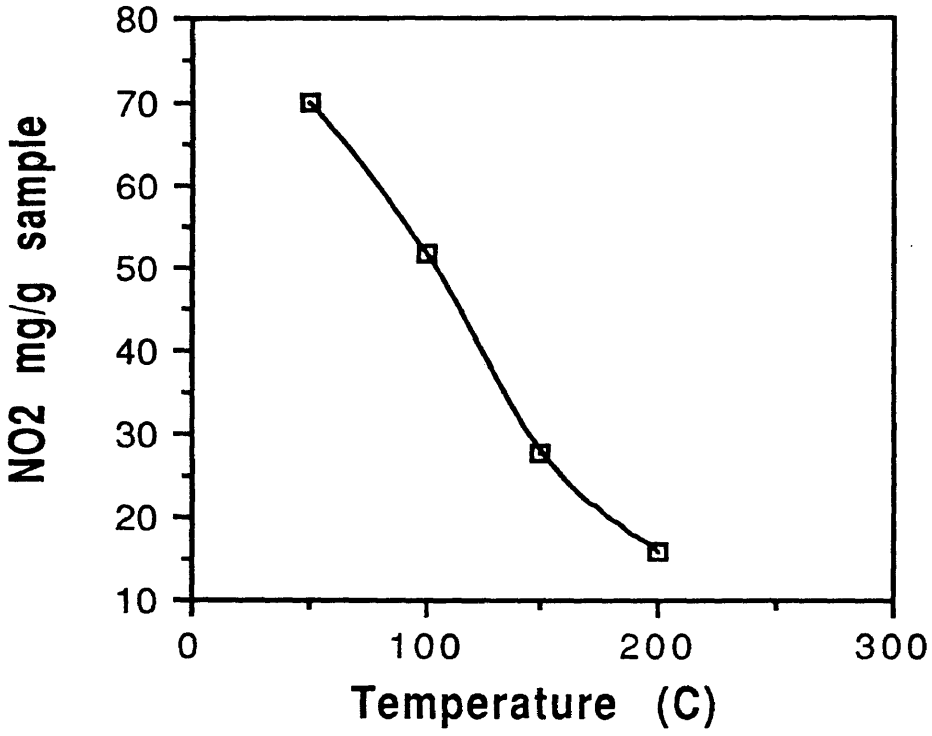

Figure 4.11 Nitrogen dioxide adsorption

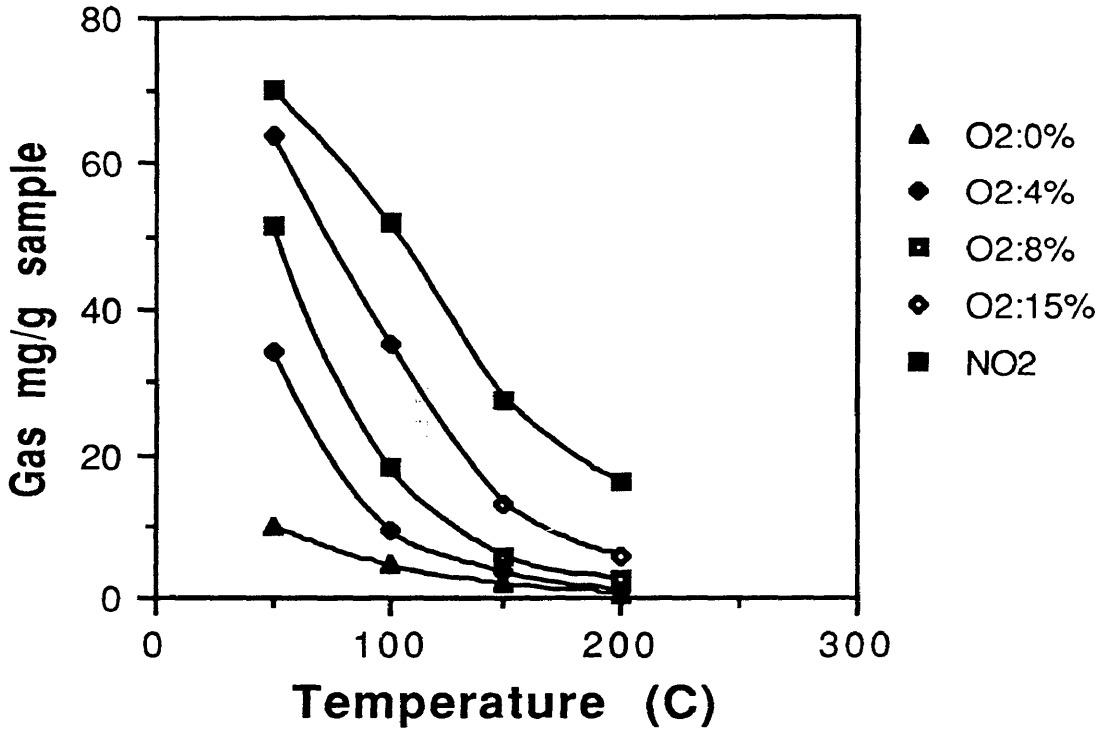

Figure 4.12 Comparison of NO2 and NO/O2 adsorption

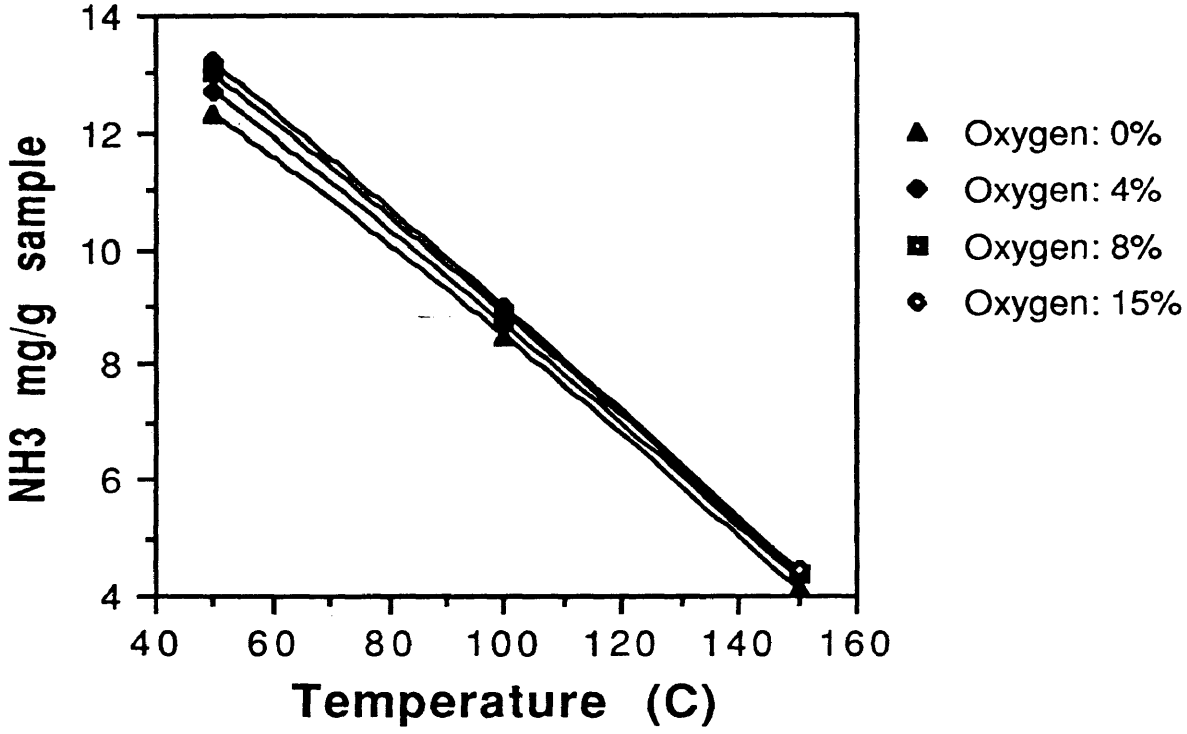

Figure 4.13 NH3 adsorption at various O2 concentrations

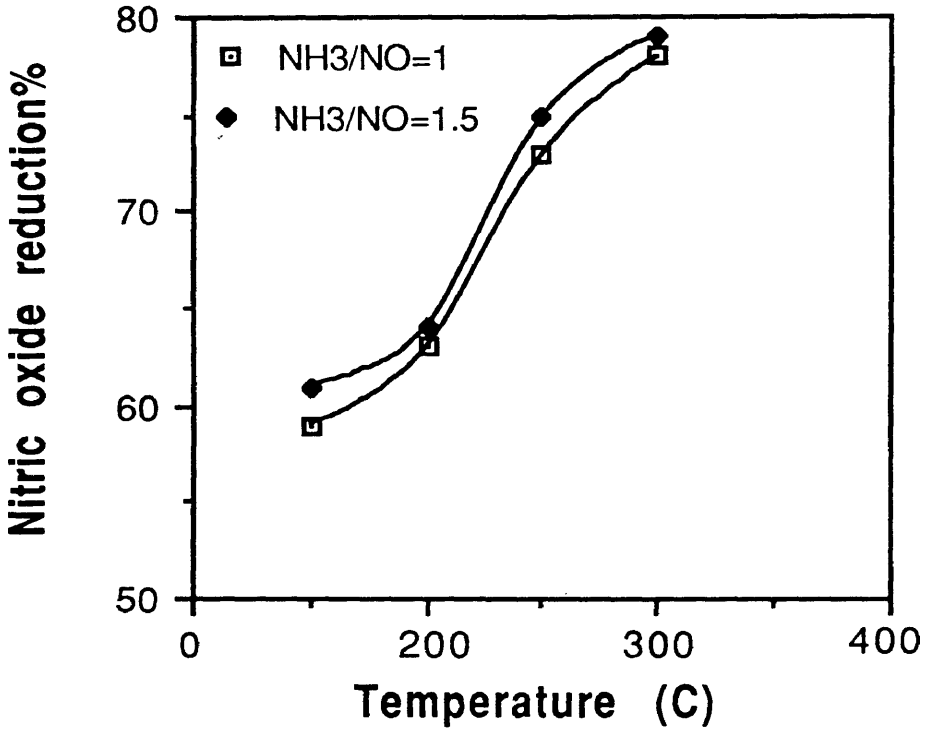

Figure 4.14 Nitric oxide conversion as a function of NH3/NO ratio

4.2.3 Comparison of activated carbon with vanadia/titania

Sample SP1, which had the highest conversion of all the commercial samples was compared with V_2O_5/TiO_2 for NO reduction. The characterization data for V_2O_5/TiO_2 from nitrogen adsorption and mercury porosimetry is presented in Tables 4.1 and 4.2. The catalyst V_2O_5/TiO_2 had a BET surface area of about 34 m^2/g and was predominantly non-microporous with an average pore radius of 170 Å.

At temperatures around 150°C, SP1 proved to be a better catalyst at various space velocities, as shown in Figures 4.15 and 4.16. However, at temperatures higher than 150°C,V_2O_5/TiO_2 showed higher activity.

4.3 Discussion

4.3.1 The effects of space velocity and oxygen

The effect of space velocity was as expected: the NO conversion was increased when space velocity was reduced.

Several authors, using different catalysts, have pointed out that the presence of O_2 has a considerable effect on NO conversion (86), although no explanation has been given for the enhancement of the reaction rate by O_2. Markvart and Rour (87) studied the effect of oxygen on the catalytic reaction over a Pt catalyst. In the presence of O_2, the same conversion values were attained at appreciably lower temperatures than those in the absence of O_2. Juntgen and Kuhln (69) also reported strong enhancement of NO conversion with inclusion of O_2 when using char. In the present study, the need to have gas phase O_2 present for NO reduction (Figures 4.1-4.4) and NO adsorption (Figure 4.9) suggests that

Table 4.1 Vanadia/titania characterization using nitrogen adsorption at 77 K

BET surface area m^2/g	Micropore volume cm^3/g	Micropore surface area m^2/g	Average pore radius Å
34	-	0.0832	170

Table 4.2 Vanadia/titania characterization using mercury porosimetry

Macro volume cm^3/g	Macro surface area m^2/g	Meso volume cm^3/g	Meso surface area m^2/g
0.51	12.3.	0.04	4.1

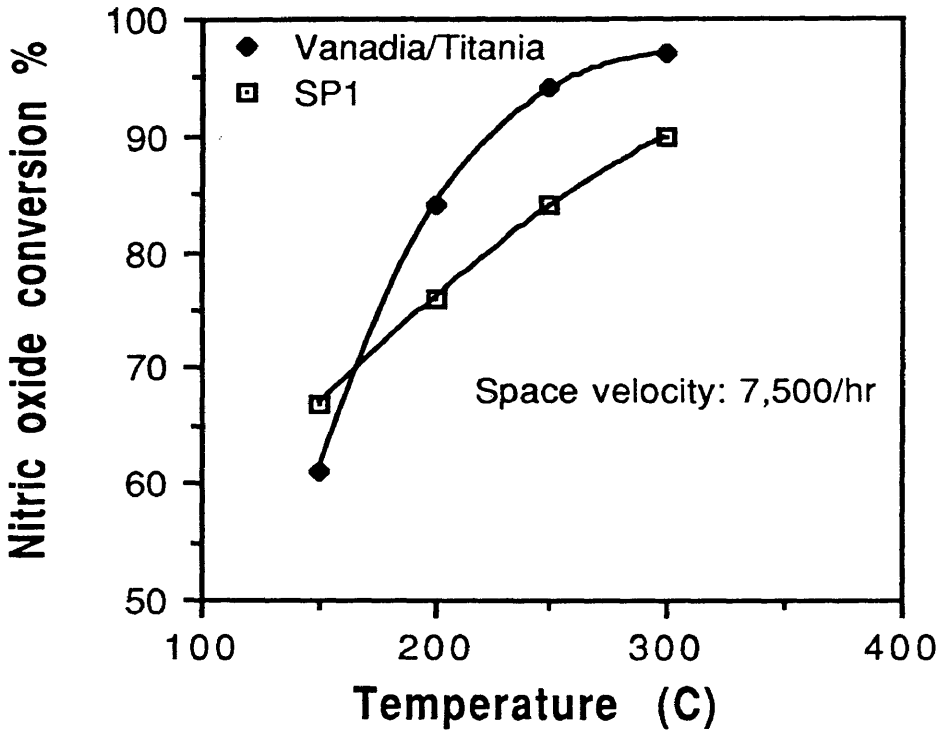

Figure 4.15 Comparison of SP1 and Vanadia/Titania

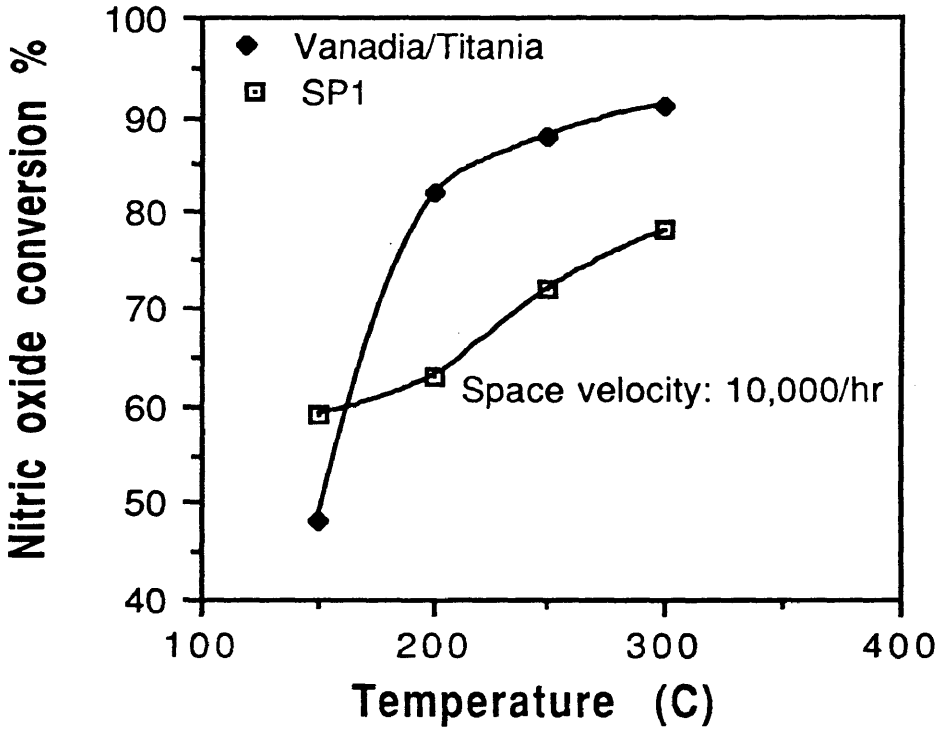

Figure 4.16 Comparison of SP1 and Vanadia/Titania

adsorption of NO is an important step in NO reduction using commercial activated carbons. There are at least two ways in which O_2 may influence NO adsorption. First it is possible that NO is oxidized by O_2 to NO_2 in the gas phase and then NO_2 is adsorbed onto the sample. It was observed that at a given temperature and in the absence of O_2, the amount of NO_2 adsorbed was considerably greater than that of NO (Figure 4.12). In part, this difference in adsorption capacities may be explained by the large difference in the polarity of two gases; NO_2 has a dipole moment of 1.054×10^{-30} C.m and is highly polar compared to NO, which has a dipole moment of 5.84×10^{-31} C.m (88). A simplified scheme for NO adsorption could be:

$$NO(g) + 1/2O_2(g) \text{ ----------> } NO_2(g) \qquad (4.4)$$

$$NO_2(g) + \text{Carbon} \text{ ----------> } NO_2\text{-Carbon} \qquad (4.5)$$

However, Rao and Haugen (89) showed that the homogeneous oxidation of NO to NO_2 is very slow compared to its heterogeneous oxidation over activated carbon. The present studies also indicated the same trend. In the absence of activated carbon, NO_2 was found to be readily reduced to N_2 by NH_3 (Figure 4.8) and NO did not reduce at all even in the presence of O_2 which suggested that the homogeneous oxidation of NO was not as important.

Second, it is possible that gas phase O_2 could react with the activated carbon surface to form carbon-oxygen structures, which would serve as active sites for NO chemisorption (forming C-NO_2 complex). The formation of the NO_2 complex on the surface was confirmed by the desorption studies (Figure 4.10).

NO_2 was also found to be more readily reduced to N_2 over activated carbon compared to when activated carbon was not used (Figures 4.6 and 4.8) and also NO2 was readily adsorbed on activated carbon (Figure 4.11). This suggested that adsorption of NO_2 was at least partially responsible for higher conversion in the presence of NH_3. It can be concluded that the intermediate step of formation of the NO_2 complex on the surface due to the presence of O_2 is very important for NO reduction. Thus when O_2 concentration was increased, the number of active sites also increased which allowed more NO adsorption, finally resulting in higher NO conversion. A simplified adsorption scheme would look like:

$$O_2(g) + 2Carbon \text{ ----------> } O{=}Carbon + O{=}Carbon \quad (4.6)$$

$$NO(g) + O{=}Carbon \text{ ----------> } ON\text{-}O\text{-}Carbon \quad (4.7)$$

The interaction of gas phase O_2 is more directed towards NO than NH_3, as changing the O_2 concentration did not affect NH_3 adsorption on activated carbon (Figure 4.13). The NO_2 conversion using NH_3 was still very high even when O_2 was not used which also confirmed that interaction of O_2 with NH_3 was not of any significance.

The different effect of O_2 on adsorption of NO and NH_3 also suggested that the adsorption sites were different for each reactant.

4.3.2 The effect of ammonia

In the present study, an excess of NH_3 had no effect on NO conversion (Figure 4.14) under the experimental conditions which suggested that the reaction rate was nearly zero order with respect to NH_3. This could be attributed to the catalyst surface being saturated with NH_3 (see Appendix D). Similar dependence on NH_3 concentration has been reported by several workers using other commercial catalysts such as V_2O_5/TiO_2, Fe_2O_3/TiO_2, WO_3/TiO_2 and activated carbons (70,90,91,92).

4.3.3 Comparison of activated carbon with vanadia/titania

At lower temperatures, SP1 had a higher activity than that of vanadia/titania (Figures 4.15 and 4.16), which suggested that activated carbons have a potential of being used as catalysts for NO_x removal from flue gas streams at low temperatures. This is advantageous for the reasons specified in Chapter 1.

4.4 Conclusions

The NO conversion over activated carbon increased significantly when oxygen was included. Nitric oxide was oxidized to NO_2 by O_2, with heterogeneous oxidation being more prominent than homogeneous oxidation. The NO_2 complex formed on the surface was readily reduced to N_2 by NH_3. The presence of O_2 did not affect NH_3 adsorption on activated carbon. Ammonia was very strongly adsorbed on the surface of activated carbon. Activated carbon was also found to be a better catalyst than a commonly used commercial catalyst such as V_2O_5/TiO_2 at reaction temperatures of 150^oC.

Chapter 5

EFFECT OF ACID TREATMENT ON ACTIVITY OF COMMERCIAL ACTIVATED CARBON

The research described previously in Chapter 3 of this thesis has shown that the activity of activated carbons for NO conversion was independent of their physical characteristics, but was influenced by the presence of oxygen functionalities on the carbon surface. Activated carbons which were more acidic (or less basic) were found to be better catalysts. The acidity of activated carbon is dependent on the presence of acidic surface oxides. These oxides are formed when the activating agent used is acidic in nature as would be the case for phosphoric, sulfuric or nitric acid. Puri (56) found that treatment of charcoal with concentrated nitric acid resulted in a 20 % increase in surface oxygen. Attempts have been made to identify the oxygen functional groups using various techniques including IR spectroscopy, X-ray photoelectron spectroscopy, neutralization of bases and temperature programmed desorption. Some of the acidic surface oxides which have been identified so far include carboxylic, phenolic hydroxyl, lactones, carboxyl acid anhydrides, aldehydes and ketones (56,57).

In this chapter, a detailed study of the effects of varying the surface oxygen concentration of coconut shell-based activated carbon on its activity for SCR of NO is presented. Sulfuric acid has been used to treat the activated carbon

surface with the aim of oxidation of the carbon surface in order to obtain a more hydrophilic surface structure with a relatively large number of oxygen-containing surface groups. The surface oxides were expected to be acidic due to the acidic nature of the oxidizing agent.

Sulfuric acid could also act as an activating agent and hence alter the physical structure of activated carbon by gasification. This effect was also investigated and is discussed in this chapter.

5.1 Experimental

5.1.1 Gases

Similar gas mixtures as described in Chapter 3 and Chapter 4 were used in this study.

5.1.2 Catalyst

Activated carbon sample SP3, which had shown a very low activity for NO reduction was used in this study to see if its activity could be improved by acid treatment.

5.1.3 Acid treatment

A schematic diagram of the experimental setup for acid treatment of the sample is shown in Figure 5.1. The reactor vessel which was made of stainless steel, was enclosed in a tube furnace. The reactor vessel had an an extension (A) which was outside the tube furnace and was used for loading the sample. Twenty grams of sample was thoroughly mixed with 40 ml of concentrated acid

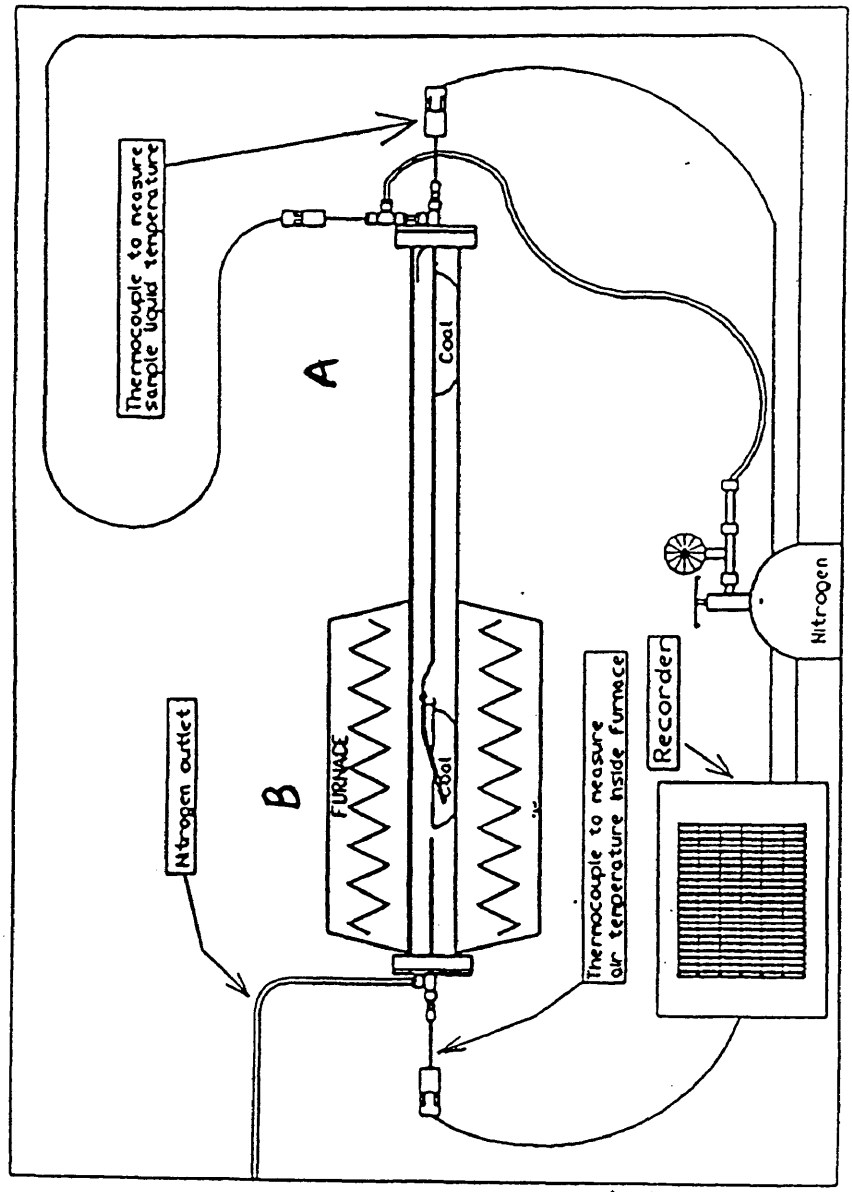

Figure 5.1 Schematic diagram of experimental set-up for acid treatment

at room temperature in the sample boat (made of quartz glass) and then placed in the reactor vessel at location A. The reactor vessel was then purged with 70 cm^3/min of nitrogen gas while being heated to the desired temperature by the furnace. Once the reactor vessel reached the desired temperature, the sample boat was pushed to location B, where it was kept for four hours under nitrogen flow. After acid treatment, the sample was allowed to cool down to room temperature and then washed with distilled water for 24 hrs. The washed sample was then dried in a vacuum oven at 100°C for 24 hrs.

Three different treatment temperatures 100°C (SP3/100), 200°C (SP3/200) and 300°C (SP3/300) were used in this study.

5.1.4 Characterization

In addition to the techniques which are described below, the acid treated samples were also characterized using nitrogen sorption, mercury porosimetry, and ultimate and proximate analysis. These techniques have already been described in Chapter 3.

5.1.4.1 Linear temperature programmed desorption

The acid treated samples were characterized by linear temperature programmed desorption (LTPD). About 15 mg of sample was heated from 25°C to 900°C at a rate of 10°C/minute under a flow of 200ml/min of He using a Seiko Scientific Instrument thermogravimetric analyzer (TGA). The gases evolved were analyzed by a VG Micromass spectrometer (MS), which was connected to the TGA .

5.1.4.2 Infrared spectroscopy

Sample SP3 and its acid treated analogues were characterized by using a Nicolet SX-20 Fourier transform infrared (FTIR) spectrometer. The pellets were prepared by mixing 1.5 mg of sample, which had been dried in a desiccator in presence of anhydrous calcium sulfate for 48 hours, with 300 mg of potassium bromide.

5.1.5 Activity measurements

The activity of the acid treated samples for SCR of NO was tested in the same manner as described in Chapter 3. The equipment setup is also described Chapter 3. Reaction conditions were the same as described in Chapter 3. The only difference was that prior to the run, the sample was heated at 100^{o}C for 4 hours under He flow, instead of 300^{o}C.

5.1.6 Adsorption of nitric oxide and ammonia on catalyst

The adsorption of each gas on SP3 and its acid treated derivatives was also investigated using the TGA/MS system described in Section 5.1.4.1. Prior to adsorption, the sample was heated at 100^{o}C for two hours under 200 ml/min of He to remove any adsorbed moisture. The relevant gas was then introduced into the system and adsorption of the reactant onto the sample was monitored by the weight gain of the sample.

In these studies, the NO concentration was 1500 ppm, and the NH_3 concentration was 10,000 ppm. The amount of sample used was 15 mg. The adsorption studies were carried out in a temperature range of 100-200^{o}C.

5.2 Results

5.2.1 Nitrogen sorption and mercury porosimetry

There was an increase in the BET surface area of SP3/200 and SP3/300, and a decrease of SP3/100 compared to SP3, as shown in Table 5.1. Corresponding increases in micropore volume and surface area were found for SP3/200 and SP3/300; and a decrease for SP3/100. As expected, the meso and macropore volume and surface area decreased for SP3/200 and SP3/300, as shown in Table 5.2. Surprisingly, a similar trend was also observed for SP3/100.

5.2.2 Ultimate and proximate analysis

The ultimate analysis of the samples is presented in Table 5.3. The sulfur content of all the samples increased after acid treatment. Sample SP3/100 had the highest sulfur content and SP3/300 had the lowest. As expected, the oxygen content of the samples increased and the carbon content decreased with increasing acid treatment temperature. Proximate analysis data are presented in Table 5.4. As shown, the ash content of the samples decreased with increasing treatment temperature, evidently due to the dissolution and subsequent volatization of inorganic constituents.

5.2.3 Linear temperature programmed desorption

Profiles of SO_2 evolved from acid treated samples during LTPD are shown in Figure 5.2. The amount of SO_2 evolved from SP3,100 was higher than from any other samples, as indicated by the area under LTPD curve.

Table 5.1 SP3 and acid treated samples characterization using nitrogen adsorption at 77 K

Sample	BET surface area m^2/g	Micropore volume cm^3/g	Micropore surface area m^2/g	Average pore radius Å
SP3	739	0.361	677	11.5
SP3/100	680	0.330	613	11.8
SP3/200	835	0.410	760	11.7
SP3/300	1000	0.463	874	13.3

Table 5.2 SP3 and acid treated samples characterization using mercury porosimetry

Sample	Macro volume cm^3/g	Macro surface area m^2/g	Meso volume cm^3/g	Meso surface area m^2/g
SP3	0.62	5.80	0.24	75.50
SP3/100	0.136	1.31	0.092	46.41
SP3/200	0.117	1.80	0.083	42.11
SP3/300	0.127	1.60	0.145	73.21

Table 5.3 Ultimate analysis of SP3 and acid treated samples

Sample	Carbon %	Hydrogen %	Nitrogen %	Sulfur %	Oxygen %
SP3	91.54	0.46	0.51	0.02	2.55
SP3/100	87.94	0.86	0.85	0.36	7.57
SP3/200	85.94	0.76	0.84	0.31	11.12
SP3/300	83.58	0.87	0.80	0.11	13.02

Table 5.4 Proximate analysis of SP3 and acid treated samples

Sample	Moisture %	Ash %	Volatile %	Fixed carbon %
SP3	2.67	4.92	30.0	62.4
SP3/100	4.09	2.42	8.0	85.5
SP3/200	4.98	1.57	13.7	79.7
SP3/300	3.19	1.62	19.5	75.7

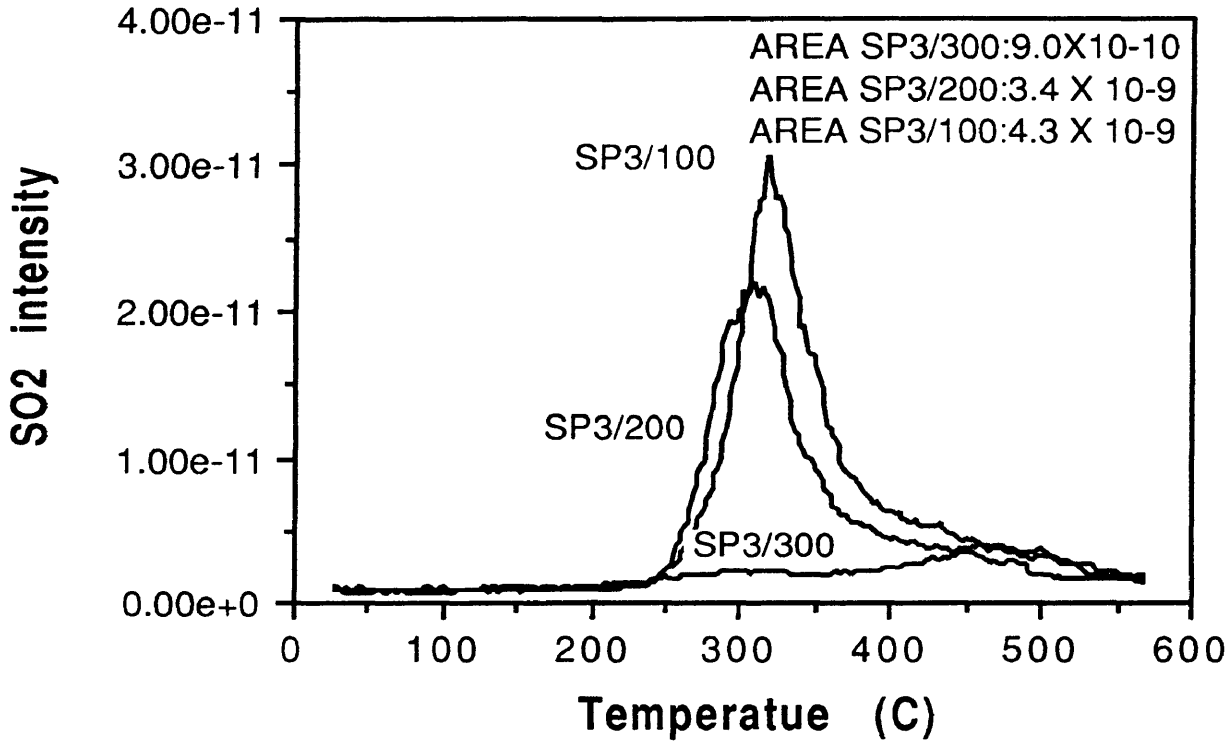

Figure 5.2 SO2 desorption for acid treated samples

Profiles of CO_2 evolved from the acid treated samples during LTPD are shown in Figure 5.3. The amount of CO_2 evolved increased with increasing acid treatment temperature as indicated by the area under each curve. A maximum in these profiles was found at temperatures near 700°C; a less intense peak also occurred around 300°C. All the surface oxides were desorbed around 950°C. No CO evolution was observed for any of the acid treated samples. Untreated SP3 did not show any evolution of CO_2 or CO.

5.2.4 Infrared spectroscopy

The FTIR spectra for SP3 and the acid treated samples is shown in Figure 5.4. It is very difficult to interprete these results quantitatively, partly due to the influence of particle size and sample preparation on the peak height. However, the ratio of two peaks in the same spectrum yields important information concerning the relative amounts of surface groups on the sample. A band at 1586 cm^{-1} was observed for all the samples; it was most intense for SP3/300 and decreased with reducing severity of acid treatment. Another absorption band, most intense for SP3/300 and absent in SP3, was located at 1725 cm^{-1}.

5.2.5 Activity measurements

The NO conversion over SP3 and its acid treated derivatives, as a function of reaction temperature, is shown in Figure 5.5. The activity of the acid treated samples was better than the parent sample. The activity of these samples increased with increasing acid treatment temperature. Sample SP3/300, which was treated at the highest temperature of all the samples, had the best activity.

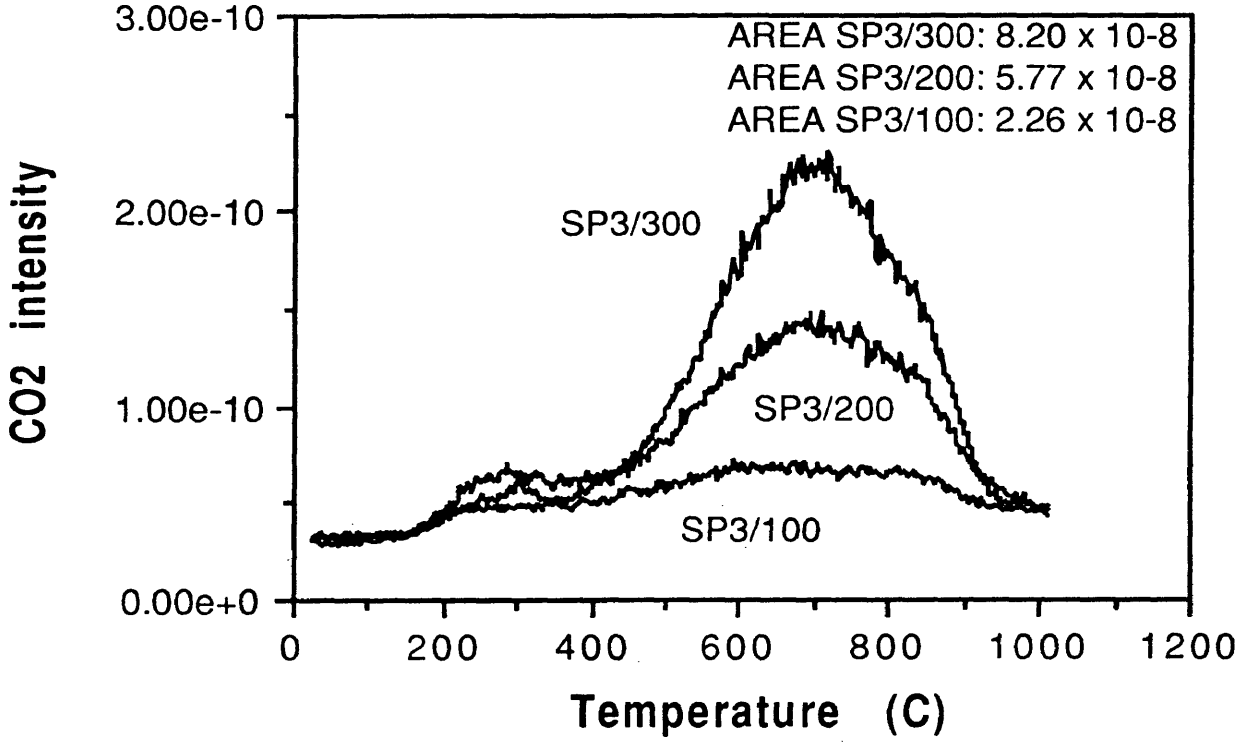

Figure 5.3 CO2 desorption for acid treated samples

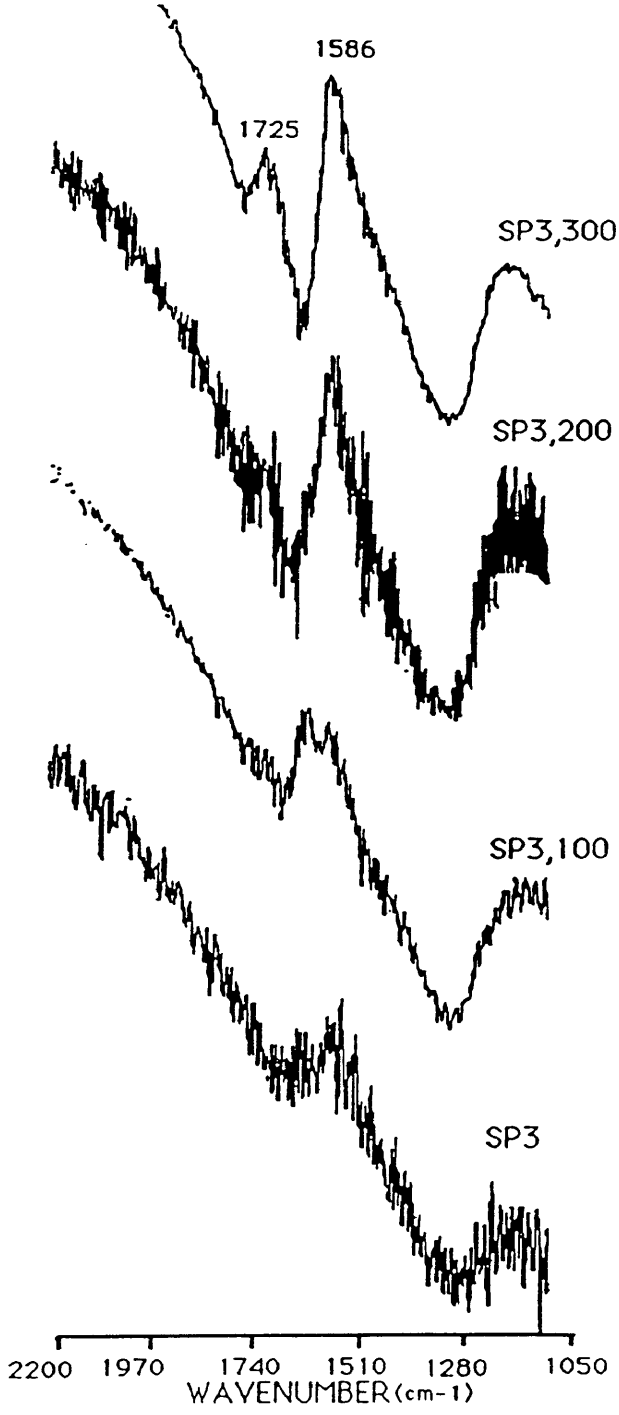

Figure 5.4 FT-IR spectra of SP3 and its acid treated analogues

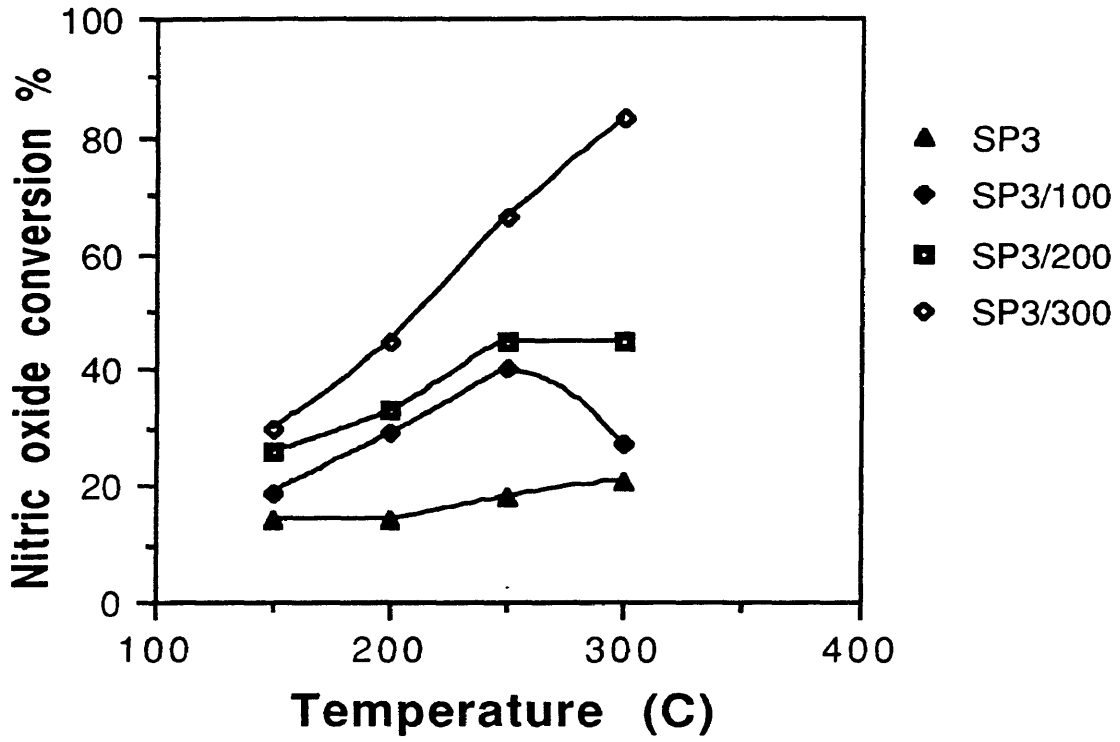

Figure 5.5 Activity of SP3 and acid treated samples

ARTHUR LAKES LIBRARY
COLORADO SCHOOL OF MINES
GOLDEN, CO 80401

At 150°C, the NO conversion was 33% and at 300°C, it was 83 %. The temperature dependence was different for each acid treated sample. The activity of SP3/300 increased uniformly with temperature, whereas above about 250°C, the activity of SP3/100 decreased while the activity of SP3/200 levelled out. This trend was consistent with the acid treatment temperature. Sample SP3/300 remained stable at 300°C and SP3/200 was less stable than SP3/300 but more than SP3/100.

The change in the activity of SP3/100 and SP3/200 at 300°C, as a function of time, is shown in Figure 5.6. The activity of SP3,100 decreased from 40 % to 27 % within three hours of operation and then remained constant. The activity of SP3/200 decreased from 50 % to 45 % within two hours of operation and then remained constant. Due to these trends the stability of these acid treated samples were also tested for longer periods. The activity of these samples did not decrease after reaching the steady state when operated at 300°C for 72 hrs, as shown in Figure 5.7.

The NO conversion did not correlate with BET surface area, as shown in Figure 5.8. Sample SP3/100, which had lower total surface area than SP3, had higher activity. Similar trends were observed for pore volume and average pore radius. The overall activity of all the samples correlated directly with the bulk oxygen content, as shown in Figure 5.9. Sample SP3/300 had the highest bulk oxygen content and the highest activity. Sample SP3 had the lowest bulk oxygen content and the lowest activity. The activity of these samples also correlated directly with the amount of surface oxides (indicated by the amount of CO_2 evolved during LTPD), as shown in Figure 5.10.

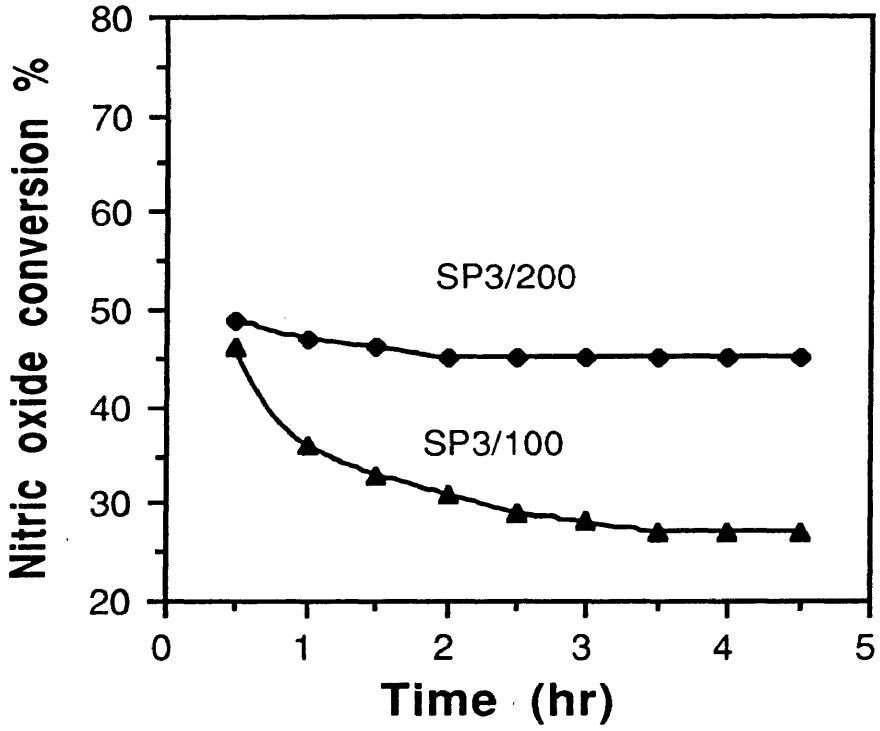

Figure 5.6 Deactiviation of SP3/200 and SP3/100 at 300 C.

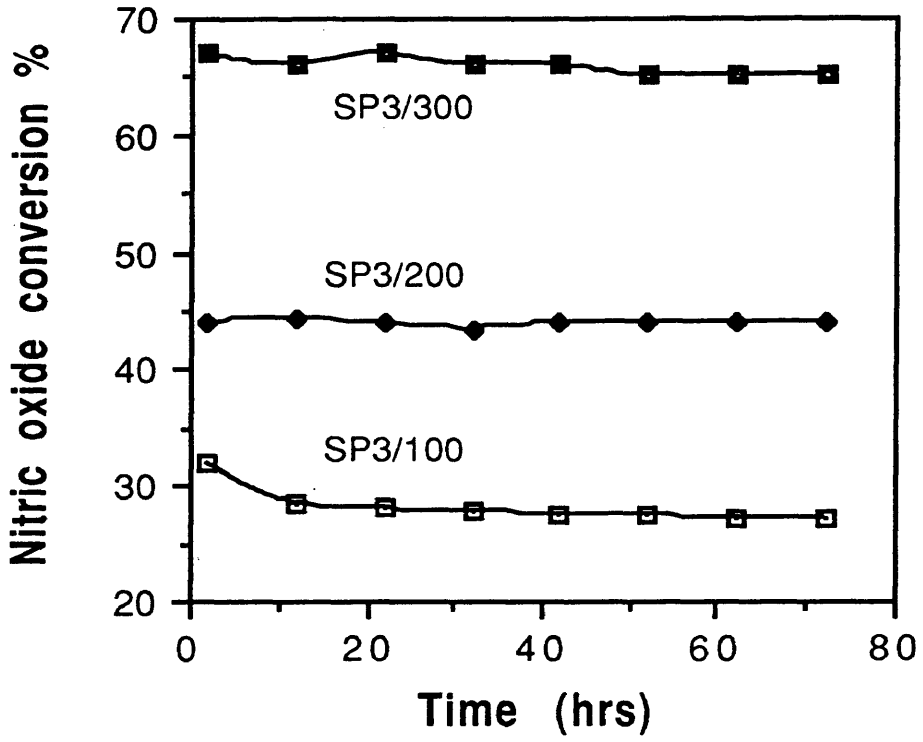

Figure 5.7 Stability of acid treated samples at 300C

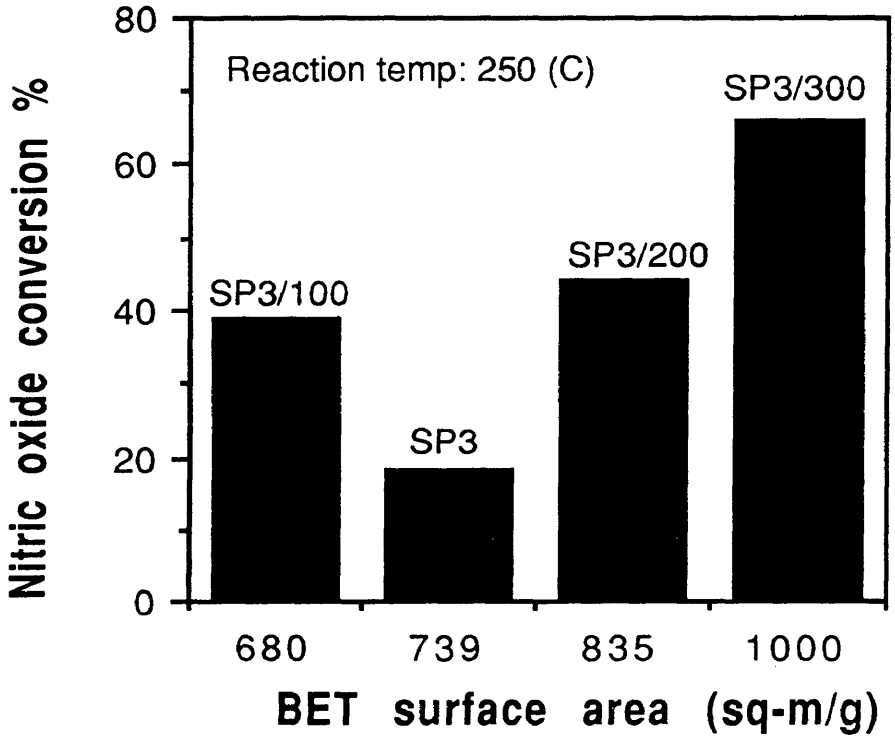

Figure 5.8 Effect of BET surface area on activity

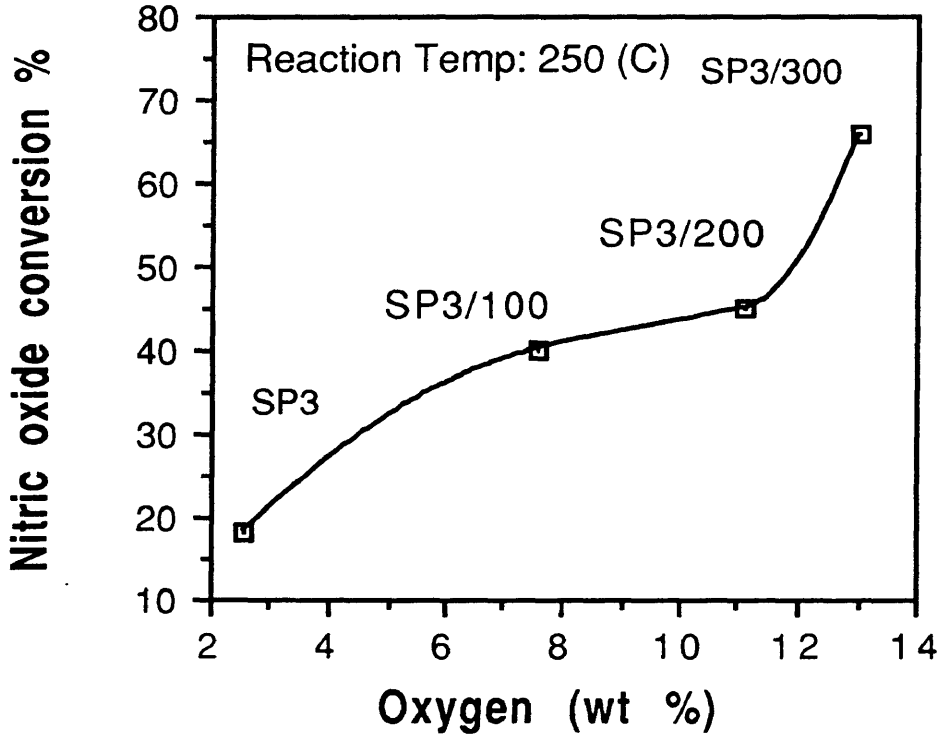

Figure 5.9 Effect of bulk oxygen on activity

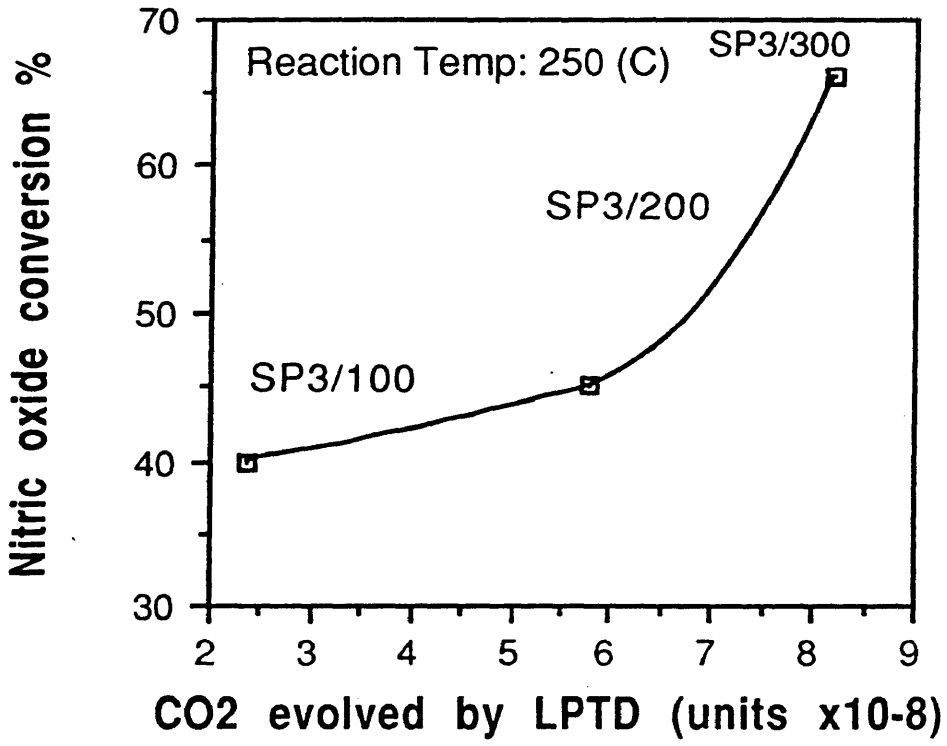

Figure 5.10 Effect of carbon surface groups on activity

5.2.6 Nitric oxide and ammonia adsorption

The adsorption capacity of SP3 and its acid treated samples for NO is shown in Figure 5.11. NO was adsorbed in the presence of 15 % O_2 as it was discovered that NO did not adsorb in the absence of O_2 . This has already been discussed in Chapter 4. From the separate experiments in which only O_2 was adsorbed on the sample, it was determined that the weight gain of the sample in the NO-O_2 system was a good representation of NO adsorption only. The adsorption capacity of all the samples decreased with increasing temperature. This is expected because in general adsorption is an exothermic process. Treating SP3 with sulfuric acid had an adverse effect on its NO adsorption capacity and this effect became more prominent with higher acid treatment temperatures. Sample SP3 had the highest adsorption capacity and SP3/300 had the lowest.

The adsorption capacity of SP3 and acid treated samples for NH_3 is shown in Figure 5.12. The presence of O_2 did not effect the adsorption of NH_3, therefore the adsorption studies for NH_3 were carried out without O_2. The adsorption capacity of all the samples decreased with increasing temperature. Treating SP3 with sulfuric acid had a favorable effect on its adsorption capacity for NH_3 and this capacity improved with higher acid treatment temperatures. SP3/300 had the highest capacity and SP3 had the lowest. Above 200^{o}C, the amount of NO and NH_3 that was adsorbed was below detection limit.

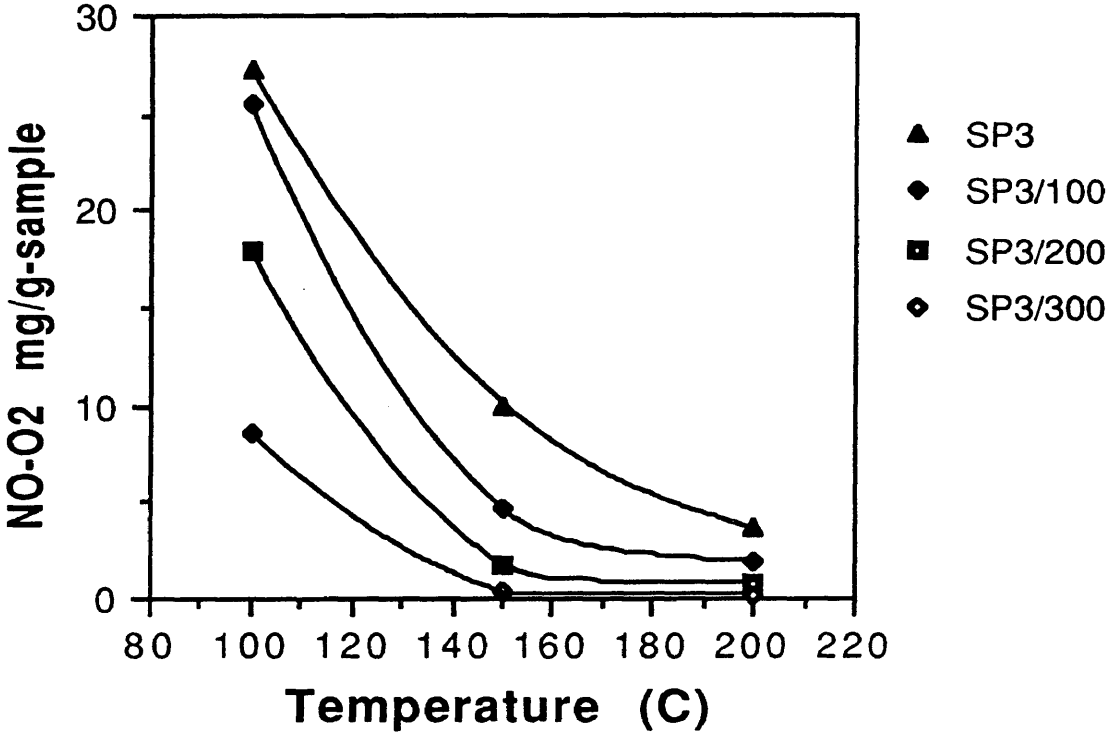

Figure 5.11 NO adsorption on SP3 and acid treated samples

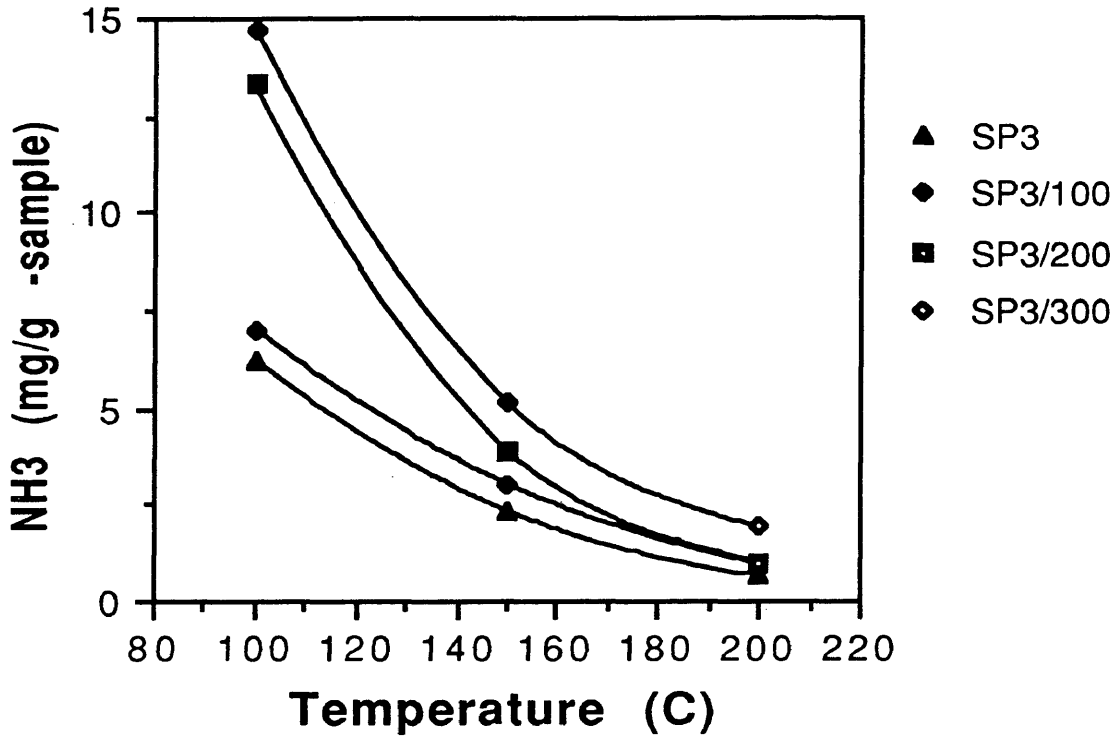

Figure 5.12 NH3 adsorption on SP3 and acid treated samples

5.3 Discussion

Sulfuric acid acted as an activating agent and changed the physical structure of SP3 (Table 5.1 and Table 5.2). The BET surface area of SP3/200 and SP3/300 increased as compared to SP3. There was corresponding increase in the micropore volume and decrease in the mesopore and macropore volume, as suggested by porosimetry data. But in case of SP3/100, the BET surface area decreased with a corresponding decrease in micropore volume and a decrease in the mesopore and macropore volume. This was an unusual trend because with a decrease in micropore region, an increase in mesopore and macropore was expected . This suggested that the micropores of SP3/100 were partially blocked by sulfur which made them inaccessible to nitrogen adsorption, resulting in a lower BET surface area. The presence of sulfur was indicated by the ultimate analysis (Table 5.3) and LTPD (Figure 5.2). During acid treatment, sulfur was retained by all the samples. Some of the sulfur came off as sulfate during the heat treatment. Since SP3/100 was treated with acid at the lowest temperature, it retained more sulfur compared to other acid treated samples.

The carbon content per unit mass of the sample decreased with acid treatment temperature partially due to gasification (as indicated by the change in total surface area) and partially due to the addition of oxygen.

According to Bansal et al. (56), the carbon-oxygen functional groups are the most important factor in determining the surface characteristics and consequently, the catalytic properties of carbons. As stated earlier, surface oxides can be acidic or basic. Acidic oxides would include functional groups

like carboxyls, phenols and aldehydes (56,57). Basic oxides would include functional groups like chromenes and pyrones (56,57). These surface oxides may also serve as adsorption sites for reactants such as NO and NH_3. Usually, the acidic oxides dominate the overall surface chemistry of activated carbons.

Sulfuric acid acted as an oxidizing reagent, and formed new functional groups on the carbon surface. The extent of oxidation increased with the treatment temperature, as indicated by the bulk oxygen content (Table 5.3) and by LTPD of these samples (Figure 5.3). Once again, in this study, the bulk oxygen content was a good representation of the presence of surface oxides, as SP3/200 and SP3/300 which had relatively lower ash content, had higher oxygen contents.

Acidic surface oxides would be removed as CO_2 during LTPD, whereas basic surface oxides would be removed as CO (56). Since no CO desorption was observed, the surface oxides were concluded to be predominantly acidic in nature. In addition to these acidic carbon-oxygen functional groups which decomposed around 700°C during LTPD experiments, there were other oxygen functional groups having a decomposition temperature near 300°C. Otake (65) concluded that acidic oxides producing CO_2 and having decomposition temperatures near 300°C were associated with carboxylic groups formed at nonadjacent, dangling carbon atoms (carbon atoms having a single C-C bond to the surface). Acidic oxides decomposing to CO_2 at temperatures near 700°C were attributed to carboxylic groups formed at adjacent dangling carbon atoms. Lower stability carboxylic groups are expected to be formed during carbonization of the precursor, whereas the latter

are formed during oxidation of activated carbon (65). This type of structural assignment was in agreement with our results since the CO_2 evolution at 700°C increased with increasing acid treatment temperatures. The formation of carboxyl groups on the carbon surface was also indicated in the FTIR data (Figure 5.4). The 1586 cm^{-1} band was close to that expected for carboxyl groups, which are known to adsorb at 1580 cm^{-1} (93). The intensity of this band increased progressively as the sulfuric treatment temperature increased. Another band, at 1725 cm^{-1} for SP3/200 and SP3/300 was assigned to carbonyl groups (94). Both of these groups are expected to be acidic in nature.

Although surface area and porosity were altered by the sulfuric acid treatment, an increase of 25 % in surface area could hardly explain the four-fold increase in the activity for SP3,300 at higher reaction temperatures (Figure 5.5). SP3/100, which showed a decrease in the surface area also had higher activity than SP3 (Figure 5.8). There was also no direct correlation between activity and average pore radius or pore volume.

In agreement with the results of Chapter 3, the concentration and the types of surface oxygen groups affected the NO conversion. Of the acid treated samples SP3/300, which had the highest amount of surface oxides, had the highest activity; SP3/100 which had the lowest amount of surface oxides, had the lowest activity (Figures 5.9 and 5.10). The surface oxides, which were formed by sulfuric acid treatment were acidic in nature. This supported our earlier finding that activated carbons acidic in nature were more favorable for NO reduction.

The unusual behavior (deactivation) of SP3/200 and SP3/100 at 300°C could be explained in terms of their acid treatment temperatures (Figure 5.6). The highest temperature that the surface oxides were exposed to were the acid treatment temperatures, which were 100°C for SP3/100 and 200°C for SP3/200. As a result of this, some of the surface oxides decomposed at higher temperatures. The bulk oxygen content of SP3/100, after the reaction, decreased to 3.44% from 7.57 % and for SP3/200, it decreased to 8.98% from 11.12 %. This may explain the initial decrease in SP3/100 and SP3/200 activity.

The trends observed for adsorption of NO and NH_3 suggested that NO adsorption sites were different from NH_3 sites. Due to increasing acidity with treatment temperature, it was not surprizing that acid treatment increased the adsorption capacity for NH_3 (Figure 5.12). The decrease in the adsorption capacity of NO (Figure 5.11) suggested that NO required oxygen sites which were not acidic. Mochida et al. (81) also suggested that the NO adsorption sites were different from NH_3 sites. They proposed the following scheme:

$$NO + O{=}Carbon \text{ ----------> } NO_2\text{-}Carbon \quad (5.1)$$

$$NH_3 + HO\text{-}Carbon \text{ ----------> } NH_4O\text{-}Carbon \quad (5.2)$$

Unfortunately, the mechanism of NO reduction over activated carbon is not yet fully understood. However, a lot of work has been done towards understanding the mechanism of NO reduction over other catalysts like V_2O_5/TiO_2. Three types of mechanisms could be distinguished in the literature

(95). The first was based on molecular adsorption of NH_3 followed by a reaction with NO in the gas phase (95,96). The second was based on dissociative adsorption of NH_3 and subsequent reaction with adsorbed NO (95.97). The third was based on oxidation of NO to NO_2 and subsequent reaction with adsorbed NH_3 (95,98). In all forgoing mechanisms, the adsorption of NH_3 was important for NO reduction. NH_3 being a Lewis base would adsorb at a acidic site. The same conclusion may be relevant for activated carbons. Based on these results, it was quite obvious why acidic activated carbons were favorable for NO reduction.

5.4 Conclusions

Treatment by use of sulfuric acid enhanced the activity of activated carbons at reaction temperatures between 150-300^{o}C. Sulfuric acid acted as an oxidizing agent and created acidic surface functionalities on activated carbon, including carboxyl and carbonyl groups. The surface characteristics of activated carbon appeared to play a more important role than their physical characteristics for NO reduction.

Chapter 6

ACTIVATED CARBONS SYNTHESIZED BY CHEMICAL ACTIVATION

Previous studies (Chapters 3) showed that commercial activated carbon originating from coal had the highest activity for NO reduction using NH_3 and that the activity of carbon (Chapter 5) could be increased further when treated with sulfuric acid which oxidized the surface and created acidic surface oxides. Based on these results, the aim of study presented in this chapter was to investigate NO reduction using NH_3 as a reductant over activated carbons that were produced from coal using sulfuric acid activation.

It is important to mention here that commercial processes using chemical activation have been limited to the use of zinc chloride ($ZnCl_2$) and phosphoric acid (H_3PO_4). Much of the literature is also concerned with $ZnCl_2$ and H_3PO_4 acid activation (56, 60). The precursors are usually cellulosic material, wood being the most common one. The application of chemical activation to coals has been more limited, apparently chemical activation is not practised industrially with coal feed stocks (60). The only published finding which involved sulfuric acid (H_2SO_4) as a chemical reagent and coal as a precursor was a patent awarded to the Carborundum Company (64) which described a process for the production of activated carbon from sub-bituminous coal using acid reagents (5% wt. of conc.H_2SO_4, HCl and H_3PO_4). The impregnated feed

was heat treated to 450°C in an inert atmosphere followed by steam activation at 800-900°C.

6.1 Experimental

6.1.1 Gases

Similar gas mixtures as described in Chapter 3 and Chapter 4were used in this study.

6.1.2 Precursor

A bituminous coal from the Illinois Basin Coal Sample Program, IBC 106, was used as a precursor. Ultimate and proximate analyses of the coal are given in Table 6.1 and 6.2; IBC 106 was a high volatile coal with a moderate ash content and high moisture content.

6.1.3 Chemical activation

The experimental setup has already ben described in Section 5.1.2. About 20 g of coal (which had been ground to -50 mesh) was mixed with 40 ml of concentrated acid. The coal-acid slurry was heated at 200°C for 1 hr under a nitrogen flow of 70 cm^3/min for better impregnation, after which the slurry was heat treated at a final temperature for 3 hrs under constant nitrogen flow. The final product was leached with distilled water for 24 hrs and then dried under vacuum at 100°C for 24 hrs. Four different treatment temperatures 300°C (SP10), 400°C (SP11), 500°C (SP12) and 600°C (SP13) were used in this study.

6.1.4 Characterization

The samples were characterized using; nitrogen adsorption; mercury porosimetry; ultimate and proximate analyses; linear temperature programmed desorption; and infrared spectroscopy. These techniques have already been discussed in previous chapters.

6.1.5 Activity measurements and reaction conditions

The activity of these samples was tested in a similar manner as described in Chapter 3. The equipment set up is also described in that chapter. Prior to each experiment, the sample was heated at 100^{o}C for 4 hrs. under He flow to remove any adsorbed moisture. The temperature was varied from 150-300^{o}C, and the total gas flow rate was 1000 SCCM with a catalyst weight of 3 g. The NO and NH_3 concentrations were 700 ppm and O_2 was 4 % with balance being He.

6.2 Results

6.2.1 Nitrogen sorption and mercury porosimetry

The data from nitrogen adsorption is presented in Table 6.1. The development of BET surface area was strongly dependent on heat treatment temperature (HTT), as shown in Figure 6.1. High BET surface area value was obtained when the HTT was about 600^{o}C. The sample that was activated at 300^{o}C (SP10) developed negligible surface area and hence is not included in further discussion. Nitrogen adsorption data also indicated that increasing HTT increased microporosity. Sample SP11 had no contribution from microporous

Table 6.1 Chemically synthesized carbons characterization using nitrogen adsorption at 77 K

Sample	BET surface area m^2/g	Micropore volume cm^3/g	Micropore surface area m^2/g	Average pore radius Å
SP10	0.5	-	-	-
SP11	6.0	-	-	67
SP12	80	0.004	16	31
SP13	247	0.100	177	14

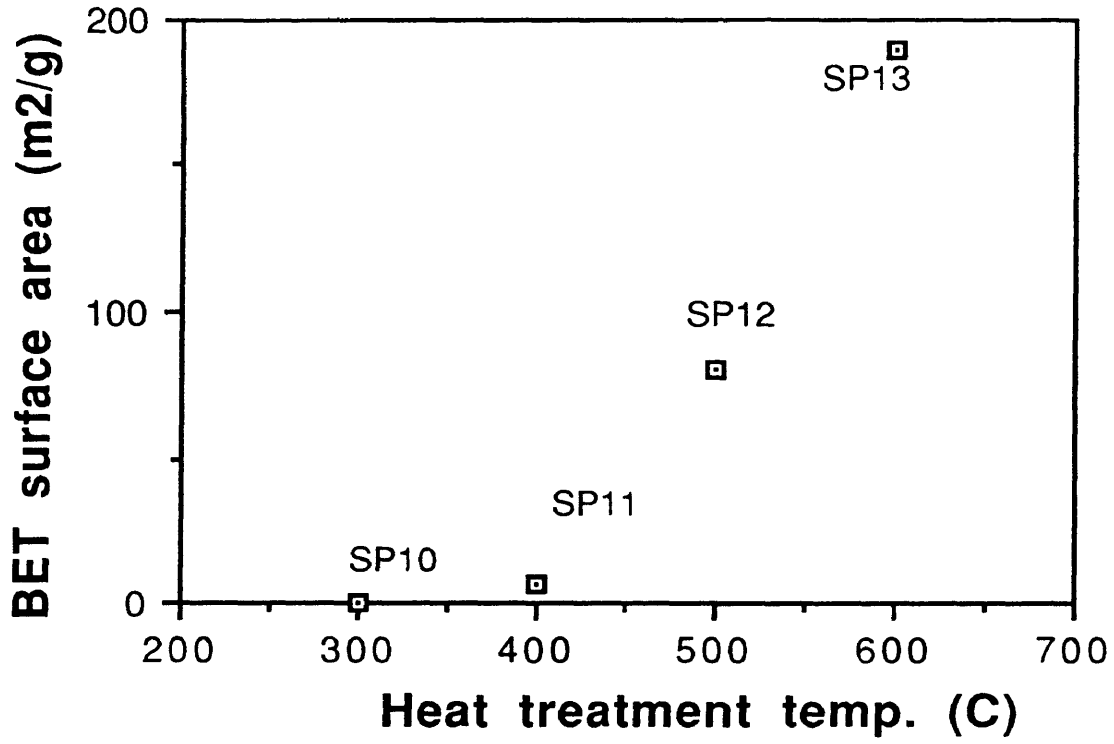

Figure 6.1 Surface area of activated carbons

surface area, whereas SP13 had significant contribution from micropores. This trend is also shown by average pore radius of the samples.

The mercury porosimetry data, Table 6.2, showed that SP11 was predominantly mesoporous and the contribution by non-micropores decreased with increasing HTT. The porosimetry results confirmed the nitrogen adsorption observations that an increase in HTT leads to a increase in microporosity (at the expense of meso and macro-porosity).

6.2.2 Ultimate and proximate analyses

The data from ultimate and proximate analyses is presented in Tables 6.3 and 6.4. There was an increase in ash content with HTT which was consistent with loss of material as volatile products and reduction in moisture level. The trend in ash content was also paralleled by an increase in sulfur content which suggested that more sulfur was deposited on carbon with increasing HTT. The presence of high ash content in the carbons reduces its mechanical strength and adsorptive capacity (56,69). The bulk oxygen content of activated carbon samples was higher than the parent coal but decreased with HTT. A decrease in H/C ratio with HTT, Figure 6.2, suggested that acid treatment promoted dehydrogenation. This is consistent with other published findings and is contributed to the loss of aliphatic C-H structures during activation (99).

6.2.3 Linear temperature programmed desorption

Profiles of CO_2 evolved during LTPD are shown in Figure 6.3. The amount of CO_2 decreased with HTT, as indicated by the area under each curve. The

Table 6.2 Chemically synthesized carbons characterization using mercury porosimetry

Sample	Macro volume cm^3/g	Macro surface area m^2/g	Meso volume cm^3/g	Meso surface area m^2/g
SP10	-	-	-	-
SP11	0.12	2.50	0.09	17.1
SP12	0.12	0.90	0.02	7.7
SP13	0.12	0.70	0.02	9.1

Table 6.3 Ultimate analysis of chemically synthesized carbons

Sample	Carbon %	Hydrogen %	Nitrogen %	Sulfur %	Oxygen %
Parent	75.2	4.97	1.81	3.53	4.88
SP10	58.82	2.02	1.60	3.38	29.18
SP11	64.13	1.88	1.62	5.62	20.55
SP12	64.68	1.30	1.88	11.7	10.15
SP13	70.08	1.42	1.83	12.35	9.08

Table 6.4 Proximate analysis of chemically synthesized carbons

Sample	Moisture %	Ash %	Volatile %	Fixed carbon %
Parent	10.8	9.6	39.9	46.7
SP10	7.81	5.00	37.4	49.8
SP11	6.45	6.20	27.9	59.4
SP12	4.42	10.29	18.1	67.2
SP13	2.70	11.99	9.5	75.8

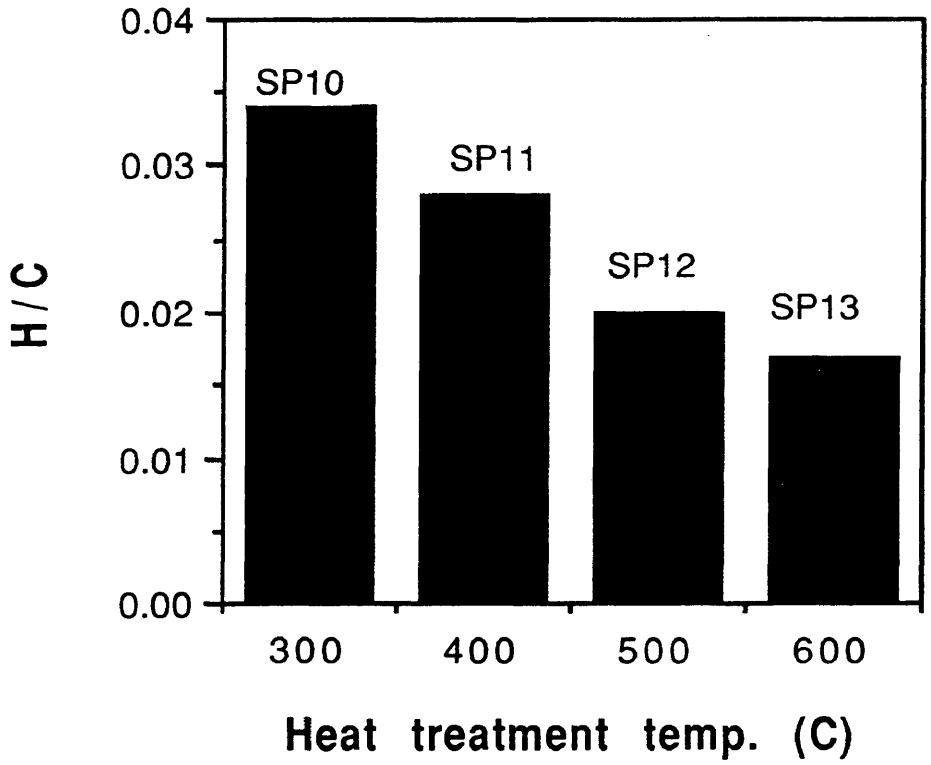

FIgure 6.2 Change in H/C ratio of carbons with HTT

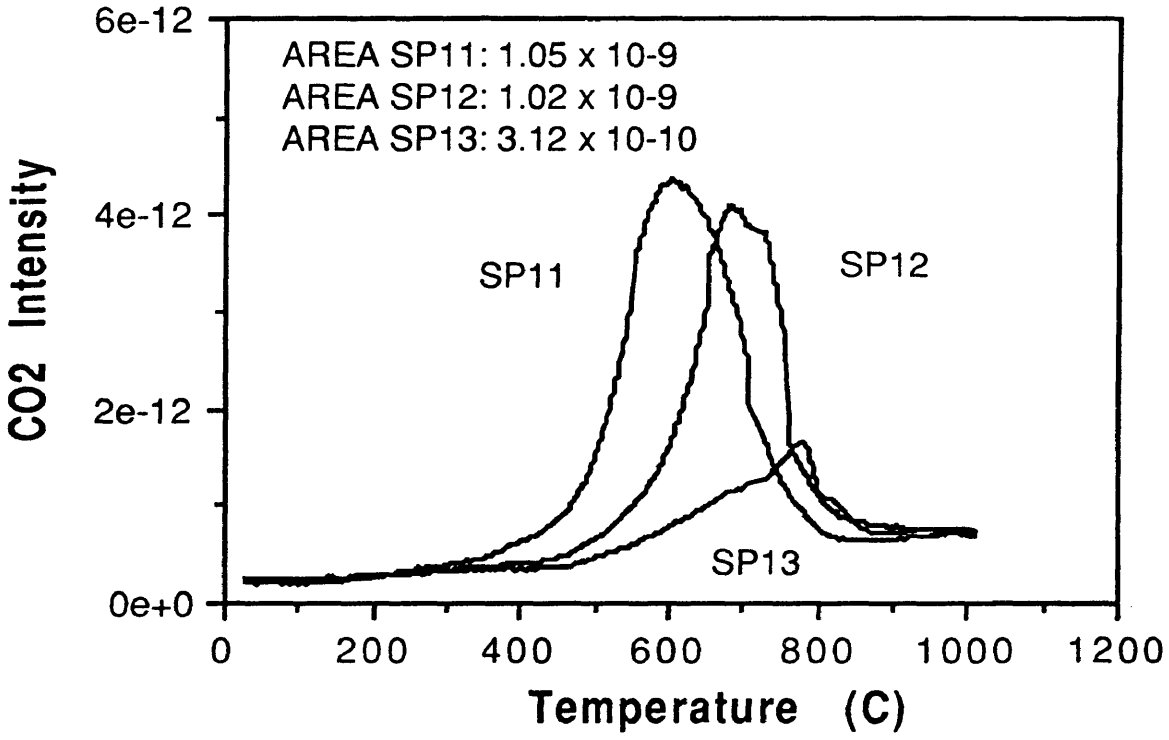

Figure 6.3 CO2 desorption from LTPD

desorption temperature for surface oxides increased with HTT. The maxima of CO_2 profiles was also different for each sample; around 600°C for SP11, 700°C for SP12 and 800°C for SP13. No CO evolution was observed for any of the samples.

6.2.4 Infrared spectroscopy

The FTIR spectra is shown in Figure 6.4. A band at 1586 cm^{-1} was observed for all the samples whose intensity reduced with increasing HTT.

6.2.5 Activity measurements

The NO conversion for the samples, as a function of temperature, is shown in Figure 6.5. Activity of all the samples increased with reaction temperature. Sample SP11 activity was less temperature-sensitive than SP12 and SP13. Sample SP12 had the highest conversion of all the samples; at 150°C the conversion was about 30 % and at 300°C, it was about 79 %. All the three carbon samples were checked for their stability at reaction temperature of 300°C. All the samples sustained their activity even after 72 hrs of operation suggesting that the surface oxides were stable against decomposition at 300°C.

The NO conversion as a function of bulk oxygen content (from ultimate and proximate analyses) is shown in Figure 6.6. Sample SP12 with intermediate bulk oxygen content had the highest activity

The NO conversion as a function of surface oxides (indicated by the amount of CO_2 evolved during LTPD) is shown in Figure 6.7. A trend similar to that of

ARTHUR LAKES LIBRARY
COLORADO SCHOOL OF MINES
GOLDEN, CO 80401

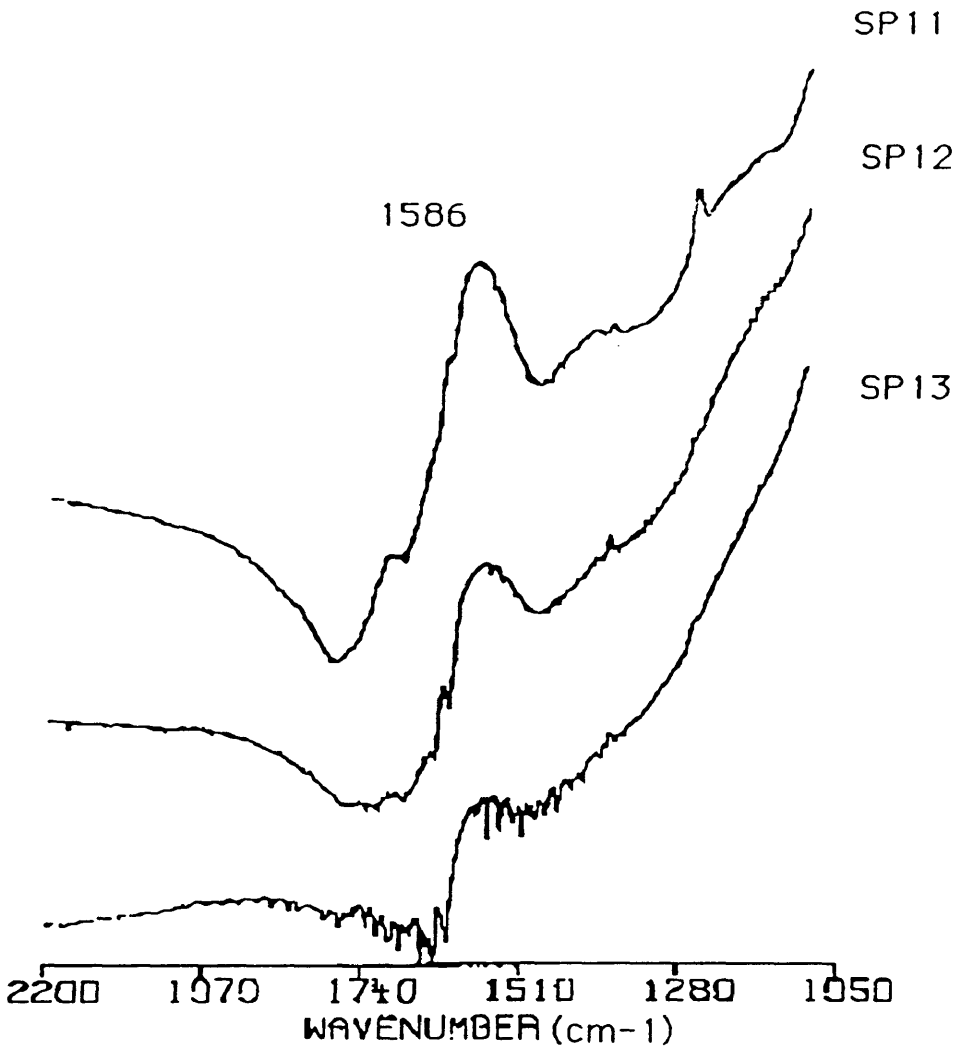

Figure 6.4 FR-IR spectra of chemically synthesized carbons

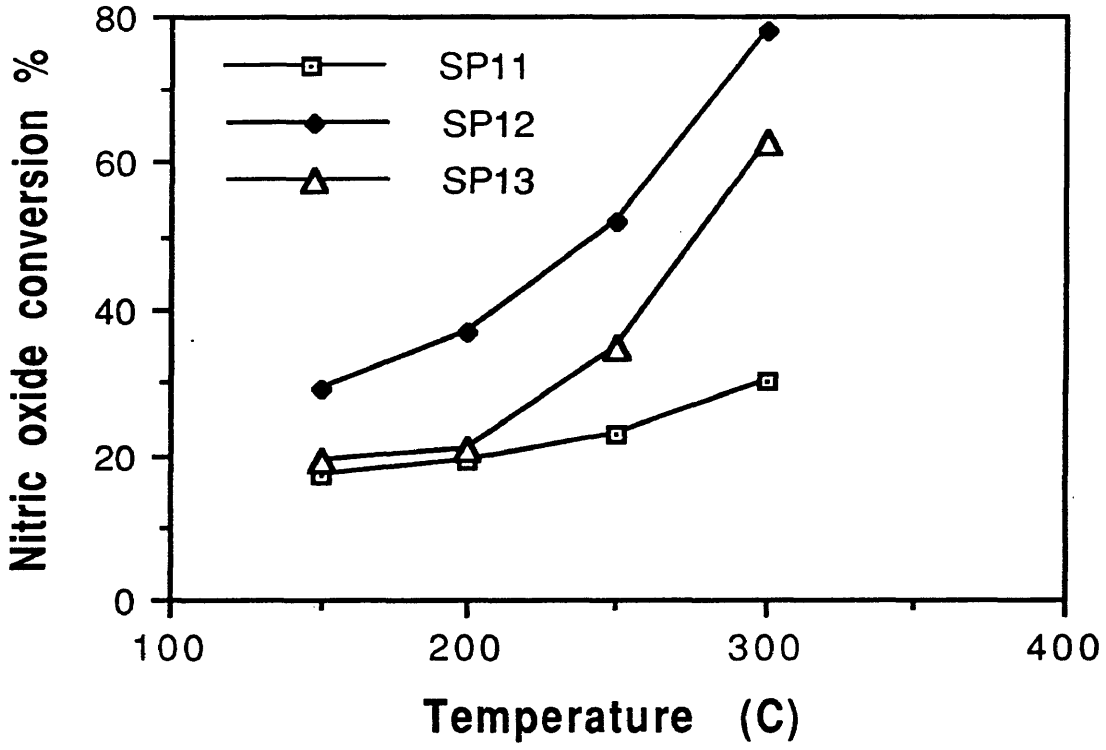

Figure 6.5 Nitric oxide conversion over chem. activated carbons

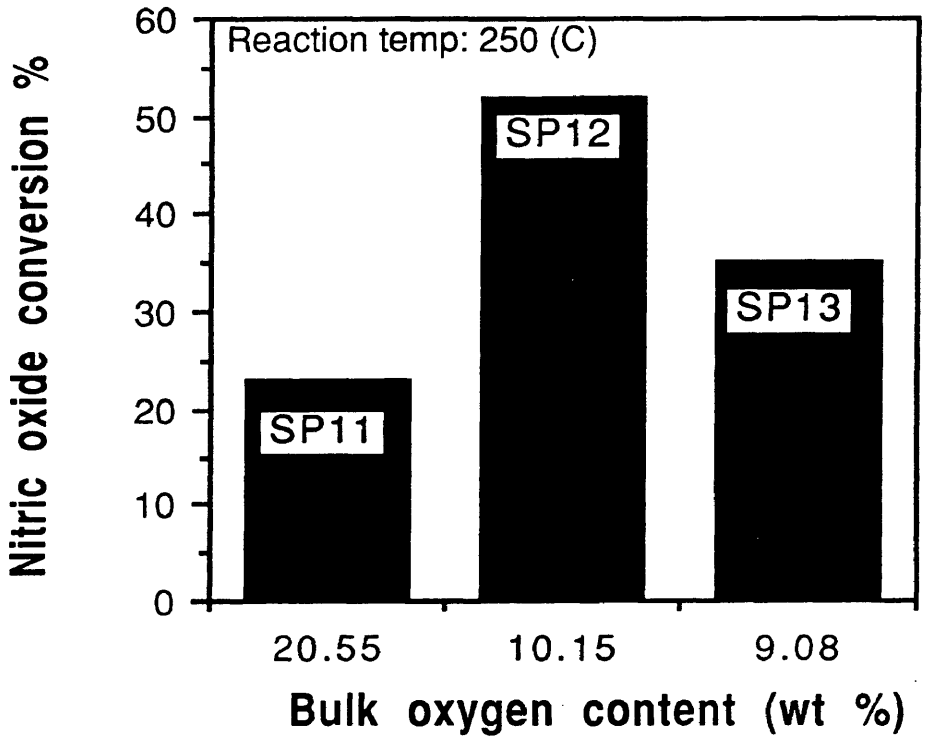

Figure 6.6 Effect of bulk oxygen content on activity of carbon

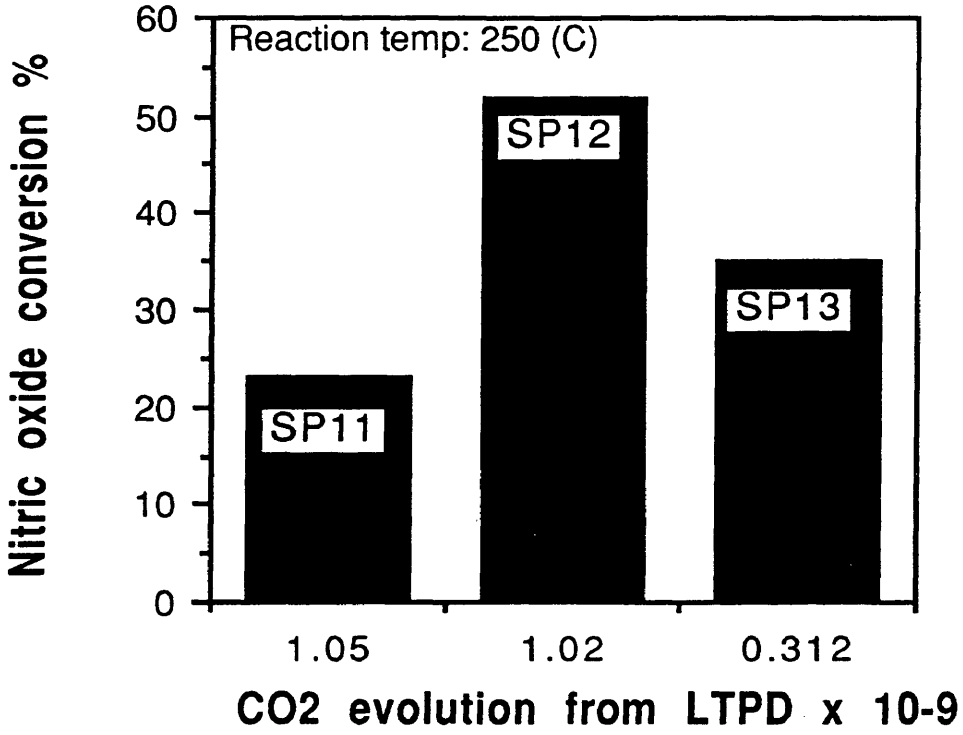

Figure 6.7 Effect of surface oxides on activity of carbon

NO verses total oxygen content was observed, where SP12 with intermediate surface oxides exhibited highest activity.

6.3 Discussion

As shown in Chapter 5, sulfuric acid acted as an activating agent as well as an oxidizing agent. The development of pore structure and hence surface area increased with HTT (Figure 6.1,Tables 6.1 and 6.2). The carbon samples also became more microporous with increasing HTT. The sample activated at 300^{o}C (SP10) did not show much pore development, whereas the sample activated at 600^{o}C (SP11) indicated the best pore development.

Due to oxidation, new functional groups were also formed on the surface. The similar trend between the bulk oxygen content (Table 6.3) and CO_2 profiles from LTPD (Figure 6.3) with HTT suggested that the bulk oxygen content was a good representation of surface oxides. The extent of oxidation decreased with treatment temperature, as indicated by the total oxygen content and LTPD profiles. This could be attributed to the elimination of surface functionalities by thermal decomposition at higher HTT, as LTPD profiles showed that surface functionalities start to desorb around 400^{o}C. These oxides were predominantly of acidic nature (since no CO desorption was observed) (56). The FTIR spectra for the carbons (Figure 6.4) showed that these surface oxides were carboxyl groups which are expected to adsorb around 1580 cm^{-1}(93). Reduction in peak intensity with increasing HTT may have resulted from the elimination of COOH groups (consistent with total oxygen content and LTPD results) by thermal decomposition as suggested earlier.

Sample SP11 had the highest amount of surface oxides of the three samples tested for SCR of NO but it did not have very high activity which could be attributed to poor surface and pore structure development compared to other two samples. Sample SP12, which had moderate surface development, had higher activity than SP13 in spite of having lower surface area. This could be explained in terms of surface functional groups. Sample SP12 had higher amount of surface oxides than SP13 which resulted in a higher activity.

In agreement with results from previous studies, the type and concentration of surface oxides of carbons (with reasonable surface area and pore structure development) were more important for NO conversion than their physical characteristics such as BET surface area.

Comparing these chemically activated carbons with their commercial counterparts (Chapter 3) which were physically activated also showed the importance of surface oxides. Activity of SP11 is comparable to SP3 and SP4; and activity of SP12 and SP13 is comparable to SP1 and SP2. But the BET surface area of these chemically activated carbons was very low compared to commercial carbons. This suggested that high activity of chemically activated samples was predominantly due to surface oxides.

6.4 Conclusions

Sulfuric acid acted as an activating and oxidizing agent by creating activated carbons from a coal precursor with acidic surface functionalities which included carboxyl groups. The structure development was strongly dependent on HTT. In agreement with the previous results, the acidic surface functionalities of

activated carbon (having reasonable surface area and pore structure development) were more important for SCR of NO than their physical characteristics.

Chapter 7

RECOMMENDATIONS

This research showed that activated carbons can be used as catalysts for NOx reduction at lower temperatures (< 300^{o}C). The physical characteristics of activated carbon such as BET surface area and porosity were not as important as chemical characteristics such as pH and ash content. Commercially synthesized activated carbon samples with low pH and low ash content exhibited higher activity. The presence of mineral matter such as CaO, MgO and Na_2O may have accounted for their high pH and reduced activity. These results suggested that coal and other material which could be cleaned by column flotation prior to activation would make better precursors for activated carbons for SCR application, since they would contain less amount of mineral matter.

Acidic surface oxides such as carboxyl groups were also found to be very important for activated carbon's activity for SCR of NO using NH_3. In cases of commercial samples as well as in-house samples, these oxides were introduced by treatment with sulfuric acid. Sulfuric acid acted as a strong oxidizing agent and oxidized the surface of activated carbon. For future work, other oxidizing agents such as nitric acid should also be investigated.

The gas phase oxygen was also found to be very important perhaps due to its role in heterogeneous oxidation of NO to NO_2 . NO_2 by itself was found to be

very readily reduced to N_2 using NH_3 over activated carbon. Based on these results, a new process could be developed which would incorporate other metal catalysts having high activity for oxidizing NO to NO_2 in presence of oxygen with activated carbon in a two stage reactor. In the first stage NO would be oxidized by oxygen over metal catalyst and in the second stage NO_2 would be reduced to N_2 using NH_3 over activated carbon.

Other reductants such as light hydrocarbons including ethane or propane could also be investigated for NO reduction in place of NH_3.

REFERENCES CITED

1. Anna-Karin, H.,"Regulations on NOx emissions, " NOx control technologies for coal combustion, IEA Coal Research, June 1990.
2. Boer, F. P., Hegedus, L. L. ,Gouker, T. R. and Zak, K. P., Chemtech, 312, May 1990.
3. Lesley L. S., "Regional emissions, concentrations and legislation," NOx emissions from coal combustion, IEA Coal Research, March 1991.
4. White, J. C., "Global climate change linkages, acid rain, air quality, and stratospheric ozone," 1989.
5. Lesley, L. S., "Effect of nitrogen oxides," NOx emissions from coal combustion, IEA Coal Research, March 1991.
6. Anna-Karin, H., "Selective catalytic reduction," NOx control technologies for coal combustion, IEA Coal Research, June 1990.
7. Anna-Karin, H., "NOx formation," NOx control technologies for coal combustion, IEA Coal Research, June 1990.
8. Shaw, J. T., "Emissions of nitrogen oxides," Fluidized beds combustion and application, Applied Science Publishers, 1983.
9 Freihaut, J., Prosica, W., and Seery, D., "Fuel bond nitrogen evolution during the devolatization and pyrolsis of coals of varying rank," Symposium on stationary combustion nitrogen oxide control, 1987.

10. Lee, Y. Y., and Hiltunen, M., "The conversion of fuel-nitrogen to NOx in circulating fluidized bed combustion," Symposium on stationary combustion nitrogen oxide control, 1989.
11. Anna-Karin H., "Control of NOx emissions through combustion measures," NOx control technologies for coal combustion, IEA Coal Research, June 1990.
12. Caton, J. A., and Siebers, D. L., Combustion Science and Technology, Vol. **65**, 277, 1989.
13. Epperly, W. R., Chemtech, 429, July, 1991.
14. Anna-Karin H., "Selective non catalytic reduction," NOx control technologies for coal combustion, IEA Coal Research, June 1990.
15 Brian, G. W., Karen, A. G., and John, W. R., Combustion and Flame, **78**, 249. 1989.
16 Chen, S. L., and Lyon, R. K., and Seeker, W. R., Environmental Progress, **10**, 182, August , 1991.
17 "NOx controls proliferates in flexible climate," Coal and Synfuels Technology, Feb. 24, 1992.
18. Anna-Karin, H., and Hermine, N. S. "Flue gas treatment," NOx control installations on coal-fired plants, IEA Coal Research, March, 1991.
19. Bosch, H., and Janssen, F., "Catalytic reduction of nitrogen oxides," Catalysis today, March, 1988.
20 Baurele, G. L., and Nobe, K., Ind. Eng. Chem. Prod. Res. Dev., **14**, 123, 1975.
21 Hahn, T., and Lintz, H. G., Surface Science, 1030, 1989.

22 Hahn, T., and Lintz, H. G., Applied Surface Science, **40**, 59, 1989.

23 Banse, B, A., Wickham, D. T., and Koel, B. E., Journal of Catalysis, **119**, 238, 1989.

24 Ravindranathan, K, Ruterana, P., and Gratzel, M., Journal of Catalysis, **126**, 572, 1990.

25 Cho., B. K., Journal of Catalysis, **131**, 74, 1991.

26 Oh, S. H., and Eickel, C. C., Journal of Catalysis, **112**, 543, 1988.

27 Oh, S. H., Journal of Catalysis, **124**, 477, 1990.

28 Murrell, L. L., and Tauster, S. J., Journal of Catalysis, **41**, 192, 1976.

29 Mizumoto, M., Yamazoe, N., and Seiyama, T., Journal of Catalysis, **55**, 119, 1978.

30 Li, Y., and Hall, K. W., Journal of Catalysis, **129**, 202, 1991.

31 Li, Y., Armor, J. N., Applied Catalysis, **76**, 1991.

32 Iwamoto, M., Yahiro, Hidenori, Shundo, S., Yu-u, Y., and Mizuno, N., Applied Catalysis, **69**, 1991.

33 Hamada, H., Kintaichi, Y., Sasaki, M., Ito, T., and Tabata, M., Applied Catalysis, Vol. **64**,. 1990.

34 Petunchi, J. O., and Hall, W. K., Journal of Catalysis, **78**, 327, 1982.

35 Tzou, M.S., and Asakura, K., Yamazaki, Y., and Kuroda, H., Catalysis, **11**, 33, 1991.

36 Takagi, M., Kawai, T., Soma, M, Onishi, T., and K. Tamaru, Journal of Physical Chemistry, **80**, 430, 1976.

37 Takagi, M., Kawai, T., Soma, M, Onishi, T., and K. Tamaru, Journal of Catalysis, **50**, 441, 1977.

38 Miyamoto, A., Inomata, M., Yamazaki, Y., Murakami, Y. Journal of Catalysis, **57**, 526, 1979.

39 Srnak, T. Z. Dumesic, J. A., Clausen, B. S. Tornqvist, E., and Topoet, N. Y., Journal of Catalysis, **135**, 246, 1992.

40 Odriozola, J. A., Heinemann, H., Somorjai, G. A., Banda, J. F., and Pereira, P., Journal of Catalysis, **119**, 71, 1989.

41 Odriozola, J. A., Soria, J., Somorjai, G. A., Heinemann, H., Banda, J. F., Grandoz, M. L. and Conesa, J. C., Journal pf Physical Chemistry, **95**, 240, 1991.

42 Gianguido, R., Busca, G., and Forzatti, P., Applied Catalysis, **64**, 259, 1990.

43. Rajadhyaksha, R. A., Hausinger, G., Zeilinger, H., Ramsetter, A., Schmelz, and H., Knozinger, H., Applied Catalysis, **51**, 67, 1989.

44 Bjorklund, R. B., Odenbrand, C. U. I., Brandin, J. G. M., Andersson, and L. H., Liedberg, B., Journal of Catalysis, **119**, 187, 1989.

45 Handy, B. T., Biaker, A., Marth, M. S., and Wokaun, A.,Journal of Catalysis, **133**, 1, 1992.

46 Topsoe, N., Slabiak, T., Clausen, B. S., Srnak, T. Z., and Dumesic, J. A., Journal of Catalysis, **132**, 742. 1992.

47 Kasoka, S., Sasaoka, E., and Nanba, H., Nippon Kagaku Kaishi, 486, 1984.

48 Chen, P. J., and Yang, T. R., Journal of Catalysis, **125**, 411, 1990.

49 Blanco, J., Avila, P., Barthelemy, C., Bahamonde, A., Odriozola, J., A., Banda, J. F. G., and Heinemann, H., Applied Catalysis, **55**, 151, 1989.

50 Eldridge, J. W., and Kittrell, J. R., Ind. Eng. Chem. Prod. Res. Dev., **25**, 192, 1986.

51 Willey R. J., Eldridge, J. W., and Kittrell, J. R., Ind. Eng. Chem. Prod. Res. Dev., **24**. 226, 1985.

52 Hyde, E. C., and Baiker, A., Ind. Eng. Chem. Res., **29**, 1985, 1990.

53 Hyde, E. C. , Musch, H., and Baiker, A., Applied Catalysis, **65**, 211, 1990.

54 Hyde, E. C. , Musch, H., Baiker, A., Marth, M. S., and Wokaun, A., Journal of Catalysis, **133**, 397, 1992.

55 Marth, M. S., Wokaun, A., Hyde, E. C., and Baiker, A., Journal of Catalysis **133**, 415, 1992.

56 Bansal, C. R., Donnet, B. J. , and Stoeckli, F., Active Carbon, Marcel Dekker, Inc., New York, 1988.

57 Vliet, B. M., "Nature and Properties of Activated carbon," Symposium on the Design and Operation of Plants for the Recovery of Gold using Activated Carbon, Johannesburg, 1985.

58 Derbyshire, F., and Thwaites, M., "Coal Precursors for Activated Carbons," 1991.

59 Jenkins, R. G., Nandi, S. P., and Walker, P. L., Fuel, **52**, 288, 1973.

60 Thwiates, M., Jagtoyen, M., and Derbyshire, F., Activated Carbons-Production and Application," 1992.

61 Laine, J., Calafat, A., and Labady, M., Carbon, 191, 1989.

62 NORIT, "Introduction to Activated Carbon, " sales brochure, Netherlands, Norit NV, 3800 AC, Amersfoot, Postbus 105.

63 Kwok, J., and Miller, A., U. S. Patent 3767592, Oct. 23, 1973.

64 Murty, H. N., U. S. Patent 4032476, June 28, 1977.

65 Otake, Y., "Characterization of Oxygen Complexes Present on Microporous Carbon," Ph. D. Thesis, Penn. State, 1986.

66 Juntgen, H., Richter, E., Knoblauch, K., and Hoang-Phu, T., Chemical Engineering Science, **43**, 419, 1988.

67 Hoechst, "Flue Gas Treatment, " sales brochure, Germany, Friedrich-Uhde-Strasse 15, Postfach 262, D-4600 Dortmund.

68 Kusakabe, K., Kawamura, H., Kim, H. J, and Morooka, S.,

69 Juetgen, H., and Kuehl, H., Chemistry and Physics of Carbon, **22**, 145, 1989.

70 Kleinshcmidt, R., Ph. D. Dissertation, GHS Essen, 1988.

71 Lenz. U., Paeffgen, H. P., and Wolfrum, E., Research report, Contract no. EN3F-005-D, RHEINISCHE BRAUNKOHLENWERKE AG, Koeln, Germany.

72 Michicharu, S., Sakuri, Y., and Yoshida, K, preprints, American Chemical Society Conference, Chicago, 1975.

73 Kapteijn, F, Mierop, J. C. A., and Moulijn, A. J., preprints, 17th Bienn. Carbon Conference, 1985.

74 deBoer, J. H., Linsen, G., Plas, T., and Zondervan, Journal of Catalysis, **4**, 649, 1965.

75 Satterfeild, C. N., Heterogeneous Catalysis in Practise, McGraw-Hill Book Company, New York, 1980.

76 deBoer, J. H., The Structure and Properties of Porous Material, Butterworth, London, 1958.

77 Schofeild, R. K., Disc. Faraday Soc., **3**, 105, 1948.

78 Smith, J. M., Chemical Engineering Kinetics, McGraw-Hill Book Company, New York,1970.

79 Mears, E. D., Ind. Eng. Chem. Process Des. Develop., **4**. 543, 1971.

80 Cheng, P. J., Buzanowski, A., and Yang, T. R., Journal of Air Waste Manag. Assoc. **40**, 1403, 1990.

81 Mochida, I., Fujitsi, H., Shiraishi, I., and Ida, S., Nippon Kagaku Kaishi, 797, 1987.

82 Nishijima, A., Kurtia, M., Kobayashi, R., Hagiwara, H., Ueno, A., Sato, T., and Todo, N., Chem. Soc. Jpn, 53, 3356, 1980.

83 Bedjai, G., Orbach, H., and Reinsenfelf, F., Industrial and Engineering Chemistry, **50**, 1165, 1958.

84 Edwards, H. W., Air Pollution and its Control, AIChe Symposium Series, 1972.

85 Richter, E., Schmidt, H., Schecker, H., Chem. Eng. Tech., **13**, 332, 1990.

86 Bosch, H and Janssen, F, Catalysis today, 2433, 1988.

87 Markvart, M., and Pour, M., Journal of Catalysis, **7**, 279, 1967.

88 Braker, W. and Mossman, A.'Matheson Gas Data Book', 6th edt.

89 Rao, M. N., and Hougen, O. A., Symposium on Chem Eng. Progress, 1952, 4, 110.

90 Imanari, M., Watanabe, Y., Matsuda, S., and Nakajima, F., "Proceedings of the 7th International Conferenc on Catalysis'," Elsveir, Amsterdam, 841, 1981.

91 Kato, A., Matsuda, S., Nakajima, F., Imanari, M., and Watanbe, Y., Journal of Physical Chemistry, **85**, 1710, 1981.

92 Kato, A., Matsuda, S., Kamo, T., Nakajima, F., Kuroda, H., and Narita, T., Journal of Physical Chemistry,.**85**, 4099, 1981.

93 Painter, P. C., Snyder, W. R., Starcinic, W., Coleman, M., Kuehn, D. and Davis, A., Applied Spectroscopy, **35**, 475, 1981.

94 Ege, N. S, "Organic Chemistry," D. C. Heath and CO., 1984

95 Lydia, S.," Low Temperature Selective Catalytic Reduction (SCR) of Nitric Oxide with Ammonia," Ph. D. thesis, University of Amsterdam, 1992.

96 Miyamoto, A., Kobyasahi, K., Inimata, M., and Murakmami, Y., Journal of Physical Chemistry, **86**, 2945, 1982.

97 Otto, K., Shelef, M., and Kummer, T. J., Journal of Physical Chemistry, **74**, 2690, 1970.

98 TaKagi, M., Kawai, T., Soma, M., Onishi, T., and Tamura. K., Journal of Catalysis, **50**, 441, 1977.

99 Jagtoyen, M., Thwaites, M., Stencel, J., McEnanaey, B., and Drebyshire, F., Carbon, **30**, 1089-1096, 1992.

APPENDIX A
CALIBRATION DATA

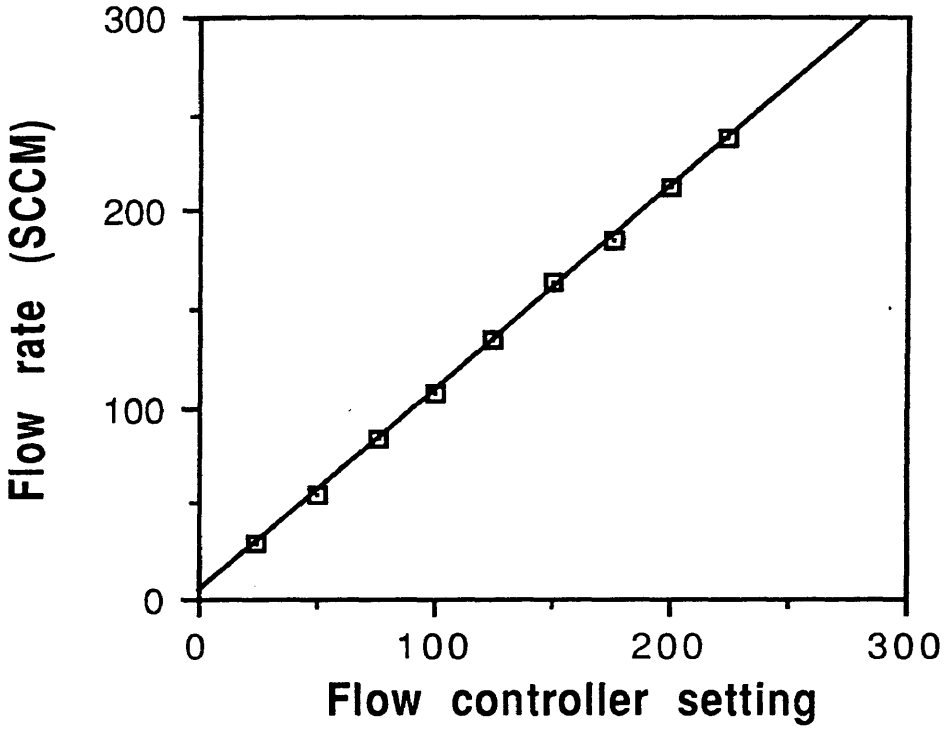

Figure A.1 Calibration graph for NO/He flow controller

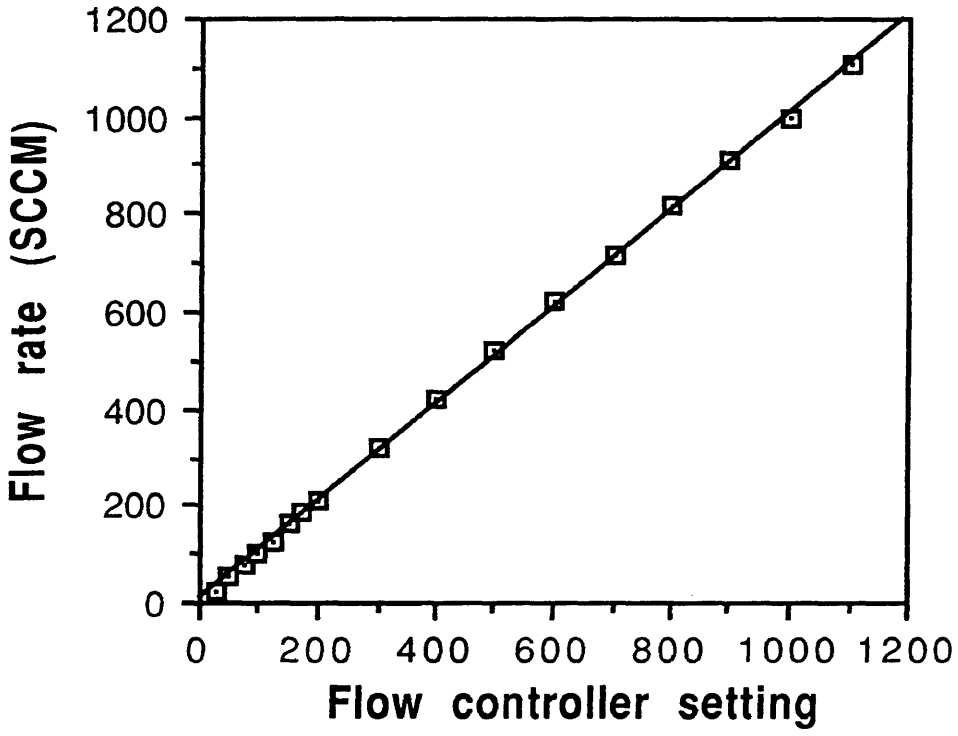

Figure A.2 Calibration graph for He flow controller

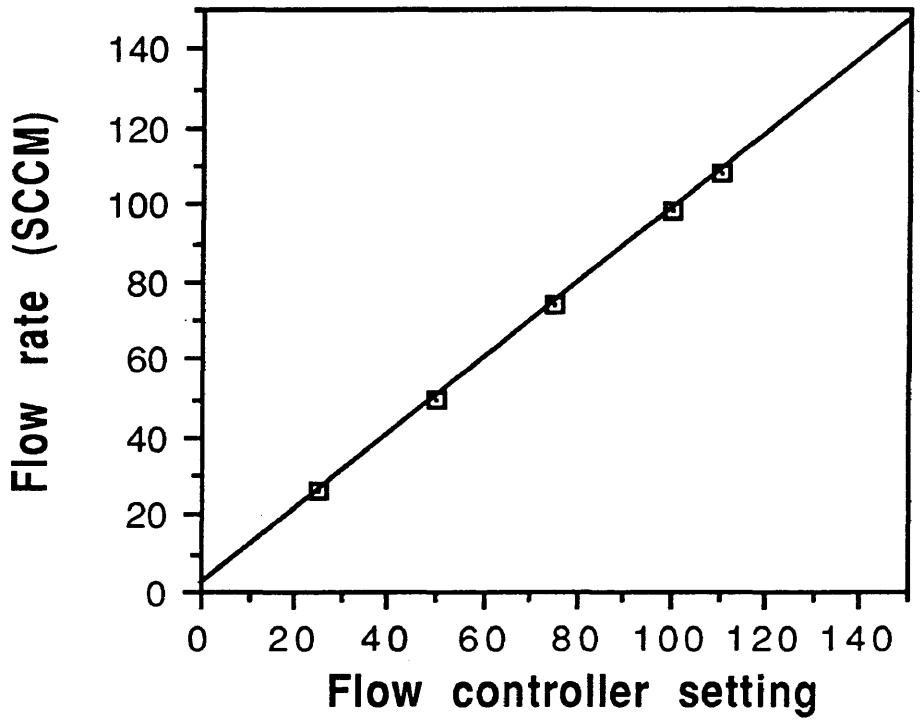

Figure A.3 Calibration graph for O2/He flow controller

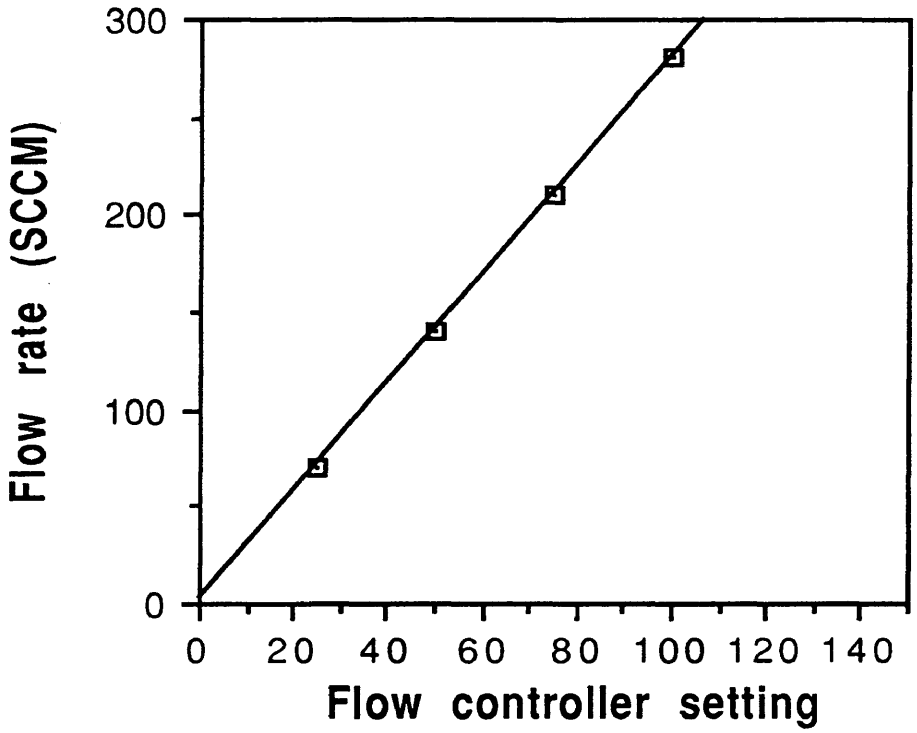

Figure A.4 Calibration graph for NH3/He flow controller

APPENDIX B

EQUILIBIRIUM CALCULATIONS

ARTHUR LAKES LIBRARY
COLORADO SCHOOL OF MINES
GOLDEN, CO 80401

Standard State: Pure gas at unit fugacity

a)

$$NO + NH_3 + 1/4O_2 \text{ ----------> } 3/2H_2O + N_2$$

$$\Delta H^o_{25C} = 3/2(-58) + 1(0) - 1(21.6) - 1(-11.02) - 1/4(0)$$

$$\Delta H^o_{25C} = -98 \text{ Kcal/g-mole}$$

$$\Delta G^o_{25C} = 3/2(-55) + 1(0) - (21) - (-3.94) - 1/4(0)$$

$$\Delta G^o_{25C} = -100 \text{ Kcal/g-mole}$$

$$\Delta G^o = -RT \ln Ka \qquad [B.1]$$

$$\ln Ka,_{25C} = \frac{-(-100000)}{(1.987)(298.16)}$$

$$\ln Ka,_{25C} = 168$$

$$\frac{d \ln Ka}{dT} = -\frac{\Delta H^o}{R T^2} \qquad [B.2]$$

Assume ΔHo is independent of temperature then Equation B.2 can be integrated to

$$\ln Ka,_2 - \ln Ka,_1 = \frac{\Delta H^o(1/T_1 - 1/T_2)}{R} \qquad [B.3]$$

$$\ln Ka,_{300C} - 168 = -\frac{98000}{1.987}(1/298 - 1/573)$$

$$\ln Ka,_{300C} = 89$$

$$Ka,_{300C} = 2.92 \times 10^{38}$$

Since operating pressure is about 1 atm therefore f/P is also approximately one.

$$Ka = ((YH_2O)^{1.5}\, YN_2)/(YNO\, YNH_3\, (YO_2)^{0.25}) \cdot P^{0.25}$$

Basis: 100 moles

	Initial moles	Moles at extent ∂
NO	0.07	$0.07-\partial$
NH_3	0.07	$0.07-\partial$
O_2	4.0	$4.0-1/4\partial$
He	95.86	95.86
N_2	0	∂
H_2O	0.0	1.5∂
Total	100.0	$100+0.25\partial$

$$Ka,_{300C}= 2.92 \times 10^{38} = \frac{(1.5\partial/100+0.25\partial)^{1.5}(\partial/100+0.25\partial)}{((0.07-\partial)/(100+0.25\partial))^{2}((4.0-0.25\partial)/(100+0.25\partial))^{0.25}}$$

Solving this equation numerically

Even for 99 % conversion of NO, the L.H.S. is greater than R.H.S which suggested that the reaction is favored towards products formation.

b)

$$NH_3 + 5/4O_2 \text{ ----------> } 3/2H_2O + NO$$

$\Delta H^o_{25C} = 3/2(-58) + 1(21.6) - 1(-11.02)-5/4(0)$
$\Delta H^o_{25C} = -54$Kcal/g-mole

$\Delta G^o_{25C} = 3/2(-55) + (21) - (-3.94)-5/4(0)$
$\Delta G^o_{25C} = -58$ Kcal/g-mole

$\Delta G^o = -RT \ln Ka$

$$\ln Ka,_{25C} = - \frac{(-58000)}{(1.987)(298.16)}$$

$\ln Ka,_{25C} = 98$

Using Equation B.3

$$\ln Ka,_{300C}\text{-}98 = \frac{-54000(1/298-1/573)}{1.987}$$

$$\ln Ka_{300C} = 54$$

$$\Delta G^{o}_{300} = -(1.987/1000)(573)(54)$$

$$\Delta G^{o}_{300} = -60 \text{ Kcal/g-mole}$$

The negative value of Gibbs free energy suggest the oxidation of ammonia is also possible under the experimental conditions.

APPENDIX C
MASS AND HEAT TRANSFER CALCULATIONS

Sample = SP1			External area	50 cm2/g
Bed Porosity=	0.5		Ea/R=	1130
Pore radius=	1.17E-07		Init Conc NH3	2.863E-08
particle porosity=	0.345		Init Conc O2	1.6358E-06
Temp (k)	NO CONC	NH3 CONC	O2 CONC	Obsereved K
	(moles/cm3)	(moles/cm3)	(moles/cm3)	(cm3/g-sec)
423	2.017E-08	2.017E-08	1.1524E-06	3.221
473	1.8038E-08	1.8038E-08	1.0306E-06	3.741
523	1.6313E-08	1.6313E-08	9.3206E-07	4.953
573	1.489E-08	1.489E-08	8.5073E-07	6.507

Sample = SP2			External area	50 cm2/g
Bed Porosity=	0.5		Ea/R=	1704
Pore radius=	1.227E-07		Init Conc NH3	2.863E-08
particle porosity=	0.695		Init Conc O2	1.6358E-06
Temp (k)	NO CONC	NH3 CONC	O2 CONC	Obsereved K
	(moles/cm3)	(moles/cm3)	(moles/cm3)	(cm3/g-sec)
423	2.017E-08	2.017E-08	1.1524E-06	1.825
473	1.8038E-08	1.8038E-08	1.0306E-06	2.656
523	1.6313E-08	1.6313E-08	9.3206E-07	4.078
573	1.489E-08	1.489E-08	8.5073E-07	5.01

Sample = SP3			External area	50 cm2/g
Bed Porosity=	0.5		Ea/R=	760
Pore radius=	1.15E-07		Init Conc NH3	2.863E-08
particle porosity=	0.605		Init Conc O2	1.6358E-06
Temp (k)	NO CONC	NH3 CONC	O2 CONC	Obsereved K
	(moles/cm3)	(moles/cm3)	(moles/cm3)	(cm3/g-sec)
423	2.017E-08	2.017E-08	1.1524E-06	0.838
473	1.8038E-08	1.8038E-08	1.0306E-06	0.838
523	1.6313E-08	1.6313E-08	9.3206E-07	1.103
573	1.489E-08	1.489E-08	8.5073E-07	1.31

Sample = SP4			External area	50 cm2/g
Bed Porosity=	0.5		Ea/R=	124
Pore radius=	1.778E-07		Init Conc NH3	2.863E-08
particle porosity=	0.5425		Init Conc O2	1.6358E-06
Temp (k)	NO CONC	NH3 CONC	O2 CONC	Obsereved K
	(moles/cm3)	(moles/cm3)	(moles/cm3)	(cm3/g-sec)
423	2.017E-08	2.017E-08	1.1524E-06	0.903
473	1.8038E-08	1.8038E-08	1.0306E-06	0.838
523	1.6313E-08	1.6313E-08	9.3206E-07	0.903
573	1.489E-08	1.489E-08	8.5073E-07	0.969

NO conversion %	Bulk Density (g/cu-cm)	G (g/cm2-sec)	Viscosity g/cm-sec	Re #	JD
44	0.00011522	0.00165463	0.00025122	0.19561875	1.76781709
49	0.00010304	0.00147972	0.00027147	0.16189052	1.90936198
59	9.3193E-05	0.00133825	0.00029172	0.13624983	2.04817309
69	8.5061E-05	0.00122148	0.00031197	0.11628827	2.18458161

NO conversion %	Bulk Density (g/cu-cm)	G (g/cm2-sec)	Viscosity g/cm-sec	Re #	JD
28	0.00011522	0.00165463	0.00025122	0.19561875	1.76781709
38	0.00010304	0.00147972	0.00027147	0.16189052	1.90936198
52	9.3193E-05	0.00133825	0.00029172	0.13624983	2.04817309
60	8.5061E-05	0.00122148	0.00031197	0.11628827	2.18458161

NO conversion %	Bulk Density (g/cu-cm)	G (g/cm2-sec)	Viscosity g/cm-sec	Re #	JD
14	0.00011522	0.00165463	0.00025122	0.19561875	1.76781709
14	0.00010304	0.00147972	0.00027147	0.16189052	1.90936198
18	9.3193E-05	0.00133825	0.00029172	0.13624983	2.04817309
21	8.5061E-05	0.00122148	0.00031197	0.11628827	2.18458161

NO conversion %	Bulk Density (g/cu-cm)	G (g/cm2-sec)	Viscosity g/cm-sec	Re #	JD
15	0.00011522	0.00165463	0.00025122	0.19561875	1.76781709
14	0.00010304	0.00147972	0.00027147	0.16189052	1.90936198
15	9.3193E-05	0.00133825	0.00029172	0.13624983	2.04817309
16	8.5061E-05	0.00122148	0.00031197	0.11628827	2.18458161

DNO-NH3 cm2/sec	DNO-02 cm2/sec	DNO-N2 cm2/sec	DNO-H2O cm2/sec	DNO-H2 cm2/sec	DNH3-O2 cm2/sec
0.40341092	0.39149216	0.39149216	1.04397908	1.30497385	0.40019198
0.47701145	0.46291817	0.46291817	1.23444845	1.54306056	0.47320524
0.55461247	0.53822646	0.53822646	1.43527057	1.79408821	0.55018705
0.63601745	0.61722633	0.61722633	1.64593689	2.05742111	0.63094247

DNO-NH3 cm2/sec	DNO-02 cm2/sec	DNO-N2 cm2/sec	DNO-H2O cm2/sec	DNO-H2 cm2/sec	DNH3-O2 cm2/sec
0.40341092	0.39149216	0.39149216	1.04397908	1.30497385	0.40019198
0.47701145	0.46291817	0.46291817	1.23444845	1.54306056	0.47320524
0.55461247	0.53822646	0.53822646	1.43527057	1.79408821	0.55018705
0.63601745	0.61722633	0.61722633	1.64593689	2.05742111	0.63094247

DNO-NH3 cm2/sec	DNO-02 cm2/sec	DNO-N2 cm2/sec	DNO-H2O cm2/sec	DNO-H2 cm2/sec	DNH3-O2 cm2/sec
0.40341092	0.39149216	0.39149216	1.04397908	1.30497385	0.40019198
0.47701145	0.46291817	0.46291817	1.23444845	1.54306056	0.47320524
0.55461247	0.53822646	0.53822646	1.43527057	1.79408821	0.55018705
0.63601745	0.61722633	0.61722633	1.64593689	2.05742111	0.63094247

DNH3-N2 cm2/sec	DNH3-H2O cm2/sec	DNH3-HE cm2/sec	DO2-N2 cm2/sec	DO2-H20 cm2/sec	DO2-HE cm2/sec
0.41532968	0.85258292	1.26147472	0.39149216	1.00047995	1.30236391
0.49110474	1.0081329	1.49162521	0.46291817	1.18301309	1.53997444
0.57099847	1.17213763	1.73428527	0.53822646	1.37546763	1.79050003
0.65480856	1.34418179	1.98884041	0.61722633	1.57735619	2.05330627

DNH3-N2 cm2/sec	DNH3-H2O cm2/sec	DNH3-HE cm2/sec	DO2-N2 cm2/sec	DO2-H20 cm2/sec	DO2-HE cm2/sec
0.41532968	0.85258292	1.26147472	0.39149216	1.00047995	1.30236391
0.49110474	1.0081329	1.49162521	0.46291817	1.18301309	1.53997444
0.57099847	1.17213763	1.73428527	0.53822646	1.37546763	1.79050003
0.65480856	1.34418179	1.98884041	0.61722633	1.57735619	2.05330627

DNH3-N2 cm2/sec	DNH3-H2O cm2/sec	DNH3-HE cm2/sec	DO2-N2 cm2/sec	DO2-H20 cm2/sec	DO2-HE cm2/sec
0.41532968	0.85258292	1.26147472	0.39149216	1.00047995	1.30236391
0.49110474	1.0081329	1.49162521	0.46291817	1.18301309	1.53997444
0.57099847	1.17213763	1.73428527	0.53822646	1.37546763	1.79050003
0.65480856	1.34418179	1.98884041	0.61722633	1.57735619	2.05330627

DNH3-N2 cm2/sec	DNH3-H2O cm2/sec	DNH3-HE cm2/sec	DO2-N2 cm2/sec	DO2-H20 cm2/sec	DO2-HE cm2/sec
0.41532968	0.85258292	1.26147472	0.39149216	1.00047995	1.30236391
0.49110474	1.0081329	1.49162521	0.46291817	1.18301309	1.53997444
0.57099847	1.17213763	1.73428527	0.53822646	1.37546763	1.79050003
0.65480856	1.34418179	1.98884041	0.61722633	1.57735619	2.05330627

DN2-H20 cm2/sec	DN-HE cm2/sec	DH2O-HE cm2/sec	total moles	YNO	YNH3
0.9535009	1.23189532	4.00191982	1000077	0.00039197	0.00039197
1.12746291	1.45664917	4.73205237	1000085.75	0.00035697	0.00035697
1.31088045	1.69361927	5.50187051	1000103.25	0.00028697	0.00028697
1.50328903	1.94220553	6.30942474	1000120.75	0.00021697	0.00021697

DN2-H20 cm2/sec	DN-HE cm2/sec	DH2O-HE cm2/sec	total moles	YNO	YNH3
0.9535009	1.23189532	4.00191982	1000049	0.00050398	0.00050398
1.12746291	1.45664917	4.73205237	1000066.5	0.00043397	0.00043397
1.31088045	1.69361927	5.50187051	1000091	0.00033597	0.00033597
1.50328903	1.94220553	6.30942474	1000105	0.00027997	0.00027997

DN2-H20 cm2/sec	DN-HE cm2/sec	DH2O-HE cm2/sec	total moles	YNO	YNH3
0.9535009	1.23189532	4.00191982	1000024.5	0.00060199	0.00060199
1.12746291	1.45664917	4.73205237	1000024.5	0.00060199	0.00060199
1.31088045	1.69361927	5.50187051	1000031.5	0.00057398	0.00057398
1.50328903	1.94220553	6.30942474	1000036.75	0.00055298	0.00055298

DN2-H20 cm2/sec	DN-HE cm2/sec	DH2O-HE cm2/sec	total moles	YNO	YNH3
0.9535009	1.23189532	4.00191982	1000026.25	0.00059498	0.00059498
1.12746291	1.45664917	4.73205237	1000024.5	0.00060199	0.00060199
1.31088045	1.69361927	5.50187051	1000026.25	0.00059498	0.00059498
1.50328903	1.94220553	6.30942474	1000028	0.00058798	0.00058798

YO2	YN2	YH2O	YHe	DNO-MIX cm2/sec	DNH3-MIX cm2/sec
0.03991993	0.00030798	0.00046196	0.95852619	1.19185324	1.1598438
0.03991083	0.00034297	0.00051446	0.95851781	1.40931392	1.37145217
0.03989263	0.00041296	0.00061944	0.95850103	1.63861213	1.59456229
0.03987444	0.00048294	0.00072441	0.95848426	1.87915742	1.82860915

YO2	YN2	YH2O	YHe	DNO-MIX cm2/sec	DNH3-MIX cm2/sec
0.03994904	0.00019599	0.00029399	0.95855303	1.19181987	1.1598438
0.03993084	0.00026598	0.00039897	0.95853626	1.4092868	1.37145217
0.03990537	0.00036397	0.00054595	0.95851278	1.63859205	1.59456229
0.03989081	0.00041996	0.00062993	0.95849936	1.87912783	1.82860915

YO2	YN2	YH2O	YHe	DNO-MIX cm2/sec	DNH3-MIX cm2/sec
0.03997452	9.7998E-05	0.000147	0.95857651	1.19179068	1.1598438
0.03997452	9.7998E-05	0.000147	0.95857651	1.40922761	1.37145217
0.03996724	0.000126	0.00018899	0.95856981	1.63849457	1.59456229
0.03996178	0.00014699	0.00022049	0.95856477	1.87899959	1.82860915

YO2	YN2	YH2O	YHe	DNO-MIX cm2/sec	DNH3-MIX cm2/sec
0.0399727	0.000105	0.0001575	0.95857484	1.19179276	1.1598438
0.03997452	9.7998E-05	0.000147	0.95857651	1.40922761	1.37145217
0.0399727	0.000105	0.0001575	0.95857484	1.63848597	1.59456229
0.03997088	0.000112	0.000168	0.95857316	1.87898315	1.82860915

DO2-MIX cm2/sec	N0-SCH #	NH3 -SCH #	O2-SCH #	KmAm-NO cm3/gcat-sec	KmAM-NH3 cm3/gcat-sec
1.79415475	1.49512292	1.52247862	1.13859843	694.298812	675.670517
2.12149034	1.51684088	1.54460294	1.15514429	733.842195	714.146694
2.46661791	1.53890487	1.56708902	1.1719607	770.324015	749.636278
2.82866346	1.56104083	1.58964892	1.1888323	804.213433	782.601886

DO2-MIX cm2/sec	N0-SCH #	NH3 -SCH #	O2-SCH #	KmAm-NO cm3/gcat-sec	KmAM-NH3 cm3/gcat-sec
1.79415475	1.4951508	1.52247862	1.13859843	694.279392	675.670517
2.12149034	1.51686032	1.54460294	1.15514429	733.828084	714.146694
2.46661791	1.53891743	1.56708902	1.1719607	770.314589	749.636278
2.82866346	1.5610572	1.58964892	1.1888323	804.200781	782.601886

DO2-MIX cm2/sec	N0-SCH #	NH3 -SCH #	O2-SCH #	KmAm-NO cm3/gcat-sec	KmAM-NH3 cm3/gcat-sec
1.79415475	1.4951752	1.52247862	1.13859843	694.2624	675.670517
2.12149034	1.51690275	1.54460294	1.15514429	733.797296	714.146694
2.46661791	1.53897841	1.56708902	1.1719607	770.268805	749.636278
2.82866346	1.56112816	1.58964892	1.1888323	804.145955	782.601886

DO2-MIX cm2/sec	N0-SCH #	NH3 -SCH #	O2-SCH #	KmAm-NO cm3/gcat-sec	KmAM-NH3 cm3/gcat-sec
1.79415475	1.49517345	1.52247862	1.13859843	694.263614	675.670517
2.12149034	1.51690275	1.54460294	1.15514429	733.797296	714.146694
2.46661791	1.53898379	1.56708902	1.1719607	770.264765	749.636278
2.82866346	1.56113726	1.58964892	1.1888323	804.138926	782.601886

INTERPARTICLE CLACULATIONS

KmAm-O2	rNO inital	rNH3 initial	rO2 initial	(Cb-Cs)NO	NO % change
cm3/gcat-sec	moles/gcat-s	moles/gcat-s	moles/gcat-s	moles/cm3	
1044.73441	6.4966E-08	6.4966E-08	1.6242E-08	9.3571E-11	0.46392129
1104.227	6.7478E-08	6.7478E-08	1.687E-08	9.1952E-11	0.50978262
1159.10166	8.0799E-08	8.0799E-08	2.02E-08	1.0489E-10	0.64297619
1210.0737	9.6887E-08	9.6887E-08	2.4222E-08	1.2047E-10	0.80911357

INTERPARTICLE CLACULATIONS

KmAm-O2	rNO inital	rNH3 initial	rO2 initial	(Cb-Cs)NO	NO % change
cm3/gcat-sec	moles/gcat-s	moles/gcat-s	moles/gcat-s	moles/cm3	
1044.73441	3.681E-08	3.681E-08	9.2024E-09	5.3018E-11	0.26286248
1104.227	4.7908E-08	4.7908E-08	1.1977E-08	6.5285E-11	0.36193763
1159.10166	6.6525E-08	6.6525E-08	1.6631E-08	8.636E-11	0.5293941
1210.0737	7.4597E-08	7.4597E-08	1.8649E-08	9.2759E-11	0.62297875

INTERPARTICLE CLACULATIONS

KmAm-O2	rNO inital	rNH3 initial	rO2 initial	(Cb-Cs)NO	NO % change
cm3/gcat-sec	moles/gcat-s	moles/gcat-s	moles/gcat-s	moles/cm3	
1044.73441	1.6902E-08	1.6902E-08	4.2255E-09	2.4345E-11	0.12070364
1104.227	1.5115E-08	1.5115E-08	3.7789E-09	2.0599E-11	0.11420048
1159.10166	1.7993E-08	1.7993E-08	4.4983E-09	2.336E-11	0.14319676
1210.0737	1.9505E-08	1.9505E-08	4.8763E-09	2.4256E-11	0.16290575

INTERPARTICLE CLACULATIONS

KmAm-O2	rNO inital	rNH3 initial	rO2 initial	(Cb-Cs)NO	NO % change
cm3/gcat-sec	moles/gcat-s	moles/gcat-s	moles/gcat-s	moles/cm3	
1044.73441	1.8213E-08	1.8213E-08	4.5533E-09	2.6234E-11	0.13006587
1104.227	1.5115E-08	1.5115E-08	3.7789E-09	2.0599E-11	0.11420048
1159.10166	1.4731E-08	1.4731E-08	3.6827E-09	1.9124E-11	0.11723242
1210.0737	1.4428E-08	1.4428E-08	3.607E-09	1.7942E-11	0.12050157

(Cb-Cs)NH3 moles/cm3	NH3 % change	(Cb-Cs)O2 moles/cm3	O2 %change	PR #	TB-TS
9.6151E-11	0.47671164	1.5546E-11	0.00134901	0.02621429	0.00014702
9.4488E-11	0.52384195	1.5277E-11	0.00148238	0.02832737	0.00017759
1.0778E-10	0.66072042	1.7427E-11	0.00186973	0.03044046	0.00024417
1.238E-10	0.83145724	2.0017E-11	0.00235288	0.03255355	0.00033261

(Cb-Cs)NH3 moles/cm3	NH3 % change	(Cb-Cs)O2 moles/cm3	O2 %change	PR #	TB-TS
5.4479E-11	0.27010206	8.8083E-12	0.00076434	0.02621429	8.3302E-05
6.7084E-11	0.37191238	1.0846E-11	0.00105245	0.02832737	0.00012609
8.8743E-11	0.54399715	1.4348E-11	0.00153942	0.03044046	0.00020104
9.5319E-11	0.64017224	1.5412E-11	0.00181158	0.03255355	0.00025609

(Cb-Cs)NH3 moles/cm3	NH3 % change	(Cb-Cs)O2 moles/cm3	O2 %change	PR #	TB-TS
2.5015E-11	0.12402495	4.0446E-12	0.00035097	0.02621429	3.825E-05
2.1166E-11	0.11734284	3.4222E-12	0.00033206	0.02832737	3.9782E-05
2.4003E-11	0.14713802	3.8809E-12	0.00041638	0.03044046	5.4376E-05
2.4924E-11	0.16739035	4.0298E-12	0.00047369	0.03255355	6.6961E-05

(Cb-Cs)NH3 moles/cm3	NH3 % change	(Cb-Cs)O2 moles/cm3	O2 %change	PR #	TB-TS
2.6956E-11	0.13364502	4.3583E-12	0.00037819	0.02621429	4.1217E-05
2.1166E-11	0.11734284	3.4222E-12	0.00033206	0.02832737	3.9782E-05
1.965E-11	0.12045842	3.1772E-12	0.00034088	0.03044046	4.4516E-05
1.8436E-11	0.12381774	2.9808E-12	0.00035038	0.03255355	4.9531E-05

D,K NO	D,K NH3	D,K O2	D, com NO	D, com NH3	D, comb O2
0.00426155	0.00566113	0.00412622	0.00424636	0.00563364	0.00411676
0.00450638	0.00598637	0.00436328	0.00449201	0.00596036	0.00435433
0.00473858	0.00629483	0.00458811	0.00472491	0.00627008	0.00457959
0.00495992	0.00658886	0.00480242	0.00494686	0.00656521	0.00479428

D,K NO	D,K NH3	D,K O2	D, com NO	D, com NH3	D, comb O2
0.00426155	0.00566113	0.00412622	0.00424636	0.00563364	0.00411676
0.00450638	0.00598637	0.00436328	0.00449201	0.00596036	0.00435433
0.00473858	0.00629483	0.00458811	0.00472491	0.00627008	0.00457959
0.00495992	0.00658886	0.00480242	0.00494686	0.00656521	0.00479428

D,K NO	D,K NH3	D,K O2	D, com NO	D, com NH3	D, comb O2
0.00426155	0.00566113	0.00412622	0.00424636	0.00563364	0.00411676
0.00450638	0.00598637	0.00436328	0.00449201	0.00596036	0.00435433
0.00473858	0.00629483	0.00458811	0.00472491	0.00627008	0.00457959
0.00495992	0.00658886	0.00480242	0.00494686	0.00656521	0.00479428

D,K NO	D,K NH3	D,K O2	D, com NO	D, com NH3	D, comb O2
0.00426155	0.00566113	0.00412622	0.00424636	0.00563364	0.00411676
0.00450638	0.00598637	0.00436328	0.00449201	0.00596036	0.00435433
0.00473858	0.00629483	0.00458811	0.00472491	0.00627008	0.00457959
0.00495992	0.00658886	0.00480242	0.00494686	0.00656521	0.00479428

D, effe NO	D, effec NH3	D, effect O2	Weiz NO	Weiz NH3	Weiz O2
0.0007325	0.0009718	0.00071014	0.48485007	0.36545662	0.00218827
0.00077487	0.00102816	0.00075112	0.5323294	0.40118934	0.00240288
0.00081505	0.00108159	0.00078998	0.67005186	0.50492775	0.00302487
0.00085333	0.0011325	0.00082701	0.84078532	0.63352858	0.00379597

D, effe NO	D, effec NH3	D, effect O2	Weiz NO	Weiz NH3	Weiz O2
0.0007325	0.0009718	0.00071014	0.27471328	0.20706561	0.00123986
0.00077487	0.00102816	0.00075112	0.37793824	0.28483263	0.00170597
0.00081505	0.00108159	0.00078998	0.55168011	0.41572691	0.0024905
0.00085333	0.0011325	0.00082701	0.64735433	0.48777904	0.00292267

D, effe NO	D, effec NH3	D, effect O2	Weiz NO	Weiz NH3	Weiz O2
0.0007325	0.0009718	0.00071014	0.12614233	0.09507999	0.00056932
0.00077487	0.00102816	0.00075112	0.11924409	0.08986813	0.00053826
0.00081505	0.00108159	0.00078998	0.1492161	0.11244404	0.00067362
0.00085333	0.0011325	0.00082701	0.16926833	0.12754302	0.00076421

D, effe NO	D, effec NH3	D, effect O2	Weiz NO	Weiz NH3	Weiz O2
0.0007325	0.0009718	0.00071014	0.13592664	0.10245493	0.00061348
0.00077487	0.00102816	0.00075112	0.11924409	0.08986813	0.00053826
0.00081505	0.00108159	0.00078998	0.12215969	0.09205527	0.00055148
0.00085333	0.0011325	0.00082701	0.12520688	0.09434289	0.00056528

Damkohler NO	Damkohler NH3	Damkohler O2
0.37433187	0.374331875	0.37433518
0.41857998	0.418579976	0.41858305
0.46282742	0.462827424	0.46283075
0.50707479	0.507074793	0.50707843

Damkohler NO	Damkohler NH3	Damkohler O2
0.24823694	0.248236939	0.24823881
0.27757925	0.277579252	0.27758143
0.30692123	0.306921232	0.30692397
0.33626387	0.336263869	0.33626667

Damkohler NO	Damkohler NH3	Damkohler O2
0.5565778	0.5565778	0.55657866
0.6223675	0.622367504	0.62236819
0.68815691	0.688156907	0.68815765
0.75394639	0.753946391	0.75394712

Damkohler NO	Damkohler NH3	Damkohler O2
3.41128909	3.411289087	3.41129001
3.81451521	3.814515212	3.8145159
4.21774113	4.217741127	4.21774173
4.62096702	4.620967019	4.62096756

APPENDIX D

LANGMUIR-HINSHELWOOD RATE EQUATION

Simplified Langmuir-Hinshelwood mechanism:

$$NO + x \underset{K1}{<\text{-------}>} NO{\cdot}x \qquad (D.1)$$

$$NH_3 + y \underset{K2}{<\text{-------}>} NH_3{\cdot}y \qquad (D.2)$$

$$NO{\cdot}x + NH_3{\cdot}y \underset{K3}{\text{------->}} N_2 + H_2O + x + y \qquad (D.3)$$

$$r = K3\,[NO{\cdot}x]\,[NH_3\cdot y] \qquad [D.1]$$

$$[NO.x] = K1\,[NO]\,[x] \qquad [D.2]$$

$$[NH_3] = K2\,[NH_3\,]\,[y] \qquad [D.3]$$

$$[x] = x_{total}/(1+K1[NO]) \qquad [D.4]$$

$$[y] = y_{total}/(1+K2[NH_3]) \qquad [D.5]$$

$$r = \frac{K3\,K1\,[NO]\,K2\,[NH_3].\,x_{total}\,y_{total}}{(1+K1[NO])\,(1+K2[NH_3])} \qquad [D.6]$$

In case if $K2[NH_3] >> 1$ and $K1[NO] << 1$ then Equation D.6 becomes

$$r = K'\,[NO] \qquad [D.7]$$

where $K' = K3\,K1\,x_{total}\,y_{total}$

The results obtained (Chapter 4) under the experimental conditions employed in this study point to fact that the surface was saturated with NH_3.